Universidade de Aveiro Departamento de Electrónica, Telecomunicações e Informática,
2019

Diogo Rafael Pinto Pires

Design de Agregados de Antenas Tri-Dimensionais para Aplicação em Sistemas de Transmissão de Energia sem Fios

3D Antenna Arrays Design for WPT systems

Universidade de Aveiro Departamento de Electrónica, Telecomunicações e Informática,
2019

Diogo Rafael Pinto Pires

Design de Agregados de Antenas Tri-Dimensionais para Aplicação em Sistemas de Transmissão de Energia sem Fios

3D Antenna Arrays Design for WPT Systems

Diogo Rafael Pinto Pires

Design de Agregados de Antenas Tri-Dimensionais para Aplicação em Sistemas de Transmissão de Energia sem Fios

3D Antenna Arrays Design for WPT systems

Dissertação apresentada à Universidade de Aveiro para cumprimento dos requesitos necessários à obtenção do grau de Mestre em Engenharia Eletró nica e Telecomunicações , realizada sob a orientação científica do Professor Doutor Nuno Miguel Gonçalves Borges de Carvalho, Professor Catedrático do Departamento de Eletrónica Telecomunicações e Informática da Universidade de Aveiro e a co-orientação do Professor Doutor Pedro Pinho, do Instituto Superior de Engenharia de Lisboa.

o júri / the jury

presidente / president

Professor Doutor António José Ribeiro Neves
Professor Associado do Departamento de Electrónica, Telecomunicações e Informática da Universidade de Aveiro

vogais / examiners committee

Professor Doutor Paulo Mateus Mendes
Professor Associado do Departamento de Electrónica Industrial da Universidade do Minho (Arguente)

Professor Doutor Nuno Miguel Gonçalves Borges de Carvalho
Professor Catedrático do Departamento de Electrónica, Telecomunicações e Informática da Universidade de Aveiro (Orientador)

"Without commitment, you'll never start, but more importantly, without consistency, you'll never finish. So, keep working, keep striving, never give up, fall down seven times, get up eight. Ease is a greater threat to progress than hardship. So keep moving, keep growing, keep learning."

Denzel Washington

agradecimentos / acknowledgements

Aos meus pais, por todo o apoio prestado tanto na vida pessoal como profissional, por todo o esforço na vida e sacrifícos realizados. Sem eles não seria possivél atingir esta meta. Um especial agradecimento também aos meus irmãos e aos meus avós. Quando as raizes são profundas, não há razão para tremer. Foram e serão sempre o meu principal alicerce e motivo de orgulho.

Aos meus amigos. Aos de sempre e aos que surgiram para iniciar comigo esta caminhada. Em tudo contribuiram para tornar esta etapa inesquecivél. É demasiado elevado o sentimento de nostalgia que surge ao recordar estes últimos 5 anos. Um especial obrigado à Filipa por toda a amizade, carinho e apoio nos momentos menos bons.

Ao meu orientador, Professor Doutor Nuno Miguel Gonçalves Borges de Carvalho, por toda a orientação prestada ao longo deste trabalho, pela oporunidade de integrar um grupo de investigação de excelência e acima de tudo, por ser um exemplo de profissionalismo que ambiciono um dia alcançar.

Um especial obrigado ao Daniel Belo, à Marina Jordão e ao Diogo Matos, por todos os conhecimentos técnicos que me passaram mas acima de tudo pela disponibilidade, paciência e ajuda neste último ano.

Por último, um sincero agradecimento a todos os membros do Instituto de Telecomunicações por todo o auxílio prestado e aos meus colegas do laboratório de Rádio Frequência por terem proporcionado um ambiente calmo que contribuiu para levar a bom porto esta dissertação.

Palavras-Chave

Agregados de Antenas 3D; Antenas Patch Microstrip; "Beam-Switch"; Cobertura Hemisférica; Internet das Coisas; "Multiple-Input Multiple Output"; Transmissão de Energia sem Fios; RF to DC

Resumo

Os conceitos emergentes das redes da Internet das coisas e cidades inteligentes, juntamente com a constante inovação que se tem verificado nos sistemas de comunicação sem fios, apresentam um requisito fundamental: a capacidade de detetar, estabelecer e manter ligações de rádio com vários utilizadores, que podem ou não encontrar-se em movimento. Projetar antenas dotadas de uma cobertura robusta torna-se pois, uma necessidade prioritária para otimizar a performance destes sistemas.

Desta forma, o principal objetivo desta dissertação foca-se no desenvolvimento de diferentes agregados de antenas tridimensionais e posterior validação do seu funcionamento, quando implementados num cenário real. O propósito deste projeto alternativo provém da existência de diversas aplicações que iriam beneficiar da existência de uma antena com ganho considerável, capaz de transmitir/receber sinais ou energia de/para todas as direções. No entanto, o principal objetivo do presente trabalho, consiste em avaliar a viabilidade da implementação destes agregados em sistemas de transmissão de energia sem fios, nomeadamente, verificar se podem ser utilizados para alimentar sensores passivos ou de baixa potência que se podem encontrar espalhados por uma vasta área.

A fim de se obter um sistema funcional, os agregados projetados serão fabricados e testados por partes. Em primeiro lugar será necessário validar o funcionamento das antenas que irão constituir os agregados. Seguidamente, serão realizadas simulações que permitam estudar algumas características dos agregados desenvolvidos. Por último, medições vão ser efetuadas aos agregados fabricados. Um *setup* de medida irá ser usado com o objetivo de simular uma rede de sensores sem fios.

Os agregados desenvolvidos provaram ser uma solução válida, caso sejam implementados neste tipo de sistemas, uma vez que, são capazes de assegurar uma cobertura robusta ao longo de todo o plano azimute, o que lhes permite alimentar sensores passivos ou de baixa potência, independentemente da sua posição ao longo dos 360 graus deste plano.

Key-words

3D Antenna Arrays; Microstrip Patch Antennas; Full Azimuth coverage; Wireless Power Transmission; RF-DC; Multiple-Input Multiple-Output; Beam switch, Internet of Things.

Abstract

The emerging concept of the Internet of Things (IoT) networks and smart cities, together with the constant innovation of wireless communications systems, presents a fundamental requirement, which is the capability of tracking, establish and maintain radio links with several targets, which can or can not be in motion. These demands results in the need to develop antennas capable of robust tracking and realize a full azimuth coverage.

This dissertation focuses on the development and behavior characterization of different Three-Dimensional (3D) antenna arrays structures. The purpose of this alternative design comes from the advantages that it can bring in applications that would benefit from the possibility of having an antenna with considerable gain, capable of transmitting/receive signals or energy to/from all directions. However, the main goal of this dissertation consists on evaluating the viability of these antenna arrays implementation in Wireless Power Transmission (WPT) systems, with the primary goal of feed passive or low-power sensors, which can be scattered over a wide area.

In order to obtain a functional system, the conceived 3D arrays will be fabricated and tested in phases. First, it will be necessary to design and test individually, the antennas that will constitute the array. Then, to study the overall array characteristics, simulations will be performed. Lastly, measurements will be performed in the prototyped 3D antenna arrays. A setup system that intends to simulate a Wireless Sensor Network (WSN) will be used.

The developed antenna arrays have proven to be a reliable solution if implemented in these systems, since they are able to ensure a full azimuth coverage and so, feed passive or low-power sensors, regardless of their position over the 360 azimuth angles.

Contents

List of Figures

List of Tables

List of Acronyms

3D	Three-Dimensional
5G	Fifth Generation Cellular Network Technology
ADS	Advanced Design System
AoA	Angle of Arrival
AR	Axial Ratio
BS	Base Station
CP	Circular Polarization
CST	Computer Science Technology
DC	Direct Current
DoA	Directional of Arrival
EM	Electromagnetic
EIRP	Equivalent Isotropic Radiated Power
ERP	Equivalent Radiated Power
ETSI	European Telecommunications Standards Institute
FCC	Federal Communications Commission
FSPL	Free Space Path Loss
HPBW	Half Power Beamwidth
IoT	Internet of Things
ISM	Industrial, Scientific and Medical
LEO	Low Earth Orbiting
LHCP	Left Hand Circular Polarization
MIMO	Multiple-Input Multiple-Output
OTA	Over the Air

PCB Printed Circuit Board

PLA PolyLactic Acid

RHCP Right Hand Circular Polarization

RF Radio Frequency

RSS Received Signal Strength

RFID Radio Frequency Identification

SA Smart Antennas

SDR Software Defined Radio

SPS Solar Powered Satellite

VNA Vector Network Analyzer

VSG Vector Signal Generator

WPT Wireless Power Transmission

WSN Wireless Sensor Network

Chapter 1

Introduction

The main challenge addressed in this work was the development and behavior characterization of 3D antenna arrays. These alternative structures can bring several advantages to the Fifth Generation Cellular Network Technology (5G), as well as, in Wireless Power Transmission (WPT) applications.

In the first chapter, the motivation that led to the development of this work, as well as, the main goals are presented. Additionally, in order to provide a better understanding of the developed work, some fundamental concepts of antennas, WPT systems and Wireless Sensor Network (WSN) are introduced.

Then, in the second chapter, the state of the art will be explored. Essential concepts related to the specific areas inherent to this work are explained and some alternative Three-Dimensional (3D) antenna arrays already developed are presented. Moreover, different application scenarios for these innovative arrangements, as well as, their advantages and disadvantages, are presented.

In Chapter 3, the development of both antenna elements and the adopted 3D structures are described. Simulations performed in order to validate the antenna arrays operation and their radiation patterns can be found here.

The measurements performed in order to study the real behavior of the developed arrays will be described in Chapter 4, as well as, the obtained results.

Finally, in the last chapter, conclusions about all the developed work are drawn. The future work that can be developed in order to improve these antenna arrays operation is also described here. More precisely, different application scenarios that can benefit from the use of this type of arrays and possible improvements in the array operation are presented.

1.1 Motivation

The emerging concepts of the Internet of Things (IoT) networks and smart cities, together with the constant innovation of wireless communications systems, presents a fundamental requirement, which is, the capability of tracking, establish and maintain radio links with several targets, which can be in motion (telecommunications devices) or fixed (IoT sensors).

These requirements result in the need to have antennas capable of robust tracking and realize full azimuth coverage. Mechanically steerable antennas, which usually consists in a planar antenna attached to a mechanical positioning system, quickly meet these requirements. However, high maintenance costs and different problems that can occur due to their

moving parts, present some of their drawbacks. The electronically steerable antennas, also called Smart Antennas (SA), present better feasibility in this aspect. In recent years due to the growing demand for high-speed communications and wireless broadband services, these antennas are a hot topic and have faced massive development.

On the other hand, the developments on IoT networks will provide the generalization of the smart cities concept, which will involve extensive use of sensors. These constant developments raise a worrying issue because for feed all those sensors will be necessary a significant amount of batteries, which eventually leads to a big waste of energy to produce them and also increase the pollution. The development of passive sensors can be seen as a solution to this problem and as a small step to a sustainable future. However, it is necessary to find an efficient system to feed all these sensors. Because of this, the optimization of WPT systems has been an area of high research recently.

3D antennas arrays, more precisely, the ones that rest in quasi-spherical structures, can be explored in order to verify if they can present a valid alternative to accomplish these demands. They are capable of fed several sensors scattered over a wide area without moving and are easy to attach in every place. To the wireless communication systems, they bring the advantage of being able to transmit and receive signals from all azimuth angles.

The scientific topics covered in this work are in trend line with a lot of current scientific concepts and projects. The increasing adoption of IoT networks, the implementation of the smart cities concept, and the improvements in mobile networks are the main areas under development which can benefit from the use of this alternative antenna arrays and, consequently, boost their implementation.

1.2 Objectives

As previously mentioned, the main objective of this work is to perform an overview of 3D antenna arrays panorama. To accomplish this, the development and behavior characterization of such structures will be performed. Furthermore, measurements of these developed structures will be carried out in order to validate their operation and consequently understand which practical scenarios will benefit from the application of these types of antenna arrangements.

At the beginning of this work, the main goal was to conceive a 3D antenna array capable of realizing a full azimuth coverage. That is, project a 3D antenna array capable of receive and transmit signals from all directions and, consequently, serve multiple providers, as, sensors or communication devices. However, during the work it was verified that this type of arrays could bring several advantages if implemented in other applications, as, WPT systems and WSN networks. The main goal here, was similar to the one proposed before, only its application was adjusted since in this scenario, the main goal is to feed several sensors. So, the main objectives of this dissertation can be listed as:

- Understand the WPT systems panorama and study how they can be improved;
- Learn about the design of microstrip antennas and antenna arrays;
- Design of different 3D antenna arrays arrangements and, by simulations evaluate their overall operation (gain, operation frequency, radiation patterns);

- Perform measurements on radiation pattern that can be obtained by beam-switching techniques, in order to evaluate the 3D array coverage capabilities;
- Design and implementation of a RF-DC circuit converter;
- Simulate a real scenario where the 3D antenna array was applied to a WPT system, more precisely, measurements on the received and transmitted power in function of the distance between a receiver and transmitter;

At the end of the work, final considerations will be drawn about future improvements on the developed 3D antenna arrays, as well as, different possible application scenarios.

1.3 Contributions

It is important to mention that the development of this dissertation led to the submission of the following scientific articles:

- D.Pires, D.Belo, M.Jordão, P.Pinho and N.B.Carvalho. "3D Antenna Array for SWIPT Sensing with WPT Capabilities". In *Proceedings European Conference on Antennas and Propagation (EuCAP), 2020* [Submitted]
- D.Pires, D.Belo, M.Jordão, P.Pinho and N.B.Carvalho. "A WPT System based on a 3D Array Transmitter". In *IEEE Access* [Submitted]

1.4 Involved Concepts

In order to provide a clear understanding of the technologies involved in this work, some concepts must be a priori explained. The developed work covers several topics, all related to the Radio Frequency (RF) panorama. The most important concepts will be carefully explained in this section, while the remaining ones will be explained during the document, when necessary.

First, and because part of this work focuses on the development of antenna arrays, it will be explained some fundamental parameters that characterize the antennas, such as radiation diagram/pattern, directivity, efficiency, gain, bandwidth and polarization.

The second topic provides an overview of the WSN concept. A brief description of how it works, as well as, some advantages that may arise from the implementation of such concept, will be presented.

The last chapter describes the different possibilities to transmit power without using any physical connection. More emphasis will be given to the Electromagnetic (EM) radiation technique since it was the one explored in this work.

1.4.1 Antennas Considerations

Nowadays, the radio systems, specifically the wireless communication systems like mobile, satellite, and space communications, are facing a massive development in order to meet the actuals users demands. The antennas are the main element in a RF system because it is the component responsible for receive and transmit the EM waves, from and through several areas, respectively. Therefore, the innovation of wireless communication systems goes along

with the antennas evolution. Several parameters and figures-of-merit are used to characterize an antenna. Directly related to this work are highlighted, for example, radiation pattern, directivity, efficiency, gain, bandwidth, and polarization. A brief description of each one will be presented bellow.

Radiation Pattern

The analysis of this parameter allows an understanding of how the antenna receives and emits EM waves. The radiation pattern, usually expressed as a function of the directional coordinates and determined in a far-field position, shows the antenna radiation properties along with all the azimuth directions. The radiation pattern can be described as the parameter that describes how power distribution is performed. The radiation pattern can be:

- **Isotropic**: when the antenna has equal radiation for all directions. Is an ideal concept, not physically achievable;
- **Omnidirectional**: when in a given plane, the antenna has a maximum and constant radiation (e.g.single-wire antennas);
- **Directional**: when the antenna radiation maximum occurs in their main lobe (e.g.patch antennas);

Sometimes it is possible to identify in a radiation pattern, the existence of different lobes. These lobes are related to the radiation intensity. The primary ones are associated with the direction of maximum radiation. The remaining ones are considered secondary lobes, usually called as side or back lobes. It is essential to minimize the existence of secondary lobes to avoid eventual power/energy losses. One parameter that is important to analyze is the Half Power Beamwidth (HPBW), also called beam width at -3 dB. This parameter represents the angle between the directions where the radiated power is half than the maximum radiated power.

Directivity

The directivity of an antenna is defined in [2] as " *the ratio of the radiation intensity in the given direction from the antenna to the radiation intensity averaged of overall directions* ". In a standard antenna, it is expected, due to the occurred losses, that not all the supplied power is radiated. Thus, directivity can be considered as the ratio between the intensity of radiation produced by an antenna in a given direction and the strength of radiation that would be produced by an isotropic antenna that radiated equal power. Considering $U(\theta, \phi)$ as the radiation intensity in a determined position and

$$U_0 = \frac{P_{rad}}{4\pi} \tag{1.1}$$

as the radiation intensity of an isotropic source, the directivity of an antenna can be given by the expression 1.2

$$D(\theta, \phi) = \frac{U(\theta, \phi)}{U_o} = 4\pi \frac{U(\theta, \phi)}{P_{rad}} \tag{1.2}$$

Efficiency

The antenna's efficiency is the merit figure which considers the losses occurred both at the input terminals and within the internal antenna structure. It cat be described as the ratio between the power supplied to the antenna and the respective radiated power, as the equation 1.3 shows.

$$\eta = \frac{P_{rad}}{P_{in}} \qquad 0 \leq \eta \leq 1 \tag{1.3}$$

Gain

The gain of an antenna is defined in [2] as "*the ratio of the radiation intensity, in a given direction, to the radiation intensity that would be obtained if the power accepted by the antenna were radiated isotropically, that is, without losses*".

$$G(\theta, \phi) = \frac{U(\theta, \phi)}{U_0} = 4\pi \frac{U(\theta, \phi)}{P_{in}} \tag{1.4}$$

However, if an analysis were proceed between the expressions 1.2 and 1.4, which represents respectively, the directivity and the gain of an antenna, it is possible to conclude that the remarkable difference between them, is that the second one considers not only the directional properties but also the radiation efficiency. Due to this condition, the gain of an antenna can also be given by the Equation 1.5. In Table 1.4.1 the gains of the different antenna types are qualitatively differentiated.

$$G(\theta, \phi) = \eta D(\theta, \phi) \tag{1.5}$$

Antenna Type	**Forms/Geometry**	**Gain**
Parabolic	Aperture Antenna	High
Horn	Aperture Antenna	Medium
Dipole	Linear Antenna	Low
Patch	Planar Antenna	Low

Table 1.1: Gains of the different antenna types.

Bandwidth

Almost all parameters that characterize an antenna change with frequency. The bandwidth is known as the range of frequencies where the antennas performance about one or more basic parameters has reasonable values. Depending on the parameter under analysis, there are standard conditions that are considered acceptable. In this work, the considered bandwidth will be the frequency range for which the impedance mismatch (S11) is less than 10 dB. For Circular Polarization (CP), we will consider the range of frequencies for which the Axial Ratio (AR) is lower than 3dB.

Polarization

Each EM wave is composed by an electric and a magnetic field, orthogonal to each other and with variable phase. Polarization is a property of EM waves that describes the magnitude and orientation of the electric field vector, which can change over time. The maximum energy transfer, between a receiving and a transmitter antenna, occurs when both are carriers of the same type of polarization. If this does not happen, it will result in transmitted signal losses, what is usually denominated as polarization mismatch.

In order to characterize an antenna polarization, it is essential to analyze the geometric figure, which results from a cut on the plane perpendicular to the direction of propagation of the EM waves. Depending on the behaviour of the current and how it flows, an antenna can be endowed with three different types of polarization.

The most common polarization curve has an elliptical shape, what consequently produces elliptical polarization. However, the occurrence of individual factors can cause this form to become a circle or a straight line originating, respectively, circular and linear polarization.The three polarization types described are depicted in Figure 1.1 [3].

The wave propagation towards the z-direction can be expressed using a trigonometric form. The electric field vector of a propagation wave can be described by equation 1.6 [2].

$$E(z,t) = E_x(z,t)\widehat{x} + E_y(z,t)\widehat{y} \qquad \begin{cases} E_x(z,t) = E_{x0}cos(wt - kz + \phi x) \\ E_y(z,t) = E_{y0}cos(wt - kz + \phi y) \end{cases} \tag{1.6}$$

Where E_{x0} and E_{y0} are respectively, the maximum amplitudes of the fields in the x and y directions. The ϕx and ϕy represents the time-phase difference in x and y components, respectively.

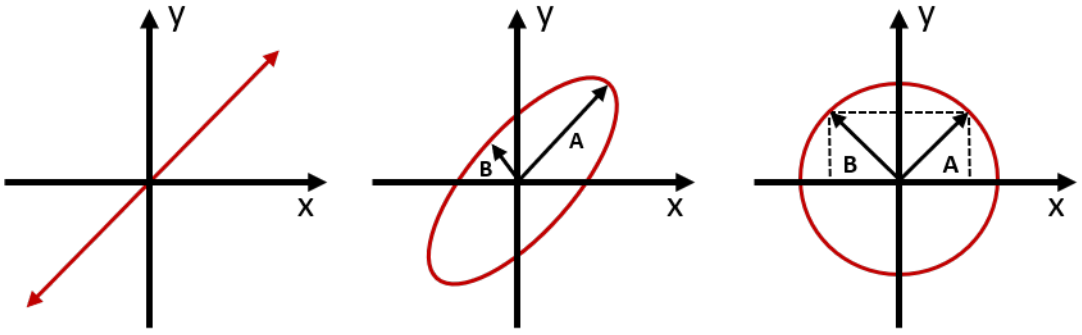

Figure 1.1: Polarization types: Linear / Elliptical / Circular.

The analysis of the time-phase difference between the two components, $\Delta\Phi = \phi_y - \phi_x$, allows to determine the type and direction of the waves propagation.

$$\begin{cases} \Delta\Phi > 0 & \text{means left polarization} \\ \Delta\Phi < 0 & \text{means right polarization} \end{cases} \tag{1.7}$$

Specifically, in the CP case, the absolute value of the electric field vector is constant over time, while the angle formed between this vector and the axis varies linearly with angular velocity ω. If the electric field follows a clockwise direction, the polarization is called Right

Hand Circular Polarization (RHCP). In its turn, if the course of the electric field vector follows an anti-clockwise direction, the polarization is named Left Hand Circular Polarization (LHCP). To ensure if the antenna has circularly polarized, the time-phase difference, $\Delta\Phi$, between the two components must be multiple of $\frac{\phi}{2}$, and as described in the equation 1.8. $\Delta\Phi$ also allows to evaluate the waves propagation direction.

$$\Delta\Phi = \begin{cases} -\frac{\pi}{2} - 2n\pi & n \in \Re \quad \text{means right-hand polarization} \\ +\frac{\pi}{2} - 2n\pi & n \in \Re \quad \text{means left-hand polarization} \end{cases} \tag{1.8}$$

Axial Ratio(AR)

The AR is a radiation pattern parameter that allows to understand what type of polarization an antenna has. However, do not provide the direction of the wave propagation. If we look again to Figure 1.1, particularly to the elliptical shape, which is the most common polarization type, the AR can be defined by

$$\text{AR} = \frac{A}{B} \qquad 0 \leq \text{AR} \leq 1 \tag{1.9}$$

AR	Polarization Type
1	Circular Polarization
∞	Linear Polarization
Other value	Elliptical Polarization

Table 1.2: Polarization types in function of the AR value.

In Equation 1.9 A and B represents the amplitudes of the field components, respectively, in the x and y directions. So, by the analysis of the AR value, the considerations presented in table 1.2 can be performed.

The AR is usually expressed in decibel (dB).

$$\text{AR}(dB) = 20 \times log_{10}(AR) \tag{1.10}$$

It is mentioned in [2] that for an antenna be considered circularly polarized, its AR needs to be equal to one, which corresponds to 0 dB. However, in practice, if an AR lower than 3 dB in the angles of maximum radiation intensity is ensured, it can be considered that an reasonable CP is achieved.

1.4.2 Antenna Arrays

The radiation pattern of a single antenna element contains a single lobe, which confers, especially in microstrip antennas, bad performance in terms of gain and directivity. A large aperture would be necessary in order to achieve a high gain antenna, which sometimes may not be desirable. Moreover, sometimes, being able to control the antennas radiation pattern can be an essential ability in several applications, where are intended the energy focus to specific positions.

The best way to accomplish these demands is by projecting antenna arrays. In [3] it is referred that an antenna array, is nothing more than several antennas strategically placed (with

specific geometrical and electrical configurations) in space to achieve desired characteristics. The implementation of antenna arrays is already generalized in the wireless communications panorama due to its better efficiency results, high gain, directivity and because overcome the limited bandwidth limitation. Usually, an antenna array is composed of identical elements.

The vector composed by the addition of the fields radiated by the individual elements results in the total radiated field (equation 1.11).

$$E_T(r, \theta, \phi) = \sum_{n=1}^{N} E_n \tag{1.11}$$

In order to optimize the radiation pattern, the fields of the array elements must constructively interfere in the direction of maximum radiation and destructive in the remaining ones. This is one the main principles of antenna arrays.

It is referred in [2] that some factors can be adjusted in order to achieve the desired directivity. Are they:

- The type of radiating elements used;
- Number of elements;
- The array geometrical configuration;
- Distance between elements;
- The phase and the amplitude applied to excite each individual array element.

Theoretical Considerations:

In order to understand the antenna arrays operation, some theoretical notions must be introduced. Initially, to introduce some features of antenna arrays, it will be consider a linear array (Figure 1.2), since is the most common used arrangement. The considerations that will be presented in this section were understood from the theoretical principles clarified in [2] and [3] , where they can be found in more detail.

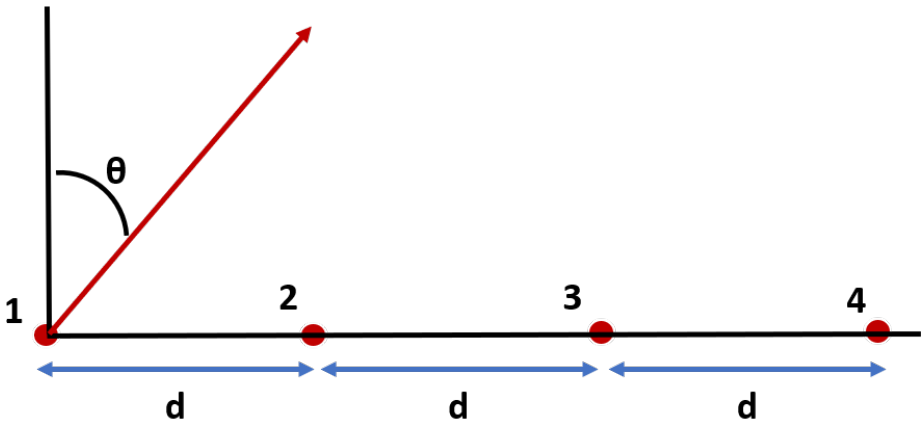

Figure 1.2: 4 elements linear antenna array.

When exited by a current **I**, an isotropic source radiates an **E-field** that can be approximated by the expression 1.12

$$E = I\frac{e^{-j\beta r}}{4\pi r} \qquad and \qquad I = Ie^{j\theta} \tag{1.12}$$

A linear and uniform array is composed by equal elements, placed along an axis with equal spacing between them and are fed by currents with equal amplitude and phase. Due to this, the following assumptions cab be assumed:

$$I_1 = Ie^{j\theta_1}; \quad I_2 = Ie^{j\theta_2}; \quad ...I_N = Ie^{j\theta_N} \tag{1.13}$$

$$(\phi_2 - \phi_1) = (\phi_3 - \phi_2) = (\phi_N - \phi_{N-1}) = \alpha \tag{1.14}$$

Where α represents the phase difference between elements. The E-field produced by each one single element can then be given by the equation 1.15

$$E_N = Ie^{j\phi_N} \times \frac{e^{-j\beta r_N}}{4\phi r_N} \tag{1.15}$$

And, the phase values can be simplified as:

$$\begin{aligned} \phi_2 &= \phi_1 + \alpha \\ \phi_3 = \phi_2 + \alpha &= \phi_1 + 2\alpha \\ \phi_N &= \phi_{N-1} + (N-1)\alpha \end{aligned} \tag{1.16}$$

Assuming the following far-field considerations (1.17) where $r \geq d$

$$\begin{aligned} \theta_1 \simeq \theta_2 \simeq ... \simeq \theta_N \\ r_1 = r - dcos\theta \\ r_2 = r_1 - dcos\theta = r - 2dcos\theta \\ r_N = r_{N-1} - dcos\theta = r - (N-1)dcos\theta \\ whereby \quad r_1 \simeq r_2 \simeq r_N \end{aligned} \tag{1.17}$$

The total field E_T, produced by an antenna array, as already mentioned, is equal to the sum of the produced fields by all elements, individually.

$$E_T = \sum_{n=1}^{N} E_n \tag{1.18}$$

Expanding the equation 1.18, will result in 1.19

$$E_T = Ie^{j\phi_1}\frac{e^{-j\beta r_1}}{4\pi r_1}[1 + e^{j(\beta dcos\theta + \alpha)} + e^{j(N-1)(\beta dcos\theta + \alpha)}] \tag{1.19}$$

From the previous equation, it is verified that the entire array field is equal to the field produced by the element positioned at the origin, multiplied by a factor. This factor is

denominated as array factor and depends on the number of elements (N), the spacing between them (d) and the excitation phase difference (α) [2].

The following expression can gives the array factor.

$$\sum_{n=1}^{N} e^{j(n-1)\varphi} \quad and \quad \varphi = \beta d cos\theta + \alpha \tag{1.20}$$

Also, and because it is a geometric progression of N terms, simplifying and normalizing, the following expression for the array factor can be obtained, which is the one usually seen in the literature.

$$|FA|_n = \frac{sin(\frac{\varphi}{2})}{Nsin(\frac{\varphi}{2})} \tag{1.21}$$

For small values of φ, for example, in the main lobe region, the expression 1.21 can be simplified, resulting in the expression 1.22.

$$|FA|_n = \frac{sin(\frac{\varphi}{2})}{N(\frac{\varphi}{2})} \tag{1.22}$$

The array factor, as mentioned before, depends on some arrays characteristics, such as the spacing between elements and the excitation phase. However, the most impact of this parameter is caused by the number of elements. As the number of elements increases:

- The main lobe becomes more narrow
- The number of lobes in the radiation diagram increases
- The level of secondary lobe decreases

The array factor is probably the most crucial parameter in order not only to study the antenna array radiation pattern but also understand how to control it. This control is intended when the array must perform steering capabilities.

On another side, when a uniform and planar array is under analysis (Figure 1.3), which is composed of elements placed over a plane, equally spaced between them and fed with the same excitation phase, the array factor can also be deduced. To obtain the array factor, these arrays can be seen as a linear aggregate of N_x elements aligned on the x-axis, in which each element, in its turn, can be considered as an aggregate of N_y elements aligned on the y-axis (Figure 1.3).

In this case, the element factor and the array factor can be determined, respectively, by the equations 1.23 e 1.24.

$$|FA|_y = \frac{sin(N_y\frac{\varphi y}{2})}{sin(\frac{\varphi_y}{2})} \quad and \quad \varphi_y = \beta d_y cos\theta_y + \alpha_y \tag{1.23}$$

$$|FA|_x = \frac{sin(N_x\frac{\varphi_x}{2})}{sin(\frac{\varphi_x}{2})} \quad and \quad \varphi_x = \beta d_x cos\theta_x + \alpha_x \tag{1.24}$$

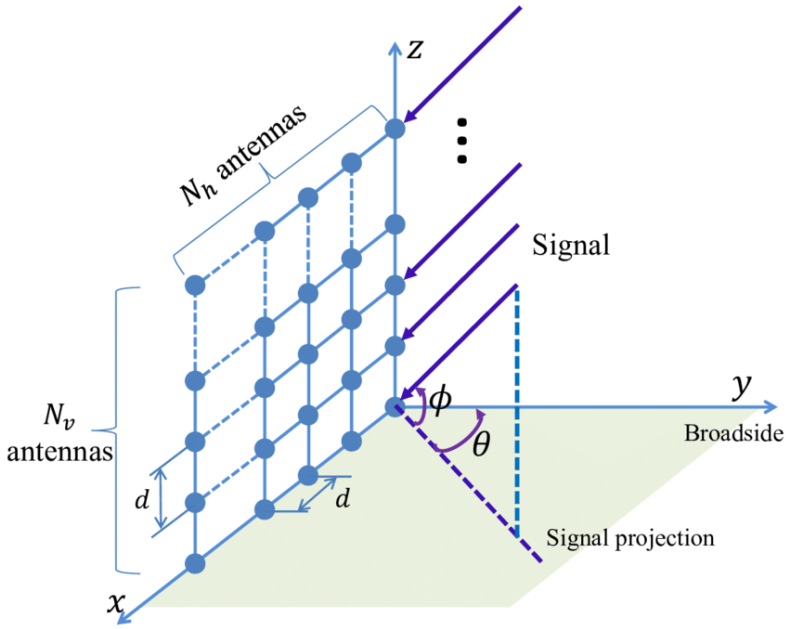

Figure 1.3: Planar array of N_x by N_y elements taken from [1].

Concatenating the two equations, the expression for the total aggregate factor of a planar array is obtained.

$$FA_T(\theta,\phi) = \frac{sin(N_y\frac{\varphi y}{2})sin(N_x\frac{\varphi x}{2})}{sin(\frac{\varphi_y}{2})sin(\frac{\varphi_x}{2})} \quad \varphi_y = \beta d_y cos\theta_y + \alpha_y \quad and \quad \varphi_x = \beta d_x cos\theta_x + \alpha_x \quad (1.25)$$

However, although the considerations presented provide important theoretical notions, that help to understand the antenna arrays operating principle, they cannot be applied to 3D antenna arrays, which are one of the main topics of this dissertation. In these arrangements, some problems arise, because in addition to the high design complexity, since the array factor is nonlinear in these structures, some adversities occur in practical implementations. The array factor of these arrangements is of high mathematical complexity, which makes the exact control of its radiation pattern a hard task.

1.4.3 Wireless Sensor Networks

In recent years, WSN's have been feeling a massive development, mainly due to the innovation and advances that occurred in semiconductors, micro-sensors, and wireless communication technologies. This concept has been seen as a reliable solution for optimizing a variety of applications, and its implementation has already been tested in most of those paradigms, such as, smart homes, environment monitoring, health applications, traffic control, and both industrial automation and management [4] [5] [6] [7].

The WSNs have been proved as an alternative in the context-awareness of informations sources and environment control, which leads to improving personal and professional lives.

The topology of these emerging networks consists of multiple sensor nodes that are connected to a gateway or sink node. These sensor nodes can be data originators or data routers, which means that the sensing information can be transmitted directly or not to the gateway.

This decision usually depends on the distance between the sensors and the gateway. The information is sent directly by the sensors that can be placed inside the gateways coverage zone. When this does not occur, the data jump between sensing nodes until they reach one that can connect directly to the gateway. A WSN architecture are depicted in Figure 1.4.

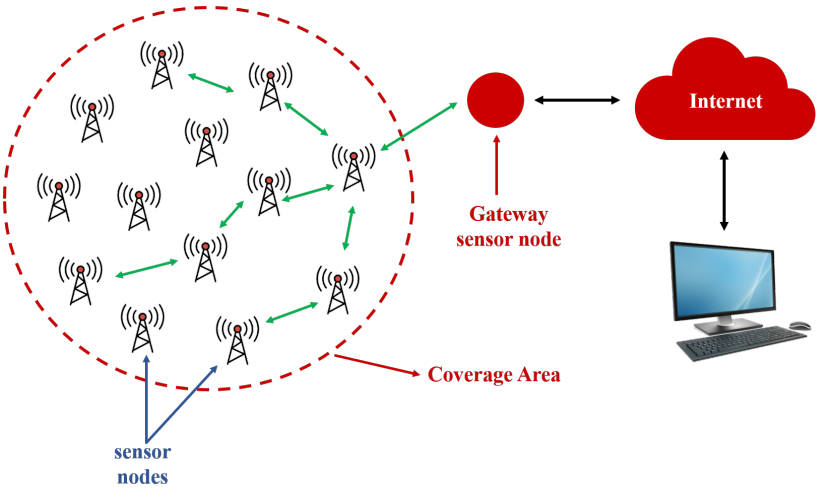

Figure 1.4: WSN architecture.

Nowadays, several applications would benefit from the implementation of the WSNs. Despite this, a worrying issue related to the power consumption arises with this scenario. If we consider a scenario where a small number of sensor nodes are used and with easy access to them, problems in both batteries consumption and replacement do not occur. However, when we face a scenario where is used a massive number of sensor nodes, the batteries production costs and pollution caused, as well as its replacement, become a serious issue.

To solve this problem, the efficiency upgrade of some alternatives based on passive sensors and WPT systems has been a topic of investigation in the past years.

1.4.4 Overview on WPT Panorama

The WPT technology was introduced in 1980 by Nikola Tesla and has been a research topic until today. Consists on the transmission of electric power between two elements without using physical connections (cables, wires). Several methods can be used for WPT, which can be implemented in both near and far filed positions. The choice of the method to use, should be done carefully and depending on the application scenario. The WPT systems can be listed as:

- Inductive Coupling
- Resonant Inductive Coupling
- EM Radiation

The first two techniques are usually applied in short-range applications where are intended to transmit significant power levels, such as cellphone chargers. In its turn, the remaining one is used in long-range applications, and only low power levels can be transmitted. In the table

1.3, taken from [8], are listed the main features of the three WPT techniques. In this section will be explained in detail WPT technique using EM waves, more precisely RF signals, since it was the one that was applied in parts of the developed work.

WPT Type	Range	Power Delivery	Functionality
Inductive Coupling	Short	High	Communication
Ressonant Inductive Coupling	Medium	High/Medium	Powering
Electromagnetic Radiation	Long	Medium/Low	Communication, Sensor & Powering

Table 1.3: Features of different WPT types.

1.4.4.1 WPT using EM radiation

This technique is the one that will be used in this work. It is a far-field method and for that, should be used when the distance between the transmitter and the receiver is quite more significant than the wavelength, λ. The basic principle of this technique is dependent on the use of two blocks: the transmitter and the receiver. The first block is responsible for transmitting EM radiation. The standard transmitter used in nothing more than a signal generator, which generates a continuous wave at a certain frequency. The receiver block is usually composed by a receiving antenna, a matching network, a rectifying circuit, and a load, like a capacitor to store the energy. The rectifying stage is based on diode capabilities of transforming the RF signals in DC energy due to their filtering characteristics. The matching network should match the impedance between the receiver's antenna and the rectifier circuit. The Low-Pass filter is responsible for removing the fundamental frequency and its harmonics obtaining the DC energy. Figure 1.5 shows, in a simplified way, the method described.

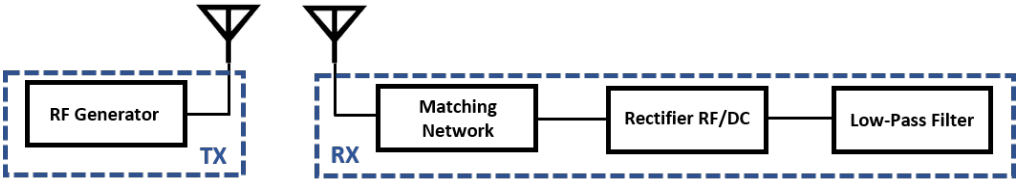

Figure 1.5: WPT system.

One of the advantages of this process is the possibility of design more compact devices, since the antennas size decrease as the frequency increases. These antennas can have multiple topologies, depending on the application where the system integration is intended. It is in this field that this work also focuses on. In the Chapter, 4 will be studied the capability of a 3D antenna array to be able to feed multiple sensors scattered over a wide area.

The optimization of these systems can bring several benefits to the WSN composed by passive or low-power sensors. They can fulfill the needs of applications where the batteries removal would be an advantage, such as the space exploration where the batteries replacement for IoT sensors can represent a hard task.

1.4.4.2 Radiated Power Considerations

In WPT systems, the level of radiated power, like in all telecommunications systems, must respect some limits imposed by specific legislations. Those limits are not universal, and because of this, they may vary from country to country. The Federal Communications Commission (FCC) and the European Telecommunications Standards Institute (ETSI) are, respectively, the regulatory entities in the United States of America and Europe.

In order to understand these limits is important to know the Equivalent Radiated Power (ERP) and the Equivalent Isotropic Radiated Power (EIRP) scales. Both are calculated in the same way (expression 1.26). However, the first one is referent to the maximum power radiated by a half-wave dipole, while the second one corresponds to the maximum power that a perfect isotropic antenna can radiate.

$$\text{ERP} \quad and \quad \text{EIRP} = TransmittedPower - Losses + AntennaGain \tag{1.26}$$

Assuming that a half-wave dipole and a perfect isotropic antenna have a gain of 1.64 dB and 1 dB respectively, the relation between these two scales is given by the expression 1.27. Usually, the transmitter is connected to the antenna by a transmission line. The considered losses in the Equation 1.26 represent the possible losses that may occur in this transmission line. These losses prevent the total supplied power to be effectively supplied to the antenna.

$$\begin{aligned} 10log(1.64) &= 2.15 \quad dBi \\ \text{ERP} &= \text{EIRP} - 2.15 \quad dB \end{aligned} \tag{1.27}$$

If we take into account the operating frequency that will be considered in this work, which are around the 5.65 GHz, the limits imposed by the FCC and for the ETSI legislations converge for similar values. The EIRP limit imposed is 1W, which corresponds respectively to 30 dBm.

1.5 Conclusion

At the beginning of this chapter, the motivational aspects that lead to the development of this work were introduced. Possible application scenarios, as well as the potential advantages that may arise from the implementation of the 3D antenna arrays, are presented.

In the second topic are listed, the main objectives that are intended to achieve with this work. However, the main goal is to perform a complete work that involves all the stages of a RF project, starting with the design and ending with performance measurements in an application scenario. During the full process, simulation, optimization, and prototyping were also important stages in order to obtain a better final prototype.

Finally, to provide a more natural understanding of the developed work, an overview of the vital concepts related to the scientific fields involved was performed. Some antennas parameters, the WSN concept, and an explanation about the WPT system used on this work were presented, as well as, the legal restrictions related to the radiated power.

Chapter 2

State of the Art

As previously mentioned, this works will focus on the design and behavior analysis of 3D antenna arrays. The main goal is to achieve a fully functional system that can bring advantages if implemented in actual application scenarios. In this chapter, state of the art about the alternative 3D arrays already developed, as well as their application will be presented. Moreover, it will also expose the state of the art of some techniques that had to be used to achieve the final prototype, such as circularly polarized antennas and WPT systems, more precisely, the RF-to-DC converters.

2.1 Circular Polarization

The utilization of antennas with CP has undergone exponential growth in several wireless communication systems. This growth can be explained due to the immunity to polarization losses, since they can transmit and receive signals in different polarization types. So, if a polarization misalignment between the transmitting and receiving antenna occur, the signal transmission quality will not be affected. Also, circularly polarized antennas bring benefits in some communications systems where sometimes, the orientation of the antenna is unknown, such as satellite communication systems.

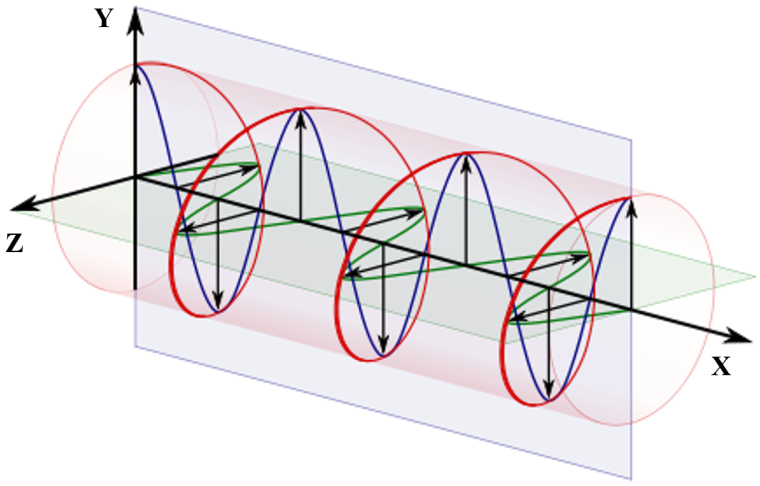

Figure 2.1: CP electromagnetic wave.

It is mentioned in [2], that, for achieve CP, three conditions must be guaranteed. Are they:

- The field must have two orthogonal linear components;
- The two components must have the same magnitude, $|E_x| = |E_y|$;
- The two components must have a time-phase difference of odd multiples of 90°.

When an antenna is circularly polarized, a EM wave, similar to the one presented in Figure 2.1, arises.

Mainly due to the symbiosis between its low cost and implementation simplicity, the use of microstrip antennas has gradually increased in the wireless communications universe. In their basic form, these antennas usually present horizontal or vertical polarization, that means linear polarization. However, CP can be achieved by doing some changes in the antenna's geometry or in their feeding techniques. Moreover, power can be supplied by one or more feed lines. Over time, several alternative techniques have been proposed in order to accomplish these polarization characteristics. Some of them, will be presented in the following section.

2.1.1 CP Techniques on Microstrip Antennas

As mentioned before, due to their flexibility, several approaches can be followed to generate CP in microstrip antennas. In Figure 2.1 is presented some alternatives that can create CP by making some changes in the antennas geometry or due to the existence of two feed lines.

If we consider an antenna with two feed lines, the quadrature-phase difference can be achieved when the patch is preceded by a power divider or by a hybrid model (Figure 2.2(b)). Both components ensure an equitable power division (3 dB) between the input and the output ports. Moreover, the hybrid model case, due to its phase characteristics, maximizes the cancellation of reflections at the input port.

However, in some application scenarios, it is intended the Printed Circuit Board (PCB) minimization, which makes non-ideal the presence of these components before the antennas. Also, it can be considered that obtain CP is more comfortable using a single feed patch. For that, it is necessary to excite two orthogonal modes with a 90 degrees phase difference, by doing some modifications in the antenna structure (Figure 2.2(a)).

All presented approaches are based on square microstrip patches because it was the geometry that will be used in this work, since it is the one that facilitates both the antenna design and matching for the predetermined frequency. However, it should be noted that the same procedures can also be applied in circular microstrip patches to reach the CP.

The circularly polarized antennas have been a research topic and different alternative techniques to accomplish this particularity were proposed, either in single elements [9], [10], [11], [12], [13] or in antenna arrays [14].

In [9] and [10], alternative designs are proposed in order to confer an AR bandwidth improvement on a single microstrip square patch. The same goal was intended in [15], but in this case, using an antenna array for vehicular communications.

In [9], was adopted a coaxial feed square patch geometry with truncated corners along one of its diagonals. In each one of these truncated corners was embedded a slot of equal dimensions. This approach, compared to the design in which the only modifications made to

the square patch structure are the truncated corners, confers improvements in AR and return loss bandwidths.

In its turn, in [10], the patch antenna has a defected ground plane, that was introduced by inserting a square ring slot just below one of the patchs top corners. This slot creates a perturbation in the patch like the conventional perturbed CP antennas.

The same approach was followed in [11], although in this case, the proposed antenna is a single-feed equilateral triangular microstrip patch. The CP was obtained by placing three triangular slots in the ground plane, below the radiating triangular patch. It is shown that if one of the triangular slots side length were slightly longer than the others, two orthogonal near-degenerate resonant modes could be excited, and CP is accomplished. An enhanced antenna gain was verified when comparing with a regular microstrip antenna with an unchanged ground plane.

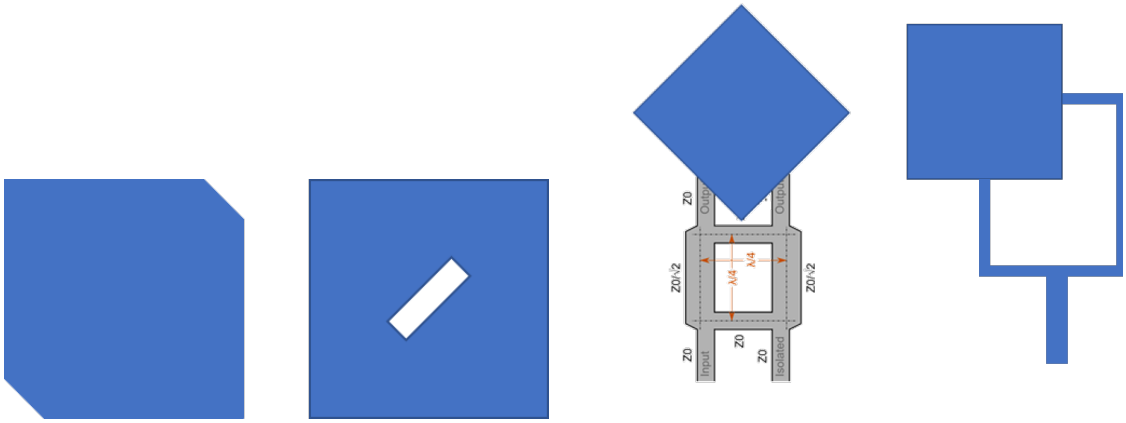

(a) (b)

Figure 2.2: CP techniques: (a) Geometry Modifications and (b) With two feed lines.

Currently, several applications benefit from the introduction of this type of antennas. An example of one, is the Radio Frequency Identification (RFID). In [12] was purpose an alternative geometry to generate CP for RFID applications. Asymmetric circular shaped slots were introduced in a single feed square patch along with the diagonal patch directions. To reduce the antenna's size, four symmetric-slits are also embedded symmetrically along with the orthogonal directions of the asymmetric-circular shaped slotted patch. This geometry presents a wide-angle of CP radiation, around 100°. Also has the particularity of the antennas operating frequency range can be tuned with robust CP radiation by changing the slit lengths along with the orthogonal directions.

As it is known, the microstrip antennas do not have very high gains. The enhancement of the gain of circular polarized microstrip patch antennas is, therefore, also a relevant research topic. In [13], a single feed microstrip patch antenna with the loading of shorting pins was developed in order to enhance the antenna gain and the directivity. In order to reach the CP, two sets of metallic pins were placed along the orthogonal diagonals of a square patch resonator. Both left-handed and right-handed CP can be achieved by changing the position of the inner pins along with the patch diagonal. The simulated and measured results demonstrate that the overall electrical radiating area of the proposed CP antenna is significantly enlarged, as well as the antenna gain. Also, the authors conclude that the resonant frequency of a

microstrip patch antenna operating in its dominant mode is substantially tuned up due to the inductive shunt effect of these pins.

2.2 Alternative 3D Antenna Arrays

The ability to establish radio links with several targets at the same time, as well as maintain the radio links with mobile targets, is increasingly a fundamental demand in wireless communication systems day life. For example, users need to be connected to their mobile vehicles such as cars, boats, and ships. Satellite communications, particularly the Low Earth Orbiting (LEO) satellites is another system where this capability is an extreme need. Moreover, the emerging concept on the IoT networks, which will boost the smart cities to a real panorama present also the need of having antennas capable of robust tracking and full azimuth coverage as the main requirements.

Figure 2.3: Smart cities panorama.

As already mentioned, mechanically steerable antennas can quickly fulfill these demands. However, they present some drawbacks related to their limited lifetime, which may not make them a better solution for some applications. The electronically steered antennas present itself as a valid alternative, with better feasibility in the lifetime aspect. However, to accomplish the full azimuth coverage is necessary to explore alternative structures. The 3D antenna arrays, mainly, the ones that rest in non-planar surfaces, have been an important research topic, not only in the communications panorama but also in other applications like localization systems.

Some examples have been proposed of antenna arrays on curved apertures. In [16], it was studied an antenna array printed on a cylindrical shape. However, this type of structure exhibits a weak degree of curvature. For this reason, the 3D antenna arrays that present spherical or quasi-spherical shapes are a research topic in the past few years. In [17], the radiation characteristics of a spherical array were studied. The arrays under tests were similar to the ones that are intended to design in this work, constituted by circularly polarized elements. More recently, in [18] was presented several design trade-offs and considerations on spherical antenna arrays, which aim to perform a full azimuth coverage.

It was concluded that antenna arrays that rest in spherical geometries are the best alternative in terms of performance and cost. It was validated that the ability of these arrays

provides hemispherical coverage while keeping a similar signal gain over all the coverage angles. It is also shown that compared to the planar phased arrays, the spherical ones require fewer elements to achieve high directivity and two-dimensional beam steering capability. In the planar arrays, the number of antenna elements can easily become very large.

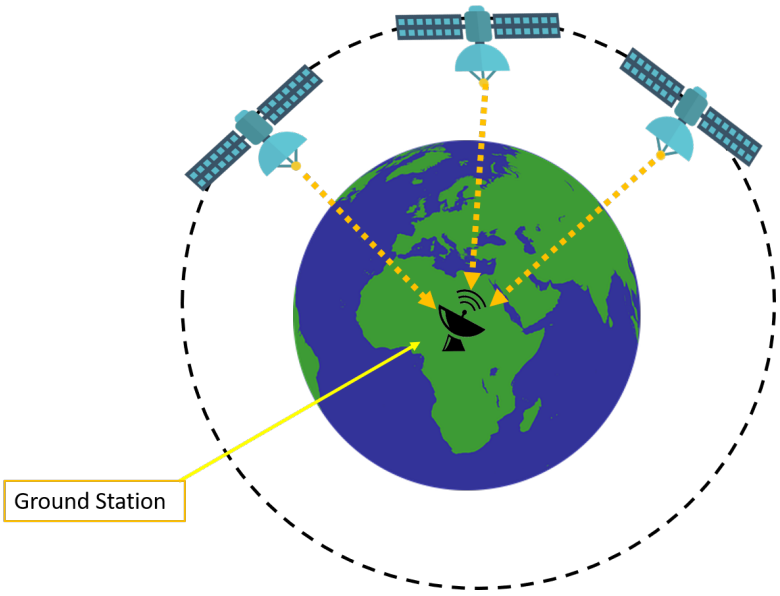

Figure 2.4: Satellite communications panorama.

In work performed in [19], an alternative spherical antenna array was developed. The antenna elements are arranged in sub-arrays, each one carrying three circularly polarized microstrip patches working at 9.5 GHz. The developed array proved itself capable of beam scanning through the hemisphere with similar directivity and beamwidth. The developed work raises a crucial paradigm since it shows that even though it is possible to control the beam width and shape, the array small aperture limits the synthesized far-field patterns. The array aperture, as well as, the spacing between elements, are crucial features that must be carefully considered when these arrays design is performed.

Being able to scan a large part of the azimuth angles with a constant gain is also an attribute that can bring advantages in satellite [20] and maritime [21] communications. In [20], an active spherical phased antenna array was proposed for satellite data transmission to the ground station. The main goal is to perform an antenna capable of maintaining a stable signal with the ground station, even if the satellite is in motion or tilted, as can be seen in Figure 2.4. Usually, the LEO satellites use a circular symmetric shaped-beam antenna. However, due to its low gain, sometimes it is necessary much RF power to maintain the required EIRP for support the radio link. This need results in a problem since, as is known, the available power in a spacecraft is limited, and their spending should be minimized.

So, an efficient solution is the use of a high-gain antenna with a narrow beam that can be pointed to the ground station continuously. The designed array shows proper beam formation through all different scan angles with reasonable cross-polarization. The measured EIRP variation is less than 1 dB among the theta plane.

On the other hand, in [21], the near-spherical antennas shape provides the stabilization of the signal gain even in low elevation angles while the beam is moving over the hemisphere. The designed antenna arrangement based on a truncated icosahedron contains square patches placed over the entire structure.

The same requirements were intended in [22], where a 3D electronically steerable antenna for mobile communications (boats, ships, trains, cars) was discussed. The designed array is composed of eight circularly polarized patch antennas placed over a heptagonal structure. The steering and the hemispherical coverage is ensured by switching between either single elements or a combination of two elements patterns.

The top element, called the zenith patch has the function of a cover, mainly the hemispheres zenith sector, while the other seven ones, known as low elevation patches, should cover and provide a stable signal with similar gain through the low hemispheres sectors. The authors also conclude that sometimes the single element radiation pattern, cannot cover a determined hemispherical region. In order to solve this problem, additional states were introduced, which were ensured by the combinations of the zenith patch with each one of the low elevation patches using a predetermined phase shift. The adopted operation procedure is presented in Figure 2.5.

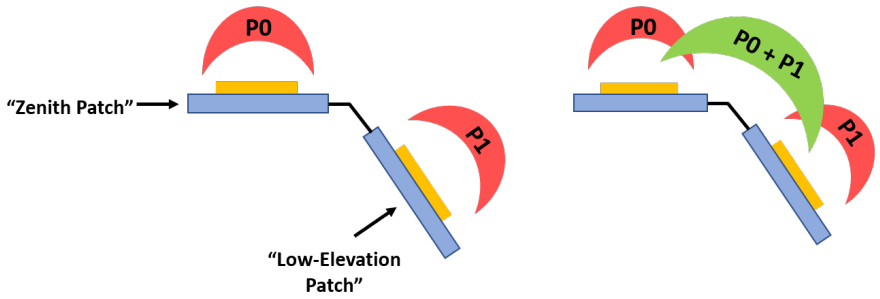

Figure 2.5: Beam switch/combination operation procedure described.

The performed measurements performed over a ground plane in order to simulate a car roof, validate the antenna operation. The measured azimuth coverage was [0-360], and the elevation coverage is [15-360]. The EIRP variation is less than +/- 2 dB at any elevation angle. The tracking algorithm implemented, based in Received Signal Strength (RSS) policy, allows to establish and maintain a stable link to the satellite with very low gain variation, even during the vehicles accelerations. The basic operation principle presented in this work, based on the beam switching techniques, shows itself as an excellent solution to accomplish the intended requirements. Due to this, this approach will be explored later.

This alternative antenna arrays has proved itself as an emerging technology that is effective improving the wireless systems performance. However, performed works also discuss their performance and possible benefits that will bring in other application scenarios, such as localization systems [23], [24].

In [23] was discussed a switched beam antenna for indoor localization systems. The antenna, composed of six patch elements arranged in a 3D shape, forming a platonic solid, enables Directional of Arrival (DoA) estimation. However, two-dimensional positioning ensured by RSS measurements was other of the main goals. The proposed solution differs from the other ones previously presented because the target does not need to be placed exactly under the antenna plane. Due to their 3D arrangement, that was specially made to ensure

full azimuth coverage, the developed system can locate a target by estimating both the azimuth theta and elevation phi DoA of the incoming messages, as can be seen in Figure 2.6. If the antenna has a fixed position, these two angles are enough to compute the absolute target position on the plane underneath the antenna. The main advantages of this system are the fact that it can be easily placed on top of any large place and does not need any configuration/calibration. Moreover, the beam switching technique helps to reduce the interference occurred in dense networks because it allows the Base Station (BS) only establish communication/direct the beam to the intended devices covered by each single element radiation pattern. The antenna shows good results, since the localization system present good accuracy.

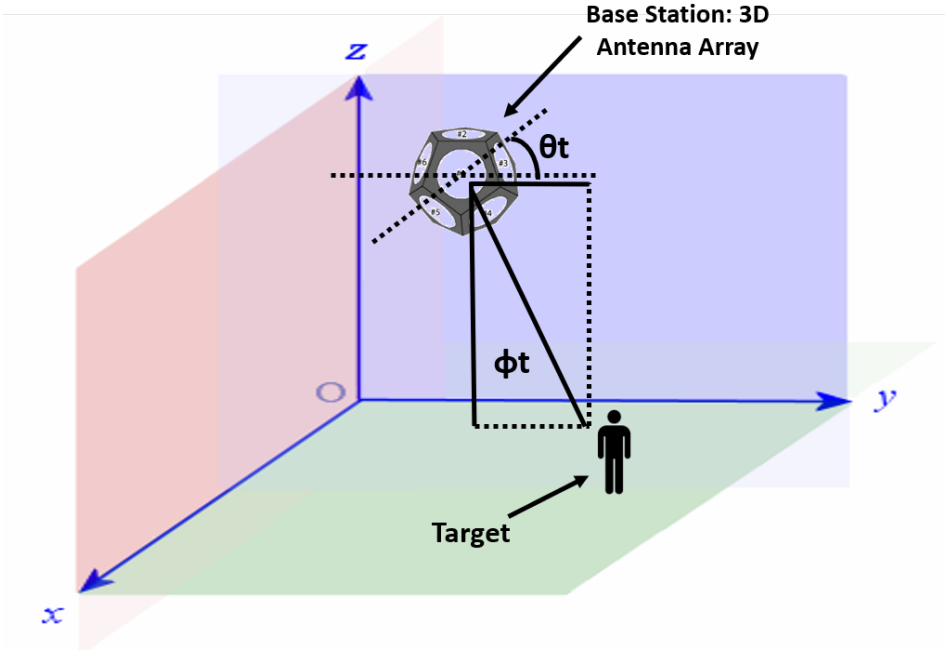

Figure 2.6: Indoor localization system with 3D antenna array as BS.

In [24], a circularly polarized pentagonal patch-excited sectorized antenna was also presented for localization applications. The target localization is based on Angle of Arrival (AoA) and RSS techniques. The developed antenna present robust semi-spherical coverage with 3 dB of maximum variation over the radiation pattern. The developed antenna also ensures a reduced coupling between elements, as well as,an increased multi-path rejection. The growing interest in these alternative structures occurs due to the agreement between good precision results and the low-cost design.

2.3 WPT Considerations

Nowadays, the WSN benefits significantly from the improvements in energy harvesting technologies. It is named energy harvesting to the process that consists of the collect of small amounts of ambient energy, and it is conversion in electrical energy. Usually, this energy collected in typical human environments came from external sources, such as thermal, kinetic energy, EM waves, and light. This technology has been seen as a reliable solution to power-

up both battery-less and low power wireless autonomous devices. Moreover, it provides a reduction of efforts in the installation and maintenance of autonomous systems, like the sensors that constitute a WSN [25]. However, on several occasions, the lack of available ambient energy leads to an insufficient amount of power produced by the energy harvesting technology. Mainly due to extended range power delivery capability, the WPT can be seen as a potential solution to this scenario if used as an additional power source.

As mentioned before, WPT is the concept of transmitting energy without using physical connections like wires or cables. The overall process is divided into three stages: transmission, reception, and RF-to-DC conversion. The RF-to-DC conversion is the most critical stage, and because of this, it will receive more emphasis in this section. The radio waves are transmitted and spread Over the Air (OTA) until they are received by a receiver antenna and converted in DC energy by the RF-to-DC converter. The rectifier circuit should be perfectly matched with the receiver antenna in order to avoid mismatches and, consequently, produce an efficient conversion. If this does not occur, some amount of power will be reflected back and, therefore, will not be available for conversion. With the increase of the mismatch between these two blocks, the conversion efficiency of the circuit will decrease, which makes the rectifier antennas, also known as rectennas, a vital component in WPT systems. For this motive, the rectennas have been a research topic with the primary goal of achieving a high conversion efficiency and consequently maximize the available DC power [26], [27], [28].

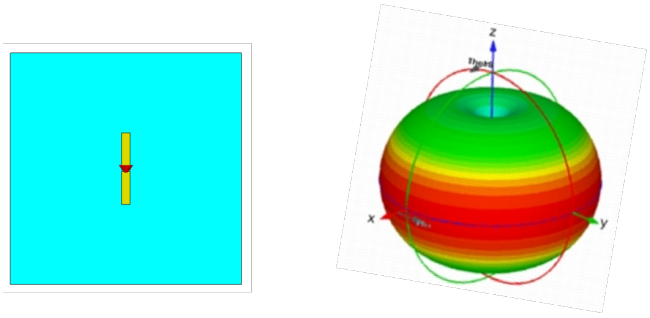

(a)

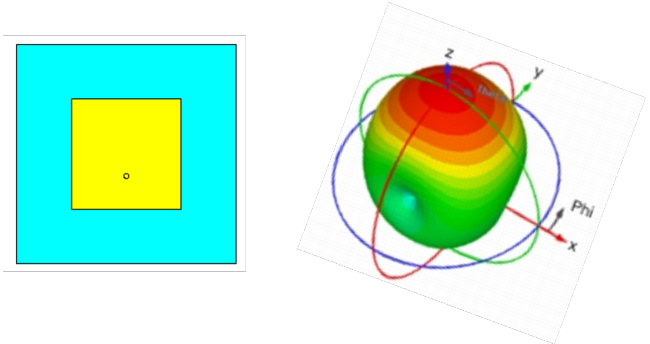

(b)

Figure 2.7: Radiation pattern of antennas used in WPT applications : (a) Dipole antenna: omnidirectional radiation pattern and (b) Microstrip patch antenna: directive Radiation Pattern.

The microstrip and dipole antennas have been widely used as transmitter antennas in

WPT applications [29], mainly due to this simplified conception process, low cost and reduce size and weight. Their radiation patterns are depicted, respectively, in Figures 2.7(a) and 2.7(b). The modest values of efficiency accomplished by these antennas can be solved with the use of antenna arrays [30]. However, depending on the application scenario, other antenna types can be used for this purpose, such as parabolic antennas. These antennas are usually used when they are intended to achieve high directivity, gain, and efficiency. Also recently, retro-directive antenna arrays have been studied in order to verify its feasibility in short-range WPT systems [31], while sometimes some applications would benefit if the transmitter arrays were able to focus its energy beam to specific positions (steering capabilities) [32]. An example of such application is the WSN, where a beam-steering antenna would be able to power up wireless sensors scattered in a specific area.

2.3.1 Point-to-Point Power Transmission Over the Air

When we look into radio-frequency, it is essential to understand the behavior of the EM waves, more precisely, the way how they propagate and all the external factors that interfere with that propagation are important theoretical notions, that must be understood.

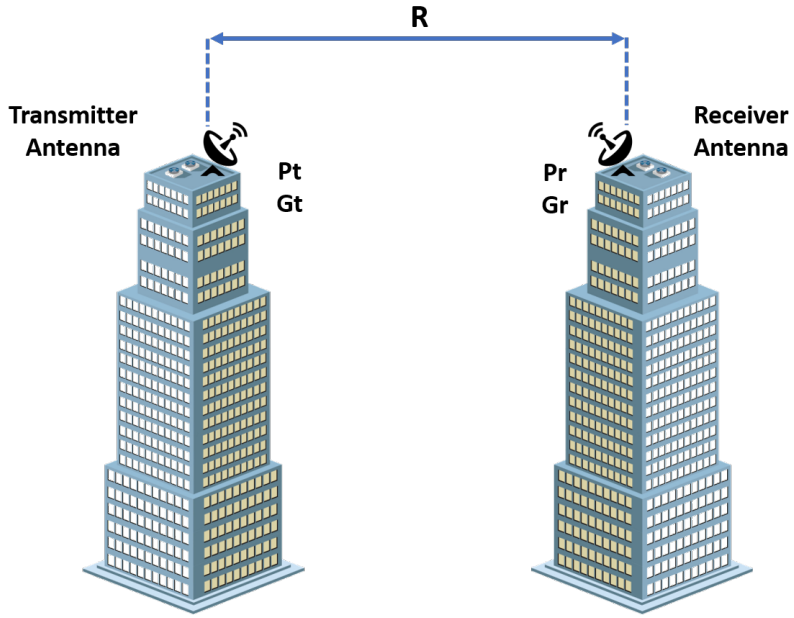

Figure 2.8: OTA signal transmission: Friis formula scenario.

The used operation frequencies are contained in the C band (4 GHz to 8 GHz), which are commonly known as the Industrial, Scientific and Medical (ISM) band. When we operate at these frequencies, the EM waves in free space propagates at the speed of light, with almost despise losses. However, when the signal propagates in a typical human environment, which carries various elements capable of interact with the signal, it can be reflected, refracted, diffracted, or absorbed, which leads to considerable losses of power. Due to these factors, it is easy to understand that the power received by the receiver antenna will be substantially lower than the one that has been transmitted. Harald Trap Friis (Naestved, August 1893 - Palo Alto, June 1976) proposes a mathematical formula that relates the power received by an antenna with the one that effectively has been transmitted by the transmitter antenna, the

distance (R) between them and the respectively gain of each one of them. The equation 2.1 represents the proposed formula, still used today. The gain and power units are, respectively, dB and dBm.

$$P_r = P_t + G_t + G_r + 20log\big(\frac{\lambda}{4\pi * R}\big)^2 \tag{2.1}$$

It should be mentioned that the Free Space Path Loss (FSPL) derives from the Friis formula and are given by the Equation 2.2

$$FreeSpacePathLosses(FSPL) = \big(\frac{\lambda}{4\pi * R}\big)^2 \tag{2.2}$$

2.3.2 RF-DC Conversion Efficiency

The conversion efficiency is one the most important RF-DC converter figures of merit, and its improvement is the aim of all related research works. As previously mentioned, to ensure maximum efficiency is necessary to minimize the losses during all conversion stages, being necessary to ensure this, to keep all these steps well matched. The RF-DC efficiency can be described as the ratio between the input RF power, $P_{In,RF}$ and the output DC power, $P_{Out,DC}$, as it is shown in equation2.3.

$$\eta = \frac{P_{Out,DC}}{P_{In,RF}} \tag{2.3}$$

However, in its turn, the DC output power, Pout, DC can be given by the equation 2.4.

$$P_{Out,DC} = \frac{V_{Out,DC}^2}{R_L} \tag{2.4}$$

And so, the efficiency of the RF-DC follows the equation 2.5. Whenever it is mentioned in this work RF-DC conversion efficiency, it will be calculated by this expression.

$$\eta = \frac{P_{Out,DC}}{P_{In,RF}} = \frac{V_{Out,DC}^2}{R_L * P_{In,RF}} \tag{2.5}$$

Usually, the mismatch between the receiver antenna and the rectifier circuit is the leading cause of power losses in a RF-DC system. So, it is crucial to guarantee the match between these two blocks. The matching circuit can be performed with passive components, like capacitors and inductors, or by using microstrip lines. The standard match impedance usually chosen when the antenna is separated from the rectifier circuit, which is the practical scenario that will be explored in this work, is 50 Ω.

2.3.3 RF-DC Converters Topologies

In this section will be slightly introduced the RF-DC converters state of the art. Different circuit topologies are used to convert RF energy into DC energy. All of these configurations use semiconductors as rectifier elements. The low cost, small size, and the better operation either to low-power input signals make them ideals to the most of practical scenarios. Usually diodes

are used as rectifier elements. However, some circuits can operate with transistors in a diode configuration. These circuits can have more than one rectifier element, which consequently will have an impact on conversion efficiency and available DC power.

2.3.3.1 Diode-based Rectifier Circuits

As mentioned before, the most common RF-DC converters are based on the basic principle of diode operation, which works as a rectifier element. However, due mainly to their high capacity junction, the standard **P-N** diodes do not present a better solution to the main objective of these circuits. The Schottky diodes are composed of a junction between an n-type material and a metal, instead of by a junction between n and p materials. This particularity results in a smaller depletion zone, which leads to a smaller junction capacity and, consequently, lower conduction voltage. These characteristics make the Schottky diodes more attractive to these applications [33] [34]. The **I-V** curve of a Schottky diode, which can be seen in Figure 2.9, is very similar to the one of a standard p-n diode, presenting only slight differences:

- The conduction voltage is lower than the one of a **P-N** diode. Typically, between 0.3-0.6 V;
- The breakdown voltage absolute value of a Schottky diode is usually lower, and the inverse current is higher than the one of a **P-N** diode with similar resistivity characteristics;

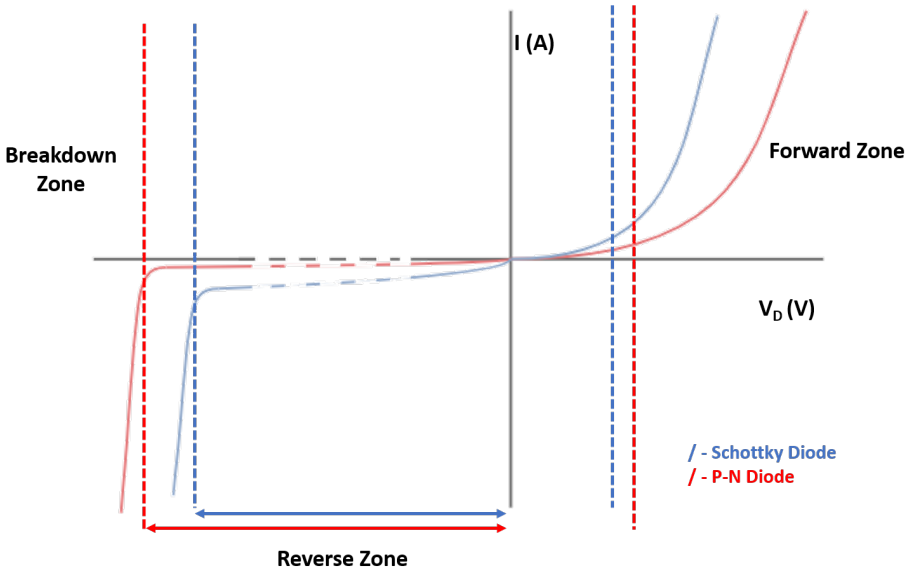

Figure 2.9: Comparison between typically Schottky and P-N diodes I-V curves.

2.3.3.2 Circuit Topologies

Several topologies have been studied and proposed for RF-DC circuits, which can be composed by one or more rectifier elements. As mentioned before, the diode-based rectifier circuits

are the most commonly used. Depending on the application, some topologies may produce better results than others. For example, for Solar Powered Satellite (SPS) applications, are used rectennas-based circuits in order to accomplish high efficiency. Alternative designs of single antennas, whether they are dipoles [35], patch antennas [36], or antenna arrays [37], have been studied in order to improve the efficiency of rectennas. The efficiency maximization is mandatory since the power density at the input is massive. On another hand, to power-up, passive sensors, or use in RFID applications, the charge-pump topologies are the ones that bring more benefits because not only rectify the RF energy to DC voltage but also produce large output voltages. Some of the most common topologies will be described in a row. The work developed in [38] was crucial for the elaboration of this section and understanding of these circuits. More topologies can be found there.

Half-Wave Rectifier

The half-wave rectifier only uses one diode and is the simplest topology used as a RF-DC converter. When at the input of the circuit is present a RF signal with peak voltage, V_P, higher than the diode threshold voltage, V_{Th}, $V_P - V_{DC} > V_{Th}$, the current will flow in the right direction producing a DC voltage that will be stored in the output capacitor. This DC output voltage directly depends on the current that flows through the diode. The more current flowing through the diode, the higher will be the voltage available in the output. However, if V_P reaches the breakdown voltage absolute value, some current will cross the diode in the reverse direction stopping the DC output voltage increment. When the input power decreases to a level where $V_P - V_{DC} < V_{Th}$, the output voltage decreases because the capacitor discharges through the load. When the power of the input signal increases again, the capacitor recharges, and the DC output voltage increase again.

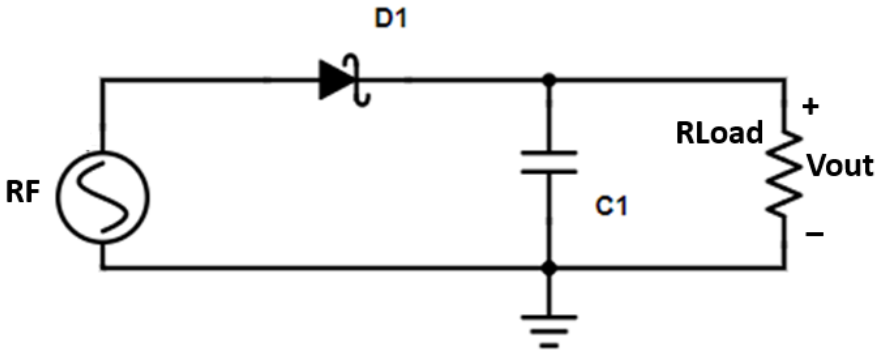

Figure 2.10: Half-wave rectifier topology.

Single-Stage Multiplier

This topology is the one that will be implemented in this work because it ensures a good balance between conversion efficiency and generated output DC power. The literature classified this circuit as a single stage voltage multiplier and is one of the most used in WPT applications. This circuit's purpose is producing at the output, the double of the peak voltage of the input signal. Based on the assumption that an RF signal is present at the input of the circuit, the operation of this circuit can be described by two individual stages:

- When the input signal is negative, the current flows through D2, and the capacitor C2 is charged with $V_P - V_{Th}$;
- When the input signal present positive values, the V_P will be added to the voltage stored in C2. Thus, the input signal voltage will double. The diode D1, the capacitor C1, and the load RL have the same operation than in the half-wave rectifier

It should be mentioned that although this architecture produces higher DC output voltage than the half-wave rectifier, its efficiency is lower for low power input signals due to the existence of two diodes.

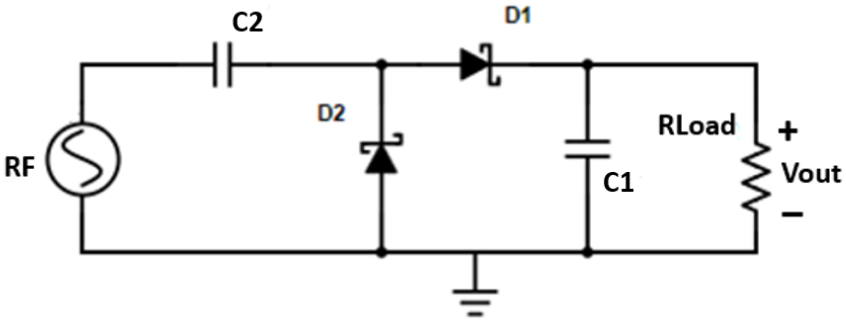

Figure 2.11: Single-stage rectifier topology.

Dickson Charge Pump

The main goal of this topology is increase the DC output voltage. This arrangement can be achieved by cascading several single-stage multipliers. The number of connected circuits defines the number of stages.

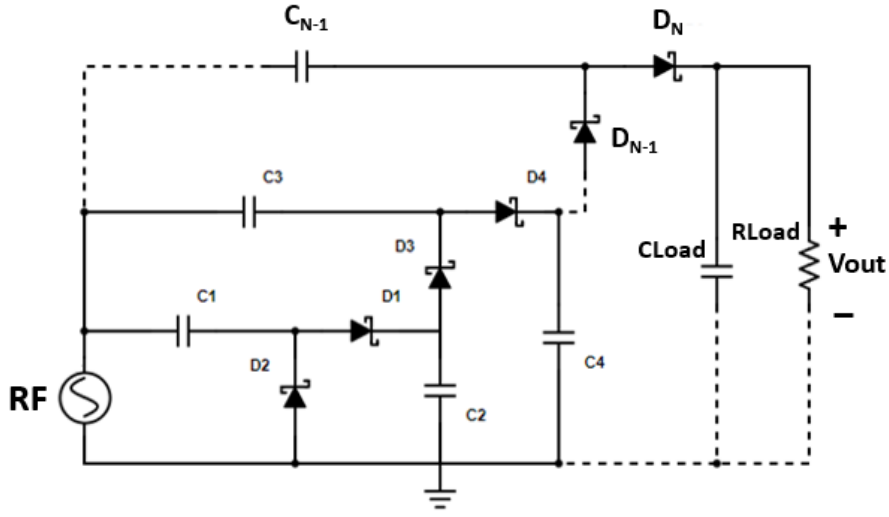

Figure 2.12: Dickson charge pump with N-stages topology.

2.4 Conclusion

A state of the art relative to the main topics addressed to the developed work main stages was presented in this chapter.

An overview of different techniques used to accomplish circularly polarized patch antennas as been made. Either by geometrical modifications, either by the use of multiple power lines, this characteristic can be achieved, always with the bandwidth and gain enhancement as main goal.

After, an analysis of 3D antenna arrays already developed, as well as, their application scenarios, was made. The literature presents several application scenarios, which will benefit from the insertion of these alternative structures. However, it was not seen the study of their advantages if implemented in WPT systems. The last topic addressed some considerations related to WPT, where a general explication about the complete process and some theoretical approaches that are important understand were given. However, the crucial objective of this section was the study of the diode-based rectifier circuits already proposed in the literature. In this way, some topologies were highlighted, and an explanation about their operation was performed.

Chapter 3

Designed Hardware

This chapter provides a complete description of all the designed components that will be part of the final system. Initially, the design of the antenna elements that will constitute the arrays will be described. Then, a full description of the process that led to the development of both 3D structures and the RF-DC converter will be provided.

In order to understand and validate each one of the components operations, simulations were performed. The obtained results will also be presented, namely, the reflection coefficients, 3D array's radiation patterns, and both conversion efficiency and DC output voltage generated by the RF-DC converter circuit.

Some concepts involved in this chapter were previously explained in Chapter 2, so it is recommended its consult for a better understanding of what will be explored here.

3.1 Antenna Elements

One of the main advantages that can be pointed to microstrip or patch antennas is based on their fabrication facility since they can be directly printed in a PCB. Usually, these antennas are made by a high conductivity metal (in this work the metal used as conductor will be cooper) placed on top of a substrate. These antennas type present also an extensive design flexibility which makes more accessible meet multiple requirements.

The designed elements are intended to be circularly polarized and work at 5.65 GHz. This polarization type was chosen in order to avoid polarization losses, that can occur if exists a polarization misalignment between the transmitting and receiving antennas.

Parameter	Symbol	Value
Dielectric Constant	ϵ_r	3.45
Loss Tangent	$tan\delta$	0.003
Dielectric Thinkness	h	0.762 mm
Conductor Thinkness (Cooper)	t	0.035 mm

Table 3.1: Substrate isola IS680 specifications.

The chosen substrate to print the antennas was the 0.762 mm Isola IS680 from *Isola Group* due to its good characteristics to RF applications and because it is available in the

"*Instituto de Telecomunicações*" manufacturing department. In Table 3.1 are presented the major substrate characteristics.

As mentioned in Chapter 2, several techniques can be followed to generate CP in patch antennas. However, this particularity is not always easy to achieve.

Different antennas were designed using the Computer Science Technology (CST) Studio Suite software, which also allows to perform EM simulations, that help to conclude about the antenna's operation. In all the attempts, the patch antenna is a square form but with slight modifications, from an attempt to attempt.

Initially, it was designed a 90 hybrid coupler to feed the patch antenna since, according to the literature, it is the method that gives a purer CP. The designed component, as well as, its S-parameters are depicted in Figure 3.1. The S-parameters analysis allows the validation of the coupler operation. It is perceptible through the reflection coefficients analysis (S_{11}, S_{22} and S_{33}) that the ports are matched with the operation frequency (5.65 GHz) and by the transmission coefficients (S_{12} and S_{13}) it can be seen that the coupler almost ensures an equitable power division. To obtain an ideal power division, the S_{12} and S_{13} should have a 3 dB magnitude to the operation frequency. However, the achieved values are reasonable. The designed 90 hybrid coupler can be then validated to generate CP when feeding a patch antenna.

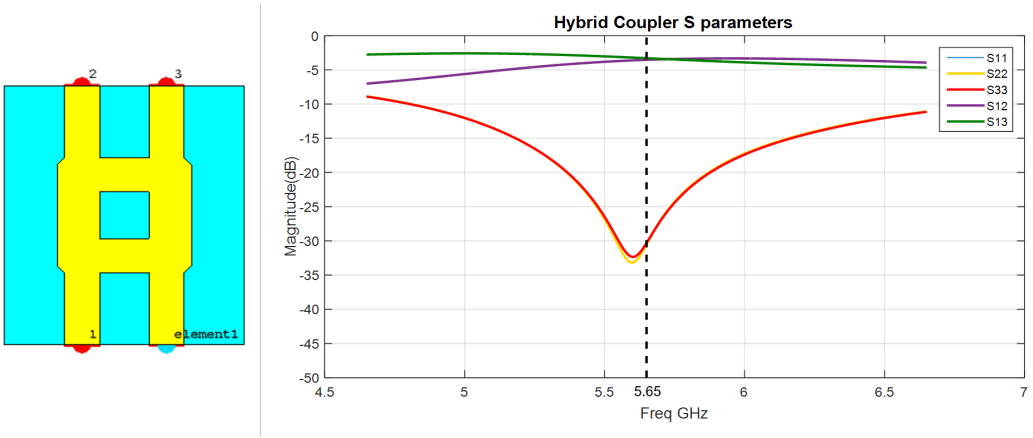

Figure 3.1: 90° hybrid coupler design and respective S parameters.

However, later, it was realized that take into account the application scenario for these antennas, exists some design limitations, namely in the feeding method. Since it is intended to attach these elements into a 3D structure, the feed performed by a transmission line is not favorable, mainly due to space limitations. In all designed antennas is used the feed by coaxial probe. This coaxial probe crosses the substrate and connects to the patch at a point that ensures the matching between the cable and the antenna (50 Ohm). Moreover, one of this feed technique advantages over the one that is made by a transmission line, is that since this one occurs in a plane opposite to the radiation plane of the antenna, there is no degradation of antenna's radiation pattern.

Based on the state-of-the-art analysis of the techniques used to generate CP on microstrip antennas, several approaches were designed and simulated. In all the designed antennas, which are presented in Figure 3.2, it is intended to achieve CP by doing some modifications in the antenna geometry. In all cases, the antenna operation was optimized to operate at 5.65 GHz and to have a AR lower than 3 dB in the angles of maximum radiation intensity.

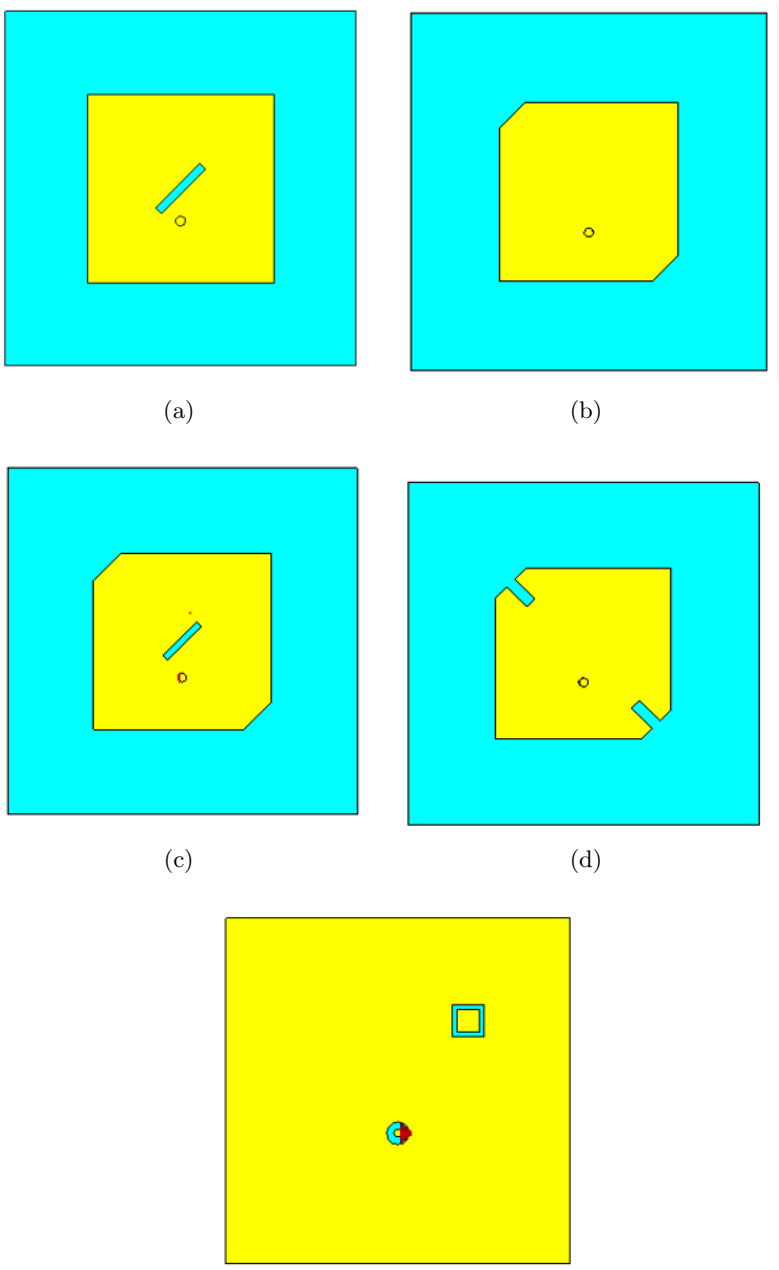

Figure 3.2: Techniques used to generate CP: (a) Central slot, (b) Truncated corners, (c) Truncated corners plus central Slot, (d) With slots embedded on the patch, (e) With square ring loaded on ground plane.

However, in some cases, like the ones presented in Figures 3.2(d) and 3.2(e), the simulated results showed that the antenna operation did not meet the requirements. It was possible to ensure the antenna matching for the operation frequency, but the AR values were too far from the ones that a circularly polarized antenna should present. Optimization attempts were

made but without effect, which led to giving up these antennas design.

The truncated corner approach shown in 3.2(b) is the one that presents better results, concerning to the antenna's matching for the intended frequency. However, the AR values between 4 and 6 dB at the angles of maximum radiation intensity are indicative that the antenna is not circularly polarized.

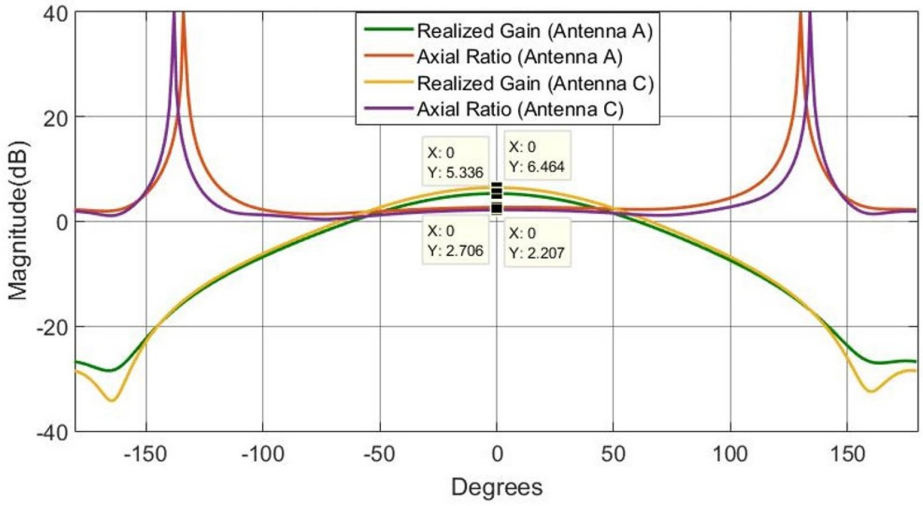

Figure 3.3: Farfield Realized gain and AR for Phi = 90 °.

In its turn, the simulations performed on the antennas depicted in figures 3.2(a) and 3.2(c) validate the CP in both antennas. In Figure 3.3 is presented the realized gain (2D radiation pattern) and the AR for the central slot and central slot plus truncated corner approaches. These antennas, from now on, will be named as antenna A and antenna C, respectively. The AR values are lower than 3dB along the plane of the highest radiation intensity for both cases. However, the antenna C has slightly higher gain than antenna A, which makes it the best choice for the intended application scenario. The maximum gain achieved by the antenna C is around 6.464 dBi at Phi = 90 and Theta = 0 while the antenna A achieves a maximum gain of 5.336 dBi at the same direction.

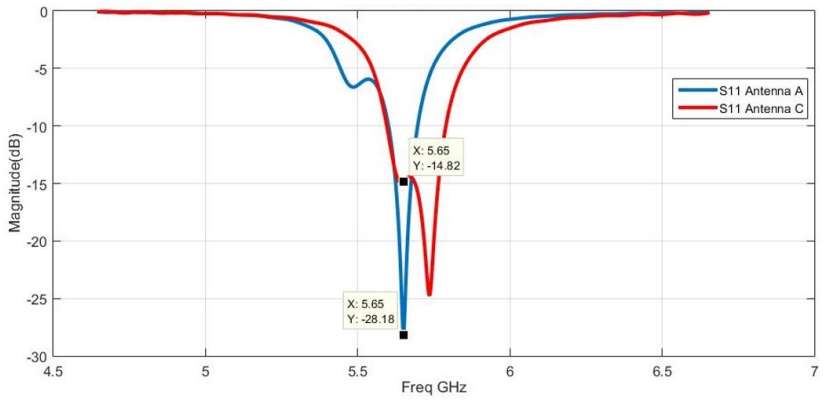

Figure 3.4: Antenna's reflection coefficient.

The reflection coefficient should also be analyzed for the required frequency in order to validate the basic operation of these elements. The antenna's S_{11} parameters are presented in Figure 3.4.

In the case of antenna C, although it can be considered to have a reasonable match for the intended operation frequency (-14.82 magnitude at 5.65 GHz), and a considerable bandwidth, larger than antenna A, the matching peak do not occur at 5.65 GHz. From the simulation performed to antenna A, it can be concluded that the antenna is perfectly matched to 50 Ohms since their S11 presents a magnitude value of -28.18 dB for the operating frequency. Several attempts were made to optimize the design of antenna C, aiming to improve the antenna matching for the operation frequency, while maintaining its AR features. However, when the antenna became perfectly matched, the AR values increases over 3 dB in the angles of maximum radiation intensity.

The antenna A, due to all the aspects discussed before, was chosen to be fabricated. In this case, the CP was obtained by cutting a slot in the center of the square patch, achieving a RHCP. In Figure 3.5 is presented the obtained prototype. The measurements performed will be present and analyzed in the following chapter.

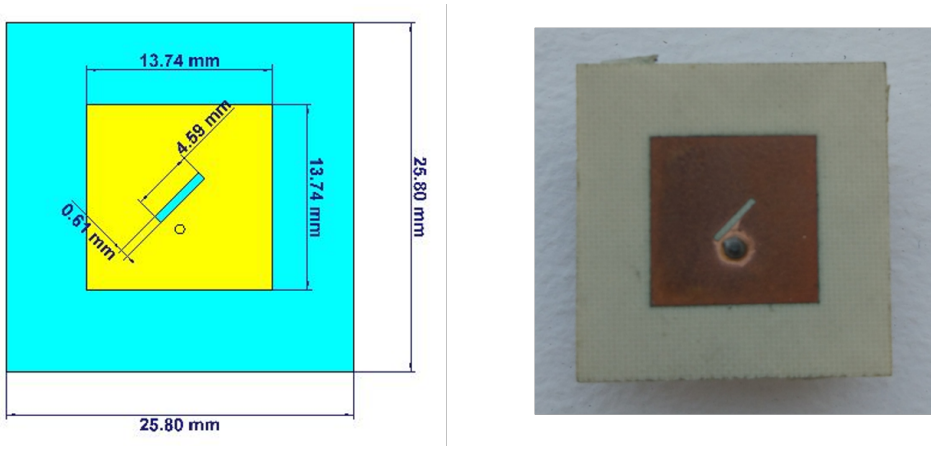

Figure 3.5: Fabricated antenna element.

3.2 Developed 3D Arrangements/Structures

At the beginning of this work, the main goal was the design and subsequent study of the 3D antenna arrays behavior in terms of coverage capabilities. The ideal scenario would be achieve an array capable of performing a full azimuth coverage, minimizing the gain variation over all the angles that radiation beams can reach. In this way, different links can be established to different target locations with stable EIRP

One of the main motivations is that exists several applications that would benefit from the implementation of these particular type of antenna arrays. Besides being easy to install in almost every place, these arrays are capable of transmitting/receiving signals or energy in/from all directions with a significant gain, and consequently, serve multiple providers, as for example, sensors or communication devices. Since that accomplish hemispherical coverage is one of the main requirements, the supporting structure must allow attaching enough antenna elements for this purpose.

At this work stage, it was interesting to design different and diversified 3D arrangements, to then, compare the performances of each one and understand in what applications they could be used in order to improve their operating system.

All the structures were designed with Solid Works software from the french company *Dassault Systèmes S.A.*. After completing this procedure the structures were printed in PolyLactic Acid (PLA) from Ultimaker supplier (dielectric constant $\epsilon_r = 2.7$ and dissipation factor, $tg(\delta) = 0.008$ @ 1 MHz) with 100 % infill. Each face of the developed structures will contain one patch antenna equal the one presented in Figure 3.2(a) and presented in the previous section. The developed 3D structures are shown if Figure 3.6.

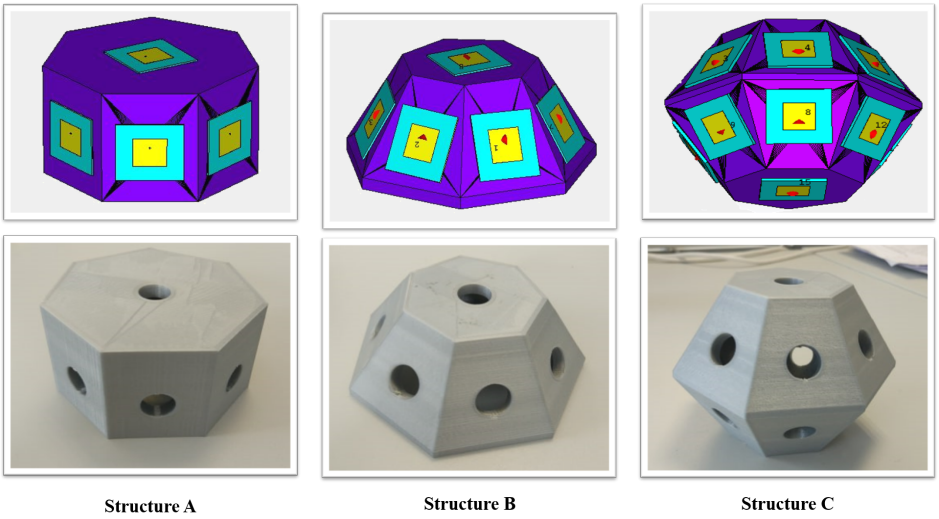

Figure 3.6: Developed 3D structures: top figures: design and bottom figures: prototypes.

For the structure A, the chosen geometry was a heptagonal prism because allows the employment of seven elements in the side faces (enough to radiate all over the hemisphere) not to distanced from each order. Due to this last particularity, it is possible to originate radiation patterns that result from the combination of two active elements. This arrangement was designed with the following objective: the top element should cover the plane below it, while the remaining seven elements are intended to cover the hemispherical sectors. These seven elements are distanced from $0.69\lambda_0$ (considering λ_0 as the free-space wavelength) from each other in order to enable the beams conjugation of different elements.

The second developed structure, structure B, was designed following also a heptagonal prism shape, but irregular, because its bases have different dimensions. This means that the lateral faces are arranged in oblique planes. This approach have the same number of antenna elements used in the previous structure in a similar configuration. The main objective of this arrangement was to analyze the impact caused by these oblique planes in the array's radiation pattern.

In its turn, the structure C was quickly developed since it was obtained by doing a mirror of structure B around its most extensive base. This procedure led to a structure twice the size of structure B and, consequently, allows attaching the double of antenna elements. The main objective is to make the radiation coverage originated by structure B more robust because, in this structure, there are elements arranged in two circular bands along the elevation axis, allowing that different elevation angles can be reached.

After the creation of these 3D structures, they were imported into CST, where it is possible to attach the antenna elements and so, get the final array. EM simulations can now be performed to the overall system, which allows the analyze of the global coverage capabilities. Discrete ports were considered to perform these EM simulations.

This work will initially follow a beam-switch approach, not being necessary for any scenario have all array elements simultaneously active. This operation procedure means that the array radiation pattern will be reconfigured by switching the active elements. It is intended to explore the radiation patterns produced by the single elements individually and the ones produced by the combination of two consecutive elements, when activated at the same time. With this technique is expected that the scanning over the azimuth plane can be ensured through the beam switch. For this reason, the antenna arrays top element will not be considered since this element must cover the plane above it.

To validate this proposition, separated simulations were performed in order to obtain the radiation patterns that are produced by the array elements individually, as well as the ones produced by the combination of two active elements. The simulated results were put together in the same plot, allowing to conclude the overall coverage capabilities of the array. For the first structure, were obtain the results depicted in Figure 3.7.

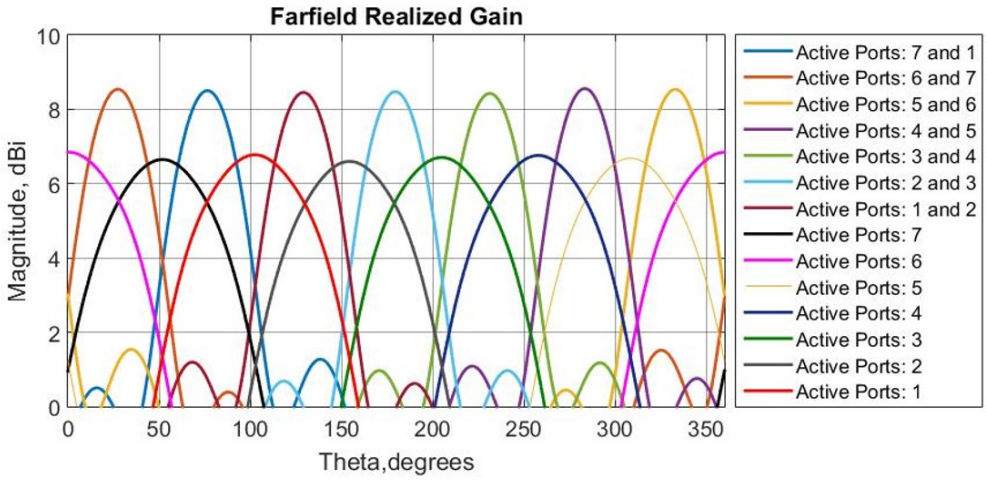

Figure 3.7: Different radiation pattern achievable by the structure A.

Through the analysis of the several radiation patterns obtained, it can be concluded that, by switching between elements, the radiation beams can cover different azimuth angles ensuring the hemispherical coverage. It is possible, in this way, to keep a similar signal gain over 360 azimuth degrees. When only a single element was active the antenna's gain is approximately constant, about 6 dBi (standard gain of a patch antenna), but in its turn, when two elements were active simultaneously, the gain obtained is as expected, a little higher (between 7 and 8 dBi). This gain variation occurs because the radio waves radiated by each antenna element individually superpose, interfering constructively and enhancing the power radiated to the desired directions. On the other hand, they interfere destructively to the other directions, reducing the radiated power to those positions. This operation procedure is one of the basic principles of antenna arrays that becomes an advantage in many application scenarios.

By analyzing these radiation patterns, it is also quickly concluded that there are some

positions where the signal quality in receiver benefits if there are two simultaneously active antenna elements. An example of those positions is, for example, when the target, which can or can not be in motion, is placed at a far-field position, in the angles between the radiation pattern main lobes, produced by single active elements. When this happens, the receiver is not directly pointed to any array element, so the solution to accomplish this connection is through a beam produced by the combination of two sequential active elements simultaneously. For this reason, it was considered essential to understanding how this beam can be controlled in order to improve the signal quality when the receiver is in these positions.

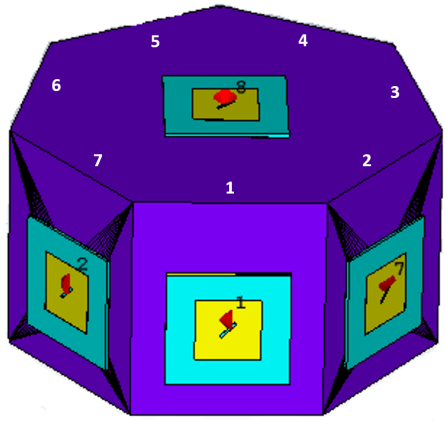

Figure 3.8: Structure A with numbered ports.

Case	Procedure/Active Ports
A	Port 7: Fixed Phase Port 1: Phase Swept
B	Port 6: Fixed Phase Port 7: Phase Swept
C	Port 5: Fixed Phase Port 6: Phase Swept
D	Port 4: Fixed Phase Port 5: Phase Swept
E	Port 3: Fixed Phase Port 4: Phase Swept
F	Port 2: Fixed Phase Port 3: Phase Swept
G	Port 1: Fixed Phase Port 2: Phase Swept

Table 3.2: Adopted procedure.

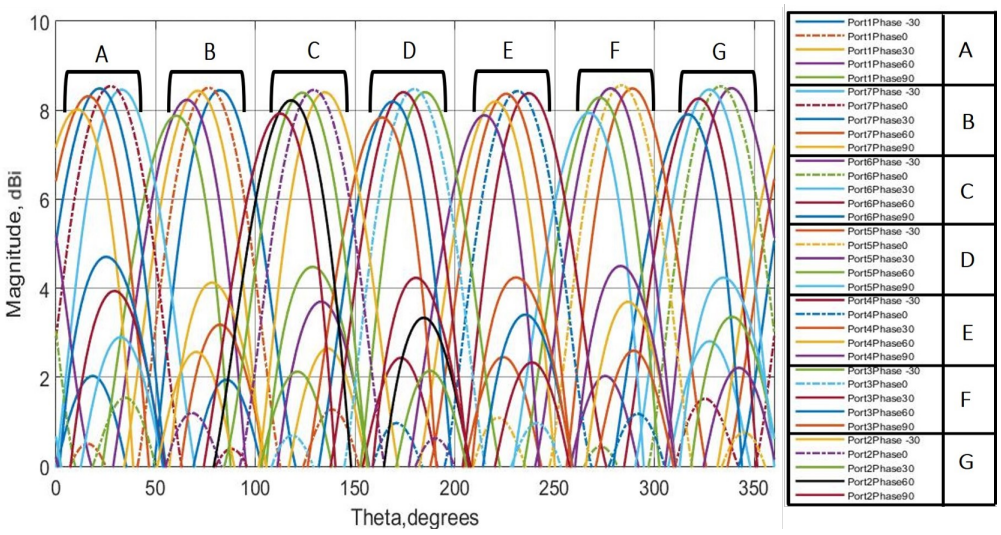

Figure 3.9: Phase sweep impact on the radiation pattern produced by two consecutive elements when active simultaneously.

Therefore, other simulations that are considered appropriate to perform consisted of a phase sweep analysis when two ports are simultaneously active. One port phase shift was

fixed at 0° while the other one was sweep from −30° to 90° with a 30° step. The adopted simulation procedure is presented in Table 3.2

The main goal was to understand the impact caused by these phase variations in the beam produced in the described circumstances, allowing to conclude which phase shift values should be introduced to accomplish a most strengthened signal on the receiver, depending on its position. Through the simulated results, presented in Figure 3.9, some considerations can be taken:

- Even with the phase shifts introduced, the signal gain remains approximately stable.
- The phase variations introduced causes, as expected, a beam shift, being the maximum signal's gain obtained for different azimuth angles depending on the phase shift introduced.

This analysis makes it possible to estimate which phase shifts should be introduced at the different ports, so that depending on the receiver position, the strengthened signal can be guaranteed. Moreover, they also indicate that if the array always operates with two consecutive elements activated, with the correct phase-shifts, a full azimuth coverage may be ensured with a higher gain.

As for structure B, initially were performed the same analysis performed to the structure A. So, maintaining the array operation procedure based on a beam switch approach, separated simulations were carried out, in order to obtain the global coverage capabilities of this array. These simulations aim to obtain not only the radiation patterns produced by each element individually but also, those which are generated by the combination of two consecutive elements, simultaneously active. It should be noted that unlike structure A, where the side faces were in perpendicular planes relative to the structure bases, in this particular case, the side faces are in an oblique plane concerning to both bases. Due to this particularity, to properly analyze the radiation patterns, the plane under analysis has to be perpendicular to the direction of antenna's radiation, which in this case occurs in a plane of approximately $Phi = 45°$ and not $Phi = 180°$, as happened in structure A.

The different radiation diagrams obtained were plotted together and are presented in Figure 3.10.

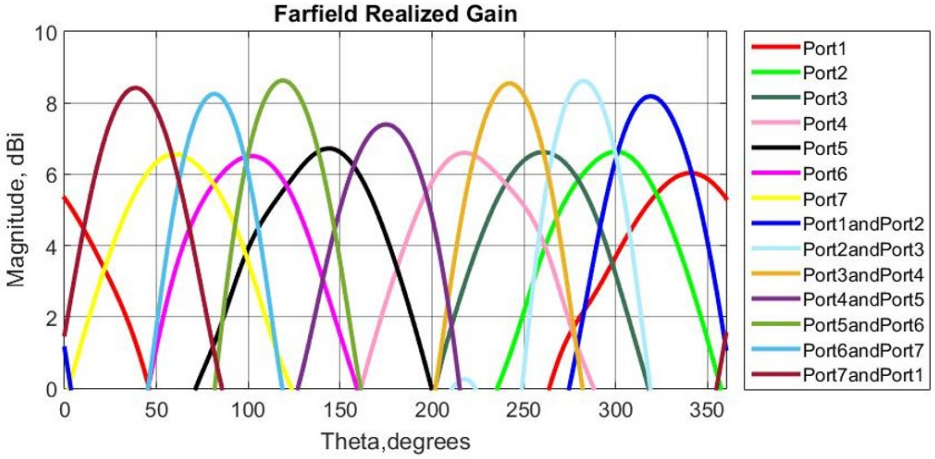

Figure 3.10: Different radiation pattern achievable by the structure B.

By analyzing the obtained results, it can be concluded that the coverage capabilities achieved by this array are in line with what was expected, since both the antennas gains obtained and global radiation pattern are similar to those obtained in structure A. However, in this structure occurs a signal's gain degradation, approximately between the 150° and 200°. This occurrence prevents the signal's power stability over the azimuth plane and occurs because the signal produced by Port 4 and Port 5 has a signal attenuation more significant than the other ones that are produced by two active elements. This occurrence, that can be caused by imperfect antenna alignments, gives it a lower gain compared with the ones, that are obtained in the remaining directions.

Finally, structure C is the one with the highest complexity due to its fifteen antenna elements. The primary purpose of this arrangement is to be able to secure a stable signal not only across all azimuth angles but also at different elevation angles. The performed simulations are similar to the previous ones, but it should be noted that the complexity of this structure makes the EM simulations much longer than the previous ones. Also, in this case, more than in the others, there is a factor that must also be taken into account, the coupling effects.

The coupling effects, reduce the antenna's efficiency and occur when two or more antennas placed near to each other interact between themselves, even if they are in transmitting or receiving mode. For example, if both antennas are transmitting, surely some energy radiated for each antenna will be received by the other one. This scenario is usually undesirable because a nearby antenna absorbs the energy that should be radiated (Figure 3.11(a)). The same occurs when antennas are in receiving mode because some energy that could be received by one antenna is instead, absorbed by a nearby antenna (Figure 3.11(b)).

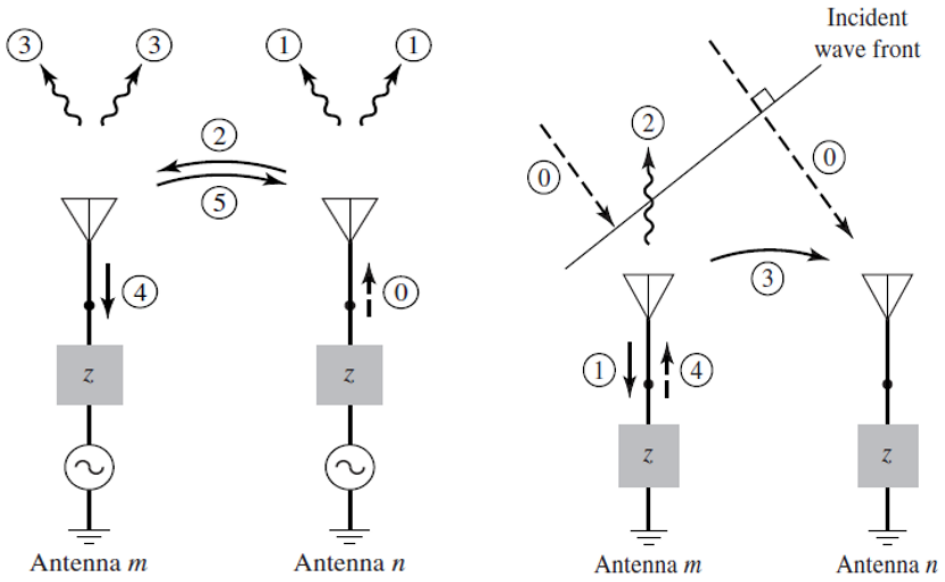

Figure 3.11: Coupling between antennas m and n (taken from [2]): (a) When transmitting and (b) When receiving.

Since this arrangement was developed in order to study its possible integration into a

WPT scenario, a system simplification is intended. Because of this, this array will differ from the previous ones, since its antenna elements will be linearly polarized, also fabricated in the same substrate. In order to understand the coupling effect among all elements, the active S_{11} parameters were simulated, and the results are presented in Figure 3.12. There is an evident difference between them, indicating that there is coupling between elements. In practice, it will be not possible to measure this directly with a two-port Vector Network Analyzer (VNA). The measurement setup that will allow performing these measurements will be presented and discussed later.

This reflection coefficient parameters were simulated for a scenario where all array's antenna elements were active simultaneously. However, this antenna array is intended to operate following the same procedure as the previous ones. That is, it is intended to follow a beam-switch approach, so in any scenario is intended to have all antenna elements simultaneously active. For this reason, this analysis should be performed, considering possible practical cases that will occur.

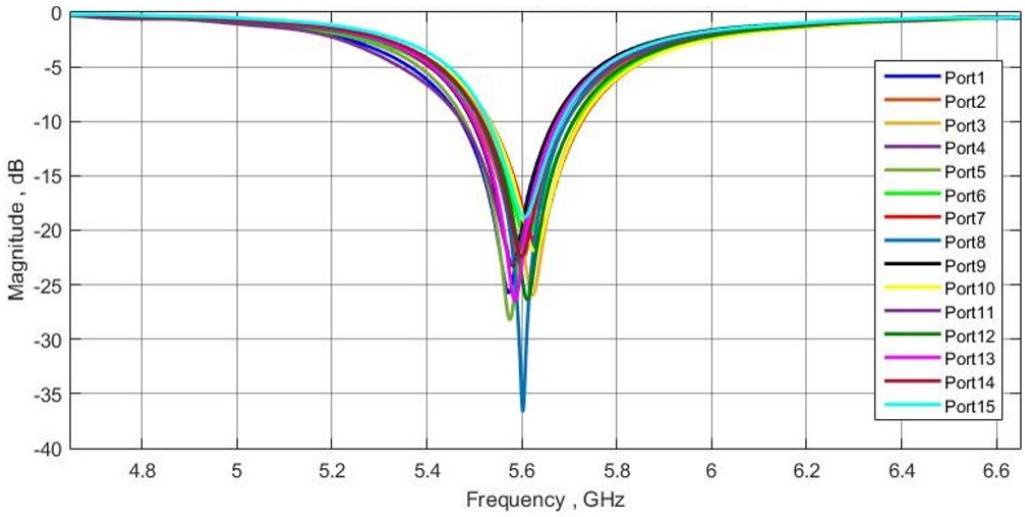

Figure 3.12: Antenna array active S11 parameters.

It is mentioned in [2], and in [3], that the mutual coupling affects the current distribution through the array elements, and hence, the input impedance as well as, the radiation pattern. The mutual coupling is highly dependent on factors such as:

- The radiation characteristics of each antenna element;
- The separation between antenna elements;
- Relative orientation of the antenna elements.

In this case, the mutual coupling will be discussed for practical scenarios that will be going to occur. From this principle, the reflection coefficient of a single port will be under analysis in different situations. It will be considered the mutual coupling introduced by the elements right next to the one that is active and what is immediately below or above, depending on whether the element is in the upper or lower circular band, respectively. For example, if we intend to analyze the coupling introduced in the antenna element number 4 (Figure 3.13) , the scenarios presented in Table 3.2 will be evaluated. It is intended to analyze not only the

changes in element four but also in the elements closest to it (elements three, five, and eight), aiming to verify possible changes that occur when these ports are simultaneously active with element 4.

The reflection coefficients in the mentioned ports were evaluated in the described scenarios. In figure 3.14 are presented the simulated results. These combinations were chosen because similar to what occurred in the previously arrays, exist some positions where the signal quality/strength benefit if exist two active elements, achieving in these situations a higher gain. It is, therefore, crucial to study the coupling effects in such situations.

Analyzing the results obtained through the simulations in the first place is possible to state that when only two ports are active simultaneously, the coupling that occurs is much less significant compared to the one that occurs when all antenna elements are active. Moreover, it can be verified evident differences between the antenna elements reflection coefficients when active simultaneously, which indicates the existence of coupling between elements. However, despite the variations presented in the reflection coefficient magnitudes, the antenna elements matching for the operating frequency can be validated, and the coupling that occurs in these scenarios is not very significant. The operation procedure based on beam switch techniques can be, therefore, implemented in practice.

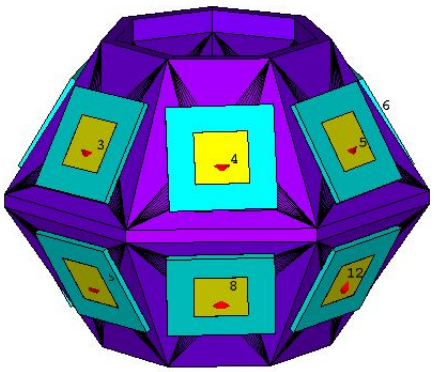

Figure 3.13: Overview on structure C.

Case	Active Ports
A	Only Element **4**
B	Elements **4** and **3**
C	Elements **4** and **5**
D	Elements **4** and **8**
E	**All** Elements Active

Table 3.3: Evaluated Scenarios.

It is now necessary evaluate the coverage capabilities of this third arrangement. To evaluate this feature, and without forgetting the primary purpose of this structure, which is to ensure a stable signal not only across all the 360 azimuth angles but also at different elevation angles, different radiation patterns were simulated. The global array's radiation pattern will be obtained following the same previous procedure, which considers the radiation patterns produced by the antenna elements individually and the ones that result from the simultaneous activation of two consecutive active elements. However, in this arrangement, this procedure can be implemented in two circular bands of antenna elements.

The following three different scenarios, depicted in Figure 3.15 will be considered:

- If the target is placed **above** the array (Case A);
- If the target is placed **at the same height as the center of the array** (Case B).
- If the target is placed **below** the array (Case C);

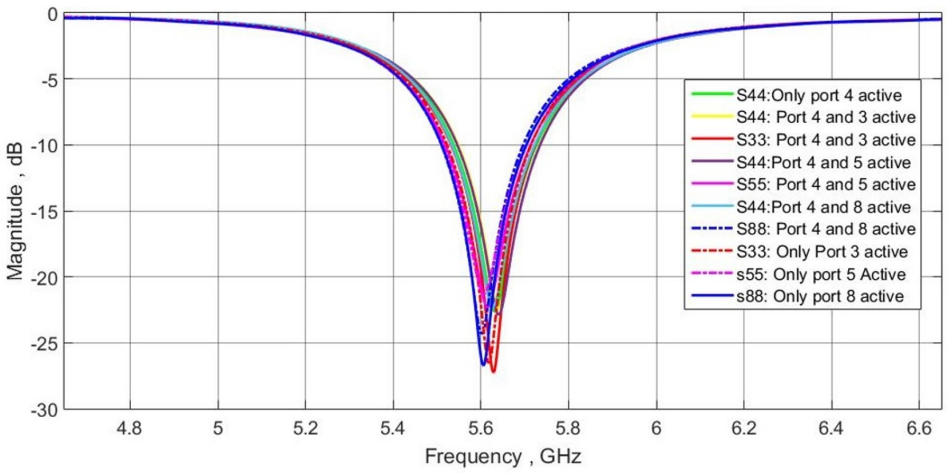

Figure 3.14: Active S_{11} parameters.

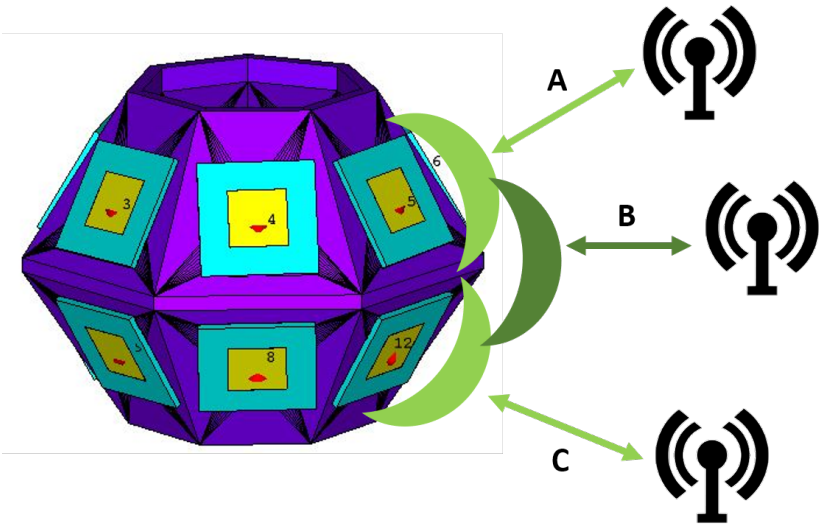

Figure 3.15: Different radiaiton scenarios for array C.

In order to ensure a stable signal, regardless of both position and target's elevation, three types of radiation patterns will be considered. In case the target is placed above the antenna array (case A), the operation procedure explained before will be tested when applied to the upper circular band of antenna elements (Figure 3.16(a)). In the case C, when the target is below the antenna array, it will be considered the coverage capabilities performed by the combination of the radiation patterns produced by the elements placed at the bottom circular band (Figure 3.16(b)). Lastly, case B is a particular one. When a target is placed with this elevation, it does not occur alignment with any antenna element. In order to ensure a robust signal in these positions, it will be tested the radiation patterns also produced by the simultaneous activation of two antenna elements. Only in this scenario, it will be considered one element of the upper circular band and the one right below it, placed in the lower circular band, right below it, as can be seen in Figure 3.16(c).

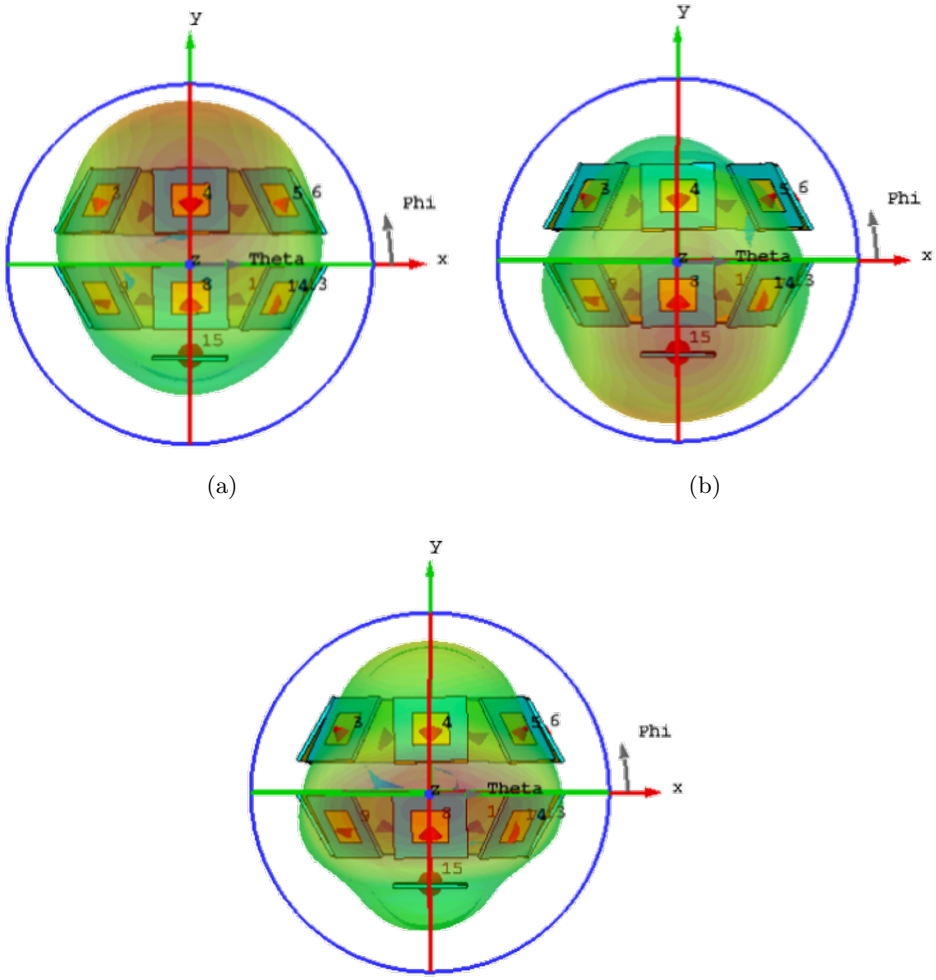

Figure 3.16: Array C: Different radiation pattern combinations: (a) Upper circular band of antenna elements, (b) Lower circular band of antenna elements, (c) Combination of elements of both circular bands.

Simulations were performed in order to analyze the coverage's robustness of this array for the three different scenarios described. The results are depicted in Figure 3.17.

By analyzing the obtained radiation patterns, it is possible to verify that in all the different situations, the signal gain is approximately constant through all the azimuth and elevation angles. However, it is also perceptible that these gain values present different values from case to case and depending on the position of antenna elements in the array.

The signal produced by the combination of elements of both circular bands is what presents better stability since the gain values are approximately 8.1 dBi in the angles of maximum radiation intensity. However, small gaps occur between the main patterns, which gives these zones a slightly smaller gain. As for the patterns produced in the upper circular band of antenna elements, can be differentiated two types of radiation lobes: the ones produced by the antenna elements individually, the widest ones, with signal's gain about 6.7 dBi and the main lobes produced by the combination of two consecutive antenna elements active

simultaneously, which are narrower,and with higher signal's gain, about 7.85 dBi.

Lastly, in the lower circular band of antenna elements, the radiation behavior is similar to the one that occurs in the upper circular one. In both circular bands, between 150° and 200°, occur a radiation efficiency degradation in the pattern produced by two active sequential elements, and hence, the gain in this width is slightly lower than expected. The average signal's gain, in this case, is about 6.5 dBi, and when two consecutive elements are excited simultaneously is about 8 dBi.

These simulations prove the primary goal of this 3D array. It was developed to be capable of transmitting and receiving signals/power from all directions with significant gain. This antenna array has a radiation behavior similar to a dipole antenna (omnidirectional), but unlike this antenna type, it presents a considerable gain, which can be an advantage in many applications. However, in an ideal case, the array elements should be individually optimized in order to ensure a more significant signal's gain stability trough all the radiation planes.

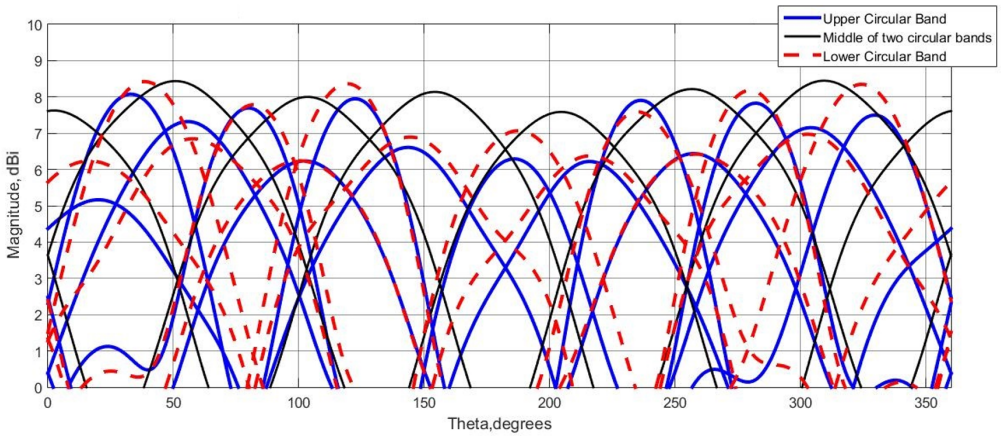

Figure 3.17: Array C: different radiation patterns for the three cases exposed before.

3.3 RF-DC Converter

As previously mentioned, several topologies can be followed to obtain a functional RF-DC converter. All of these circuits use semiconductors as rectifier elements, which present an acceptable behavior for low power input signals. This particularity gains more relevance since the WPT technique that will be explored is the one that operates based on EM radiation. Therefore, it is supposed that the signal that is going to excite the converter due to different types of attenuation will be a low power one. This acceptable behavior for low power input signals, allied to the low cost and small size, make these components very attractive for WPT applications.

The converter that will be used should be carefully chosen and take into account some features that are intended to achieve. The application scenario that was in mind was a WSN, where these circuits can feed one or more sensors. So, if, on the one hand, is intended to enhance the RF-DC efficiency, and on the other hand, the circuit must produce a considerable output DC voltage, enough to power-up these sensors, is essential to design a circuit that can reasonably balance these two variables.

Primarily, the antenna and the converter should be perfectly matched to avoid power

losses and, consequently, maximize the conversion efficiency. Moreover, to produce enough DC output voltage, the used circuit must contain more than one rectifier element. However, it should be noted that even though the DC output voltage rises with the increase of rectifier elements in the circuit, by another side, for the same input powers, the RF-DC conversion efficiency decreases. This occurs because a full biased diode has an associated resistance, so how many more of these elements the circuit contains, more losses will be introduced in the signal path. Due to all of these described aspects, the followed topology was the single-stage multiplier, already presented in Figure 2.11.

Due to all the advantages previously mentioned, the Schottky diodes are the crucial components in RF-DC converter circuits. The designed circuit consisted of two SMS7630-079LF Schottky diodes from Skyworks Solutions, whose SPICE parameters are presented in Table 3.4.

Parameter	**SPICE**	**Descritpion**	**Value**
I_s	Is	Saturation Current	5E-6 A
R_s	Rs	Series/Parasitic Resistance	20Ω
N	N	Emission Coefficient	1.05
C_j	Cjo	Zero Bias Junction Capacitance	0.14 pF
V_T	Vj	Junction Potential	0.34 V
V_{br}	Bv	Reverse Breakdown Voltage	2 V
I_{br}	Ibv	Reverse Breakdown Current	1E-4 A
W_g	Eg	Gap Band Energy	0.69 eV
p_t	Xti	Is Temperature Exponent	2
M	m	Junction Grading Coefficient	0.4

Table 3.4: SMS7630-079LF SPICE parameters.

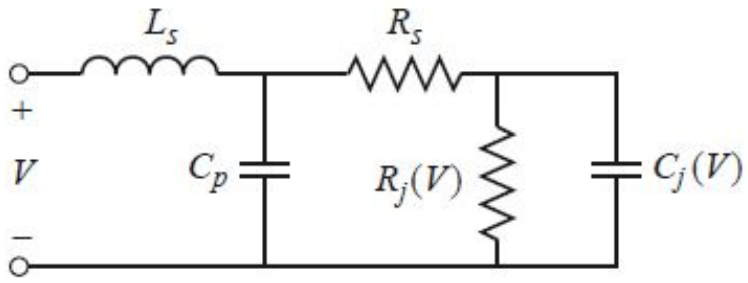

Figure 3.18: Schottky diode equivalent model.

A equivalent AC circuit model for a Schottky diode from [39] are presented in Figure 3.18. The diode's package leads are modeled as a series inductance (L_s) and for a shunt capacitance (C_p), whose suggested values are provided in the component data-sheet. The series resistance (R_s) represents the opposition to current propagation, while both the junction resistance and capacitance are bias dependent. It is possible to verify the existence of some parameters highly dependent on both the operating frequency and the power of the input signal. Due to these dependencies, these types of circuits must be optimized for a predetermined signal's frequency and power.

The single-stage multiplier overall design process will cover the following steps:

- Optimize the circuit for an operating frequency of 5.65 GHz and a signal's input power of 0 dBm ;
- Analysis of the load's value influence on circuit behavior. Check which one confers better efficiency;
- Design a matching network in order to match the circuit to the desired frequency.

The RF-DC converter was matched at the desired frequency using a open-circuit stub in parallel with a series line, which is responsible for realizing the impedance's match between the receiver antenna and the converter circuit.

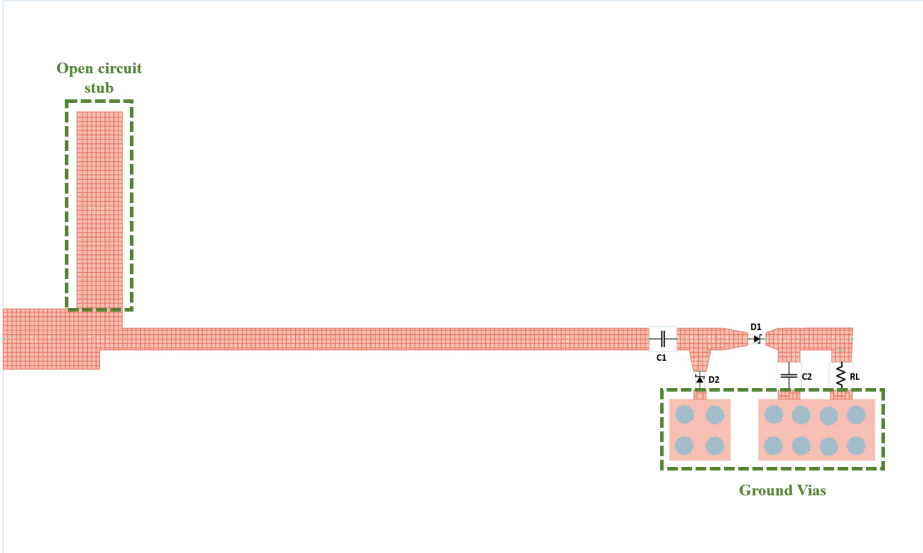

Figure 3.19: Schematic of the first RF-DC converter approach.

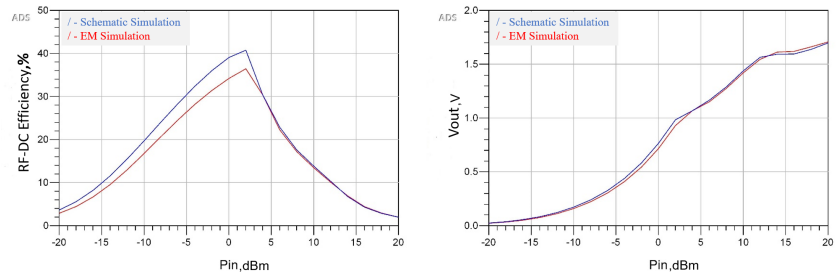

Figure 3.20: Simulation results of the circuit composed by discrete components.

Initially, an approach where C2 was a discrete component (Figure 3.19) was followed. However, despite the acceptable simulation results obtained and presented in Figure 3.20,

in practice, this circuit presented poor results, in both efficiency and output DC voltage for low-power input signals. The capacitor package used has dimensions (precisely its width) considerably larger than the line in which it was applied. This feature was not considered for simulation purposes.

It should be mentioned that all the presented simulations were performed using the software Advanced Design System (ADS) from *Keysight Technologies*.

In a second approach, only one modification of the previous circuit was performed. The load capacitor (C2 in Figure 2.11), which was previously a discrete component, was replaced by an open stub that also ensures capacitive characteristics. All the lines and the stub dimensions can be found in the table 3.5 and in Figure 3.21 is depicted the new designed circuit.

Widths		**Lengths**	
Variable	**Dimension (mm)**	**Variable**	**Dimension (mm)**
W50	1.974	**L50**	6.244
WStub	1.591	**LStub**	12.575
WCap	3.499	**LCap**	9.045
Wline	1.119	**L1**	13.362
		L2	2.344
		L3	2.554
		L4	3.238
		L5	17.602

Table 3.5: Dimensions of the 2nd Designed Circuit.

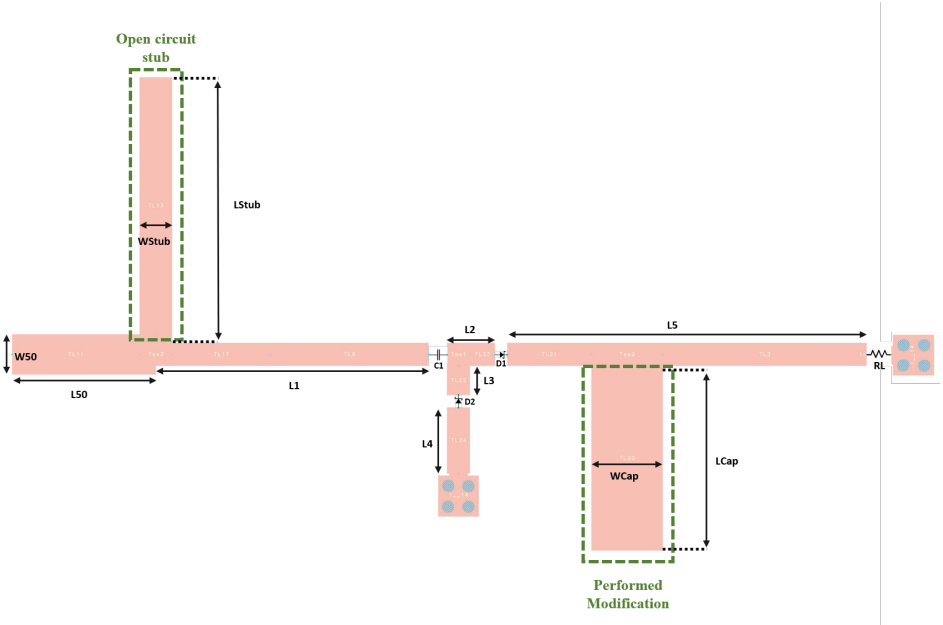

Figure 3.21: Schematic of the second RF-DC converter approach.

The widths of the lines that are not distinguished in the circuit schematic presented in

Figure 3.21 are shown in that table as **Wline**. This new design approach has led to a slightly increase in the total circuit size.

To evaluate this new circuit performance, simulations were performed again in ADS software. In Figure 3.22 are presented the obtained results for both conversion efficiency and DC output voltage.

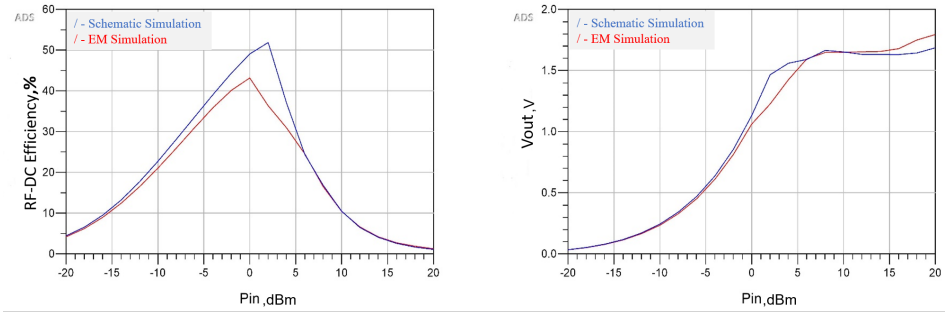

Figure 3.22: Simulation results obtained for second the RF-DC converter approach.

As can be seen, both parameters values have undergone significant improvements, and for low input power, the results of the schematic and EM simulations show an serious agreement. For the input power for which the circuit has been optimized (0 dBm), the efficiency and output DC voltage have values of 43.14 % and 1.06 V, respectively.

Simulations were also performed ir order to verify if the converter circuit was correctly optimized for the considered load resistance. So, the load resistance value was swept between 1 $k\Omega$ and 3 $k\Omega$ with a 200Ω step, in order to analyze what is the best value to use. Both the conversion efficiency and DC output voltage were analyzed for the different RLoad values. The results are presented in Figure 3.23 and shown that a 2.6 kΩ load resistance was the one that confers to the circuit the maximum conversion efficiency as well as, a considerable generated output DC voltage.

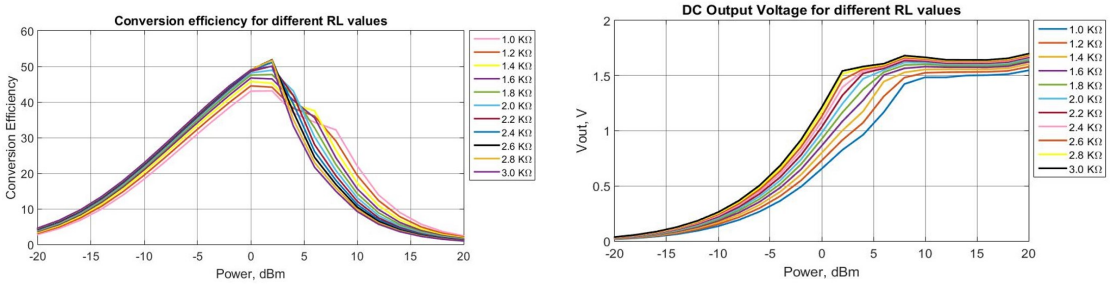

(a) (b)

Figure 3.23: (a) R_{Load} Sweep impact on: conversion efficiency and (b) Output DC power.

These obtained results are satisfactory and are in line with what was intended since the output DC voltage should be enough to feed low power devices. This circuit was fabricated (Figure 3.24), and its practice performance will be analyzed in chapter 4.

3.4 Conclusion

This chapter provided a full description of the fabricated components that will constitute the final system.

The first topic gives a full description of the procedure followed to design the antenna elements that would constitute the 3D antenna arrays. Different alternatives were presented, and based on the results obtained by the simulations, it was chosen to fabricate the one that best fulfilled the intended requirements.

Then, a full system overview was presented. Initially, was described the development of the 3D arrangements. The antenna elements were then, attached in the structures, which allows performing EM simulations that help to study these alternative arrays behavior. Coverage capabilities, radiation intensity, signal gain, and coupling effects are the topics presented and analyzed.

Finally, the entire RF-DC converter circuit design process is presented. Simulations were performed to analyze the circuit operating frequency as well as its conversion efficiency and output DC power generated. Both the circuit and the matching network have been optimized in order to meet the desired requirements. The circuit was fabricated after its operation was validated theoretically.

Now that all the components required to simulate the intended system are built, measurements can be performed in order to analyze the real performance of the components and validate them. In Chapter 4, the performed measurements are described, and considerations about the overall system will be made.

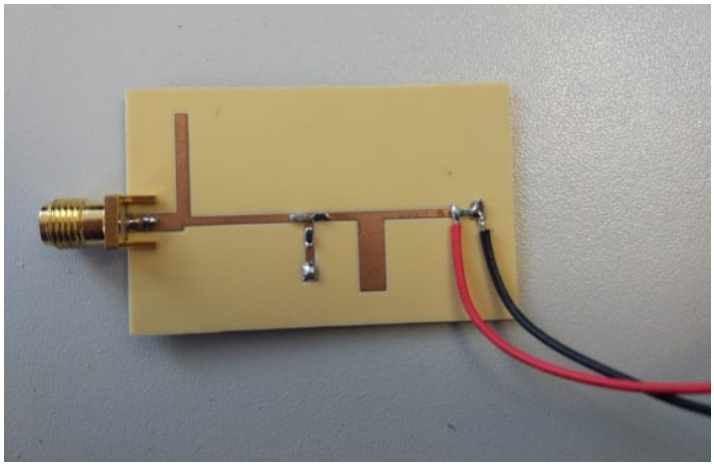

Figure 3.24: RF-DC converter prototype.

Chapter 4

System Measurements and Analyze

During this chapter will be exposed all the measurements and tests performed on the different developed components. Initially, both the antennas and the RF-DC converter circuit will be tested individually in order to validate their real operations. Then, it will be presented the measurements performed to the complete system with the primary goal of understanding its viability if implemented in a real application scenario.

4.1 Measurements Performed to the Antennas

4.1.1 Antennas Scattering Parameters

In Section 3.1, several antennas were designed and simulated, aiming to achieve the desired requirements. At the end of that chapter, based on the obtained results trough the simulations, a circularly polarized antenna was chosen to be fabricated. It is now necessary to validate its real operation. One of the main parameters that should be measured in antennas is its reflection coefficient. The scattering parameters, namely the S_{11} parameter, which represents the antenna's reflection coefficient, will be measured with a VNA, which will allow evaluating the antenna's matching at the operating frequency.

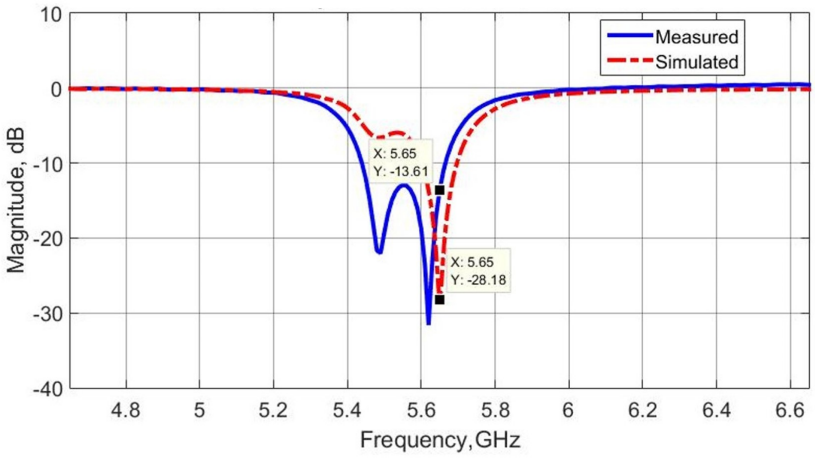

Figure 4.1: Fabricated antenna S_{11} parameter.

The main goal is to ensure the lowest reflection possible, so the antenna will present a better matching to the frequencies where this parameter has lower magnitudes. However, it is usually considered that an antenna has an acceptable matching for a specific frequency if the value of this parameter is lower than -10 dB at the respective frequency. In Figure 4.1 is presented the measured reflection coefficient of the fabricated antenna.

The measured S_{11} indicates approximately a 230 MHz bandwidth, between 5.45 GHz and 5.68 GHz. This means that this antenna is capable of operating correctly at frequencies within this range, where the reflection coefficient is bellow than -10 dB. The minimum antenna power reflection occurs at approximately 5.61 GHz, where the S_{11} parameter magnitude is minimal. For the intended operating frequency, 5.65 GHz, the power reflection (-13.61 dB) can also be considered acceptable. These results validate the antenna operation for the desired frequency. However, when operating with these antennas, it is necessary to ensure high accuracy when defining the operating frequency, since they should be as close as possible, to the frequencies where the antenna is present better matching.

4.1.2 Circular Polarization Validation

As mentioned earlier, the antennas that compose the array are designed to be circularly polarized. This feature brings several advantages that have already been exposed in Section 2.1. Mainly, this polarization type removes the need for the transmitting and receiving antennas to be continuously aligned in order to maximize the received power.

Aiming to evaluate if the fabricated antenna is circularly polarized, it is necessary to measure its AR. To achieve this, measurements of the antenna's radiation patterns were performed in the anechoic chamber. Two sets of measures were made, both of them in the antenna planes of maximum radiation intensity (horizontal and vertical), which are orthogonal to each other. The radiation pattern obtained are depicted in Figure 4.2.

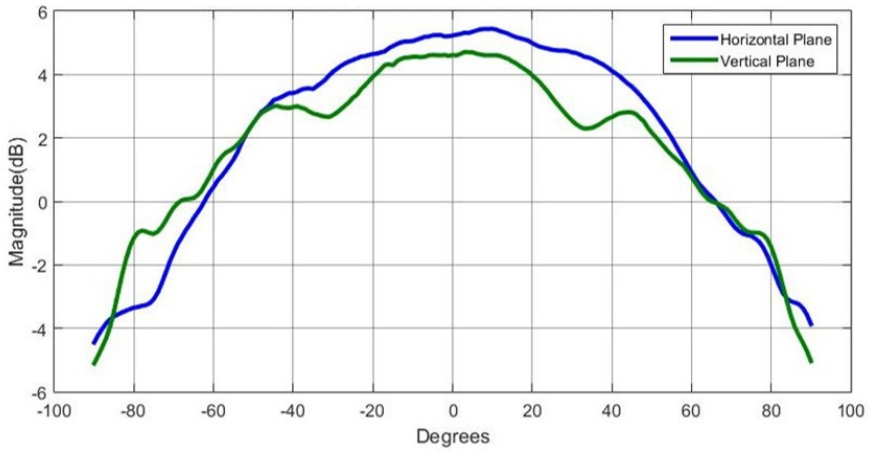

Figure 4.2: Radiation patterns measured in anechoic chamber.

In both planes, the antenna presents similar radiation characteristics but with gain slightly lower in the vertical one. In both measurements, but especially in the vertical plane, can be seen the existence of a small jitter that should occur due to the antenna rotation motion inside the chamber. This particularity may eventually cause small discrepancies between the measured gains in both radiation planes. In order to analyze the antenna's polarization type, the AR was calculated and plotted in function of the same angles that the antenna's radiation

patterns were measured. The achieved results are shown in Figure 4.3. Since the units used are dB's, the AR is easily obtained by calculating the difference of antenna gain in both planes over the measured angles.

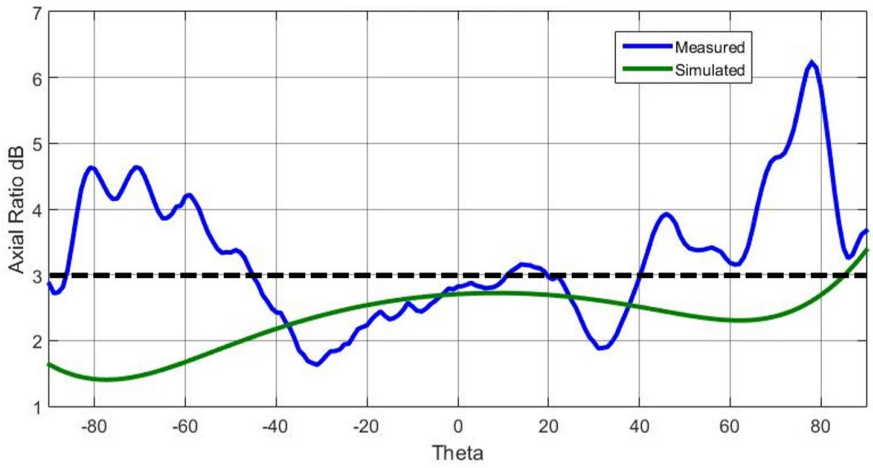

Figure 4.3: Real antenna AR.

Through the analysis of the obtained results, it is possible to conclude about the antenna's polarization. Assuming that a AR of less than 3 dB is indicative of an acceptable CP, the fabricated antenna is circularly polarized approximately throughout the maximum radiation angles. Only between angles fifteen and twenty the AR slightly exceed 3 dB.

The slight differences verified between the simulated and practical results can occur because the antenna is fed by coaxial probe, which leads to the existence of solder in the patch. During simulations, this solder disposition is considered regular and with the same height than the cooper that constitute the patch antenna. However, in practice, this does not occur, since the solder is irregularly placed and is higher than the patch. This particularity should be considered when simulations were performed.

However, this antenna can be considered well circularly polarized and adequately matched to the intended operating frequency. The developed antenna operation can thus, be validated.

4.2 RF-DC Converter

During the work was developed the rectifier circuit presented in Figure 3.24. This circuit must be perfectly matched with the receiver antenna in order to minimize the power losses. For this reason, this circuit was projected and optimized to match the fabricated antenna, which operation is presented and analyzed in the previous section (Section 4.1). So, this circuit was designed to operate at 5.65 GHz and have the best efficiency value for 0 dBm input power.

4.2.1 Scattering Parameters

Aiming to validate if the RF-DC converter is matched to the operation frequency, the first measurement performed was the circuit's reflection coefficient using a VNA. The converter's S_{11} parameter is shown in Figure 4.4.

Analyzing the obtained results, it is possible to conclude that the circuit is well matched for the frequency of 5.65 GHz since its S_{11} parameter, presents at this frequency, -14.75 dB of magnitude. However, the frequency for which the signal's reflections are minimized is at 5.55 GHz (S_{11} parameter with -20 dB of magnitude). Therefore, it is at this frequency that the received signal will be stronger. The operation frequency profoundly influences the circuit efficiency, so it becomes vital to understand how the efficiency levels vary with different frequencies, even more, when like in this case, the minimum reflection coefficient does not occur for the desired frequency. In this circuit, it is required to evaluate mainly the difference of its efficiency for the designed frequency (5.65 GHz) and for the frequency where the minimum of reflection occurs (5.55 GHz).

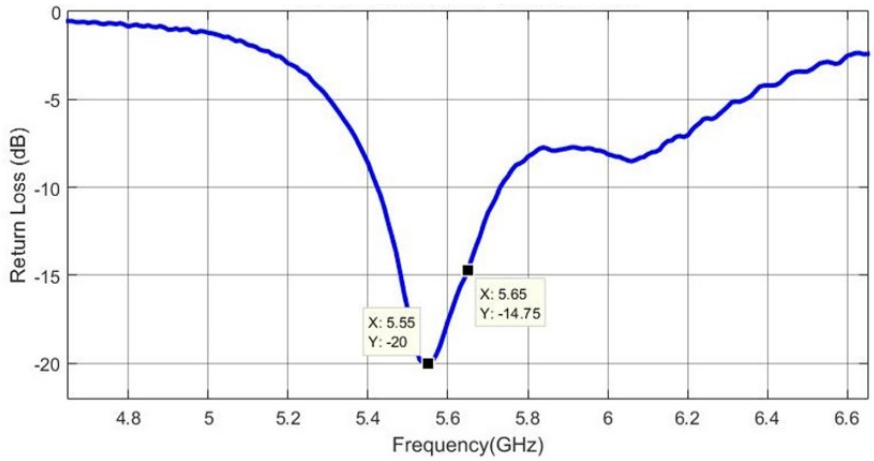

Figure 4.4: Fabricated circuit S_{11} parameter.

4.2.2 RF-DC Converter Performance

After fabricated, the RF-DC converter was subjected to different measurements in order to evaluate its real performance. In Figure 4.5 is depicted the experimental setup used.

An R&S SMW200A Vector Signal Generator (VSG) produces a sinusoidal signal that represents the RF waves at the RF-DC converter input. The signal generated by the VSG is transmitted to the RF-DC converter circuit input through a directional coupler. This coupler is used because it allows us to connect a power meter, which helps to perform a measurement system calibration. This power meter will allow real-time measurement of the power that actually, is supplied to the circuit. Finally, a multimeter is connected to the circuit's output to measure the DC voltage generated by RF-DC.

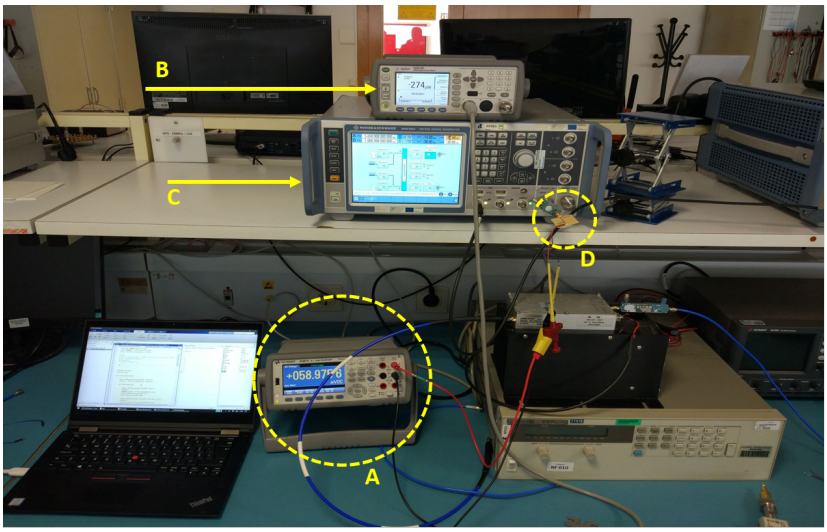

Figure 4.5: Experimental setup used for RF-DC converter measurements.

4.2.2.1 Conversion Efficiency Vs Operation Frequency

The first measurement consisted of calculating the conversion efficiency for different frequencies with fixed input signal power. In this way, it is possible to conclude which frequency gives the circuit the best performance. In order to achieve these measurements, the signal's frequency was swept from 5 GHz to 6 GHz with a 20 MHz step, and the input power was fixed at 0 dBm, since it was the power for which the circuit was optimized. For each step, the efficiency level was calculated. In Figure 4.6 are presented a plot with the obtained results. The maximum efficiency occurs at 5.54 / 5.55 GHz and not for the frequency for which the circuit was designed, 5.65 GHz. However, these results were already expected given the considerations made in the previous section, where it was concluded that in this circuit, the minimum reflections occur with a signal's frequency of 5.55 GHz.

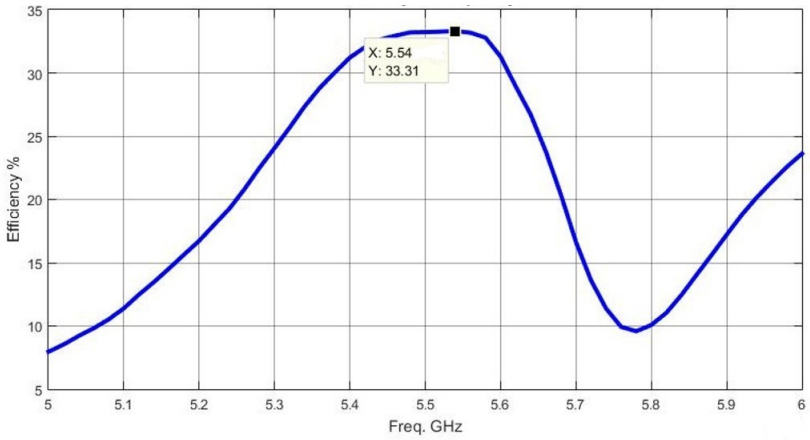

Figure 4.6: RF-DC converter: conversion efficiency Vs signal's frequency.

At this point, some optimizations should be performed in order to match the antenna with the RF-DC converter circuit. In this way, the power losses due to possible reflections will be minimized.

It is more comfortable performing the antenna matching for the desired frequency than the converter circuit. For this reason, to simulate the global WPT system, the 3D array will be composed of linear polarized antennas designed to operate at 5.55 GHz. Both the simulated and measured reflection coefficients of this new antenna are presented in Figure 4.7. Based on the obtained results, antenna operation was then validated at the desired frequency. However, it can be seen that the conversion efficiency presents a broad peak, remaining constant approximately between 5.4 GHz and 5.6 GHz. This particularity protects the circuit efficiency for small frequency variations. Since the circuit's conversion efficiency values for the optimal frequency and the surrounding ones are not very significant, the circuit can operate in these frequencies without significant losses.

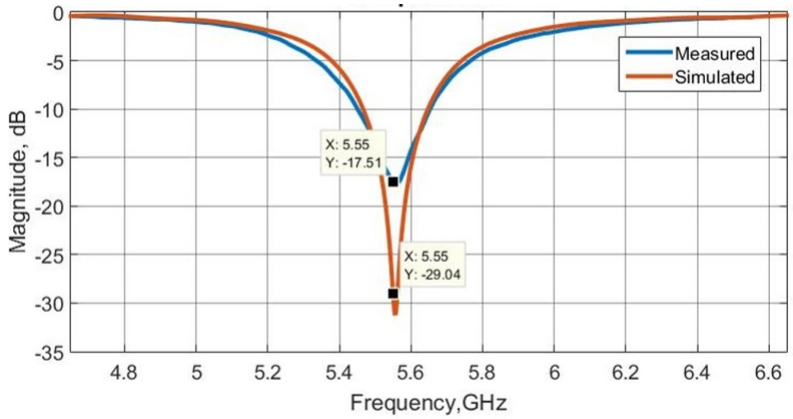

Figure 4.7: Linearly Polarized Antenna designed to operate at 5.55 GHz

4.2.2.2 Conversion Efficiency Vs RF Input Power

Now that it is well known which frequencies confer the best conversion efficiency to the designed circuit, it is also crucial to evaluate how the efficiency levels vary for different input signal powers. To perform this analysis, a measurement similar to the one previously described (Section 4.2.2.1) was performed. However, now, the operating frequency will remain fixed while different input signal powers will be tested. The input signal power will be swept between -15 and 20 dBm in two different scenarios: For the optimal frequency, 5.55 GHz, and 5.65 GHz, which is the frequency for which the circuit was initially designed. Although it was already been concluded that the circuit has the higher conversion efficiency at 5.55 GHz, this comparison will be performed to see how different the efficiency levels will be. The results are depicted in Figure 4.8.

First, it is concluded that the conversion efficiency is higher for the frequency of 5.55 GHz than for 5.65 GHz. The difference between efficiency levels remains, approximately, constant over all the different input signal powers tested. For 0 dBm of input signal power, that was the power for which the circuit was optimized, a difference of approximately 8% occurs. In both scenarios, the maximum efficiency conversion occurs for an input signal power of about 10 dBm. However, at 5.55 GHz the conversion efficiency measured for a 0 dBm input signal

power has reasonable values, take in account the followed circuit topology.

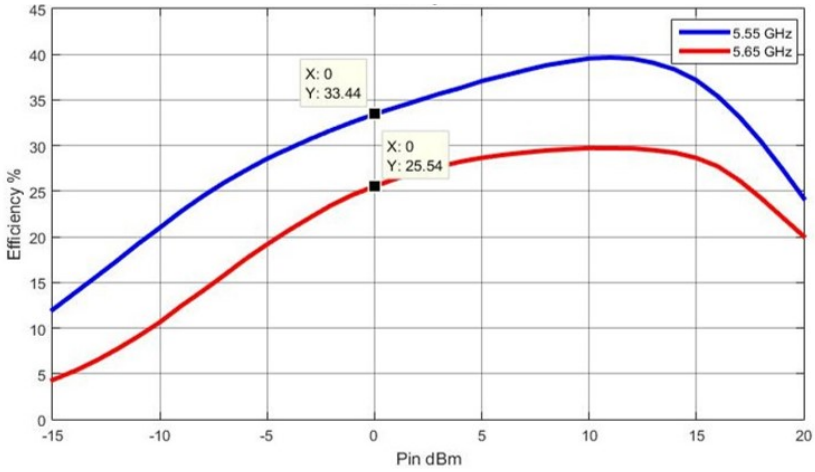

Figure 4.8: RF-DC converter: conversion efficiency Vs input signal power.

4.2.2.3 Output DC Voltage Vs RF Input Power

One of the main features of an RF-DC converter circuit is the generated output DC voltage. It is intended to achieve considerable DC output voltage values, capable of power-up low power devices or low-power sensors. To validate this capability, the circuit was tested at the optimal frequency. The input power was swept between -15 dBm and 20 dBm with a 1 dB step. For each step, the generated DC voltage was measured. The results are plotted and presented in Figure 4.9.

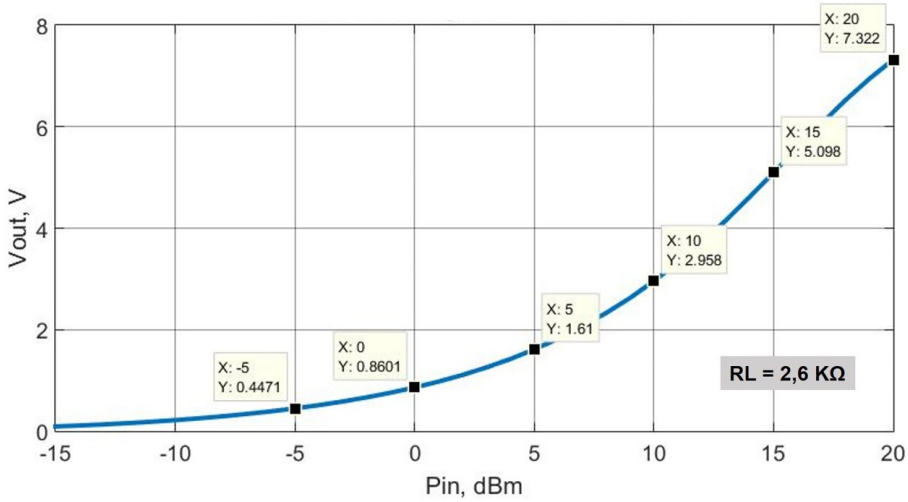

Figure 4.9: RF-DC converter: generated DC output voltage Vs input signal power.

As expected, the output DC voltage increases as the input RF power increases. At 0 dBm of input power, the designed circuit generates 0.86 V, which depending on the load considered, can be able to generate enough current to fed low power devices. From 0 dBm of

input signal power, the generated DC voltage increases exponentially. For the power that gives the highest conversion efficiency (10 dBm), the circuit is capable of generating approximately 3V. However, 10 dBm is a considerable high power, and it is intended to operate with lower powers. Moreover, in a standard human area, ensure that 10 dBm of power is effectively delivered to a receiver can be a hard task for different motives:

- The receiver and the transmitter can be in non line-of-sight conditions;
- Due to several reflections and multi-path propagation that can occur, it may be necessary to emit high power values, not allowed by the FCC or ETSI rules.

The circuit's behavior was then validated. It is expected that this circuit would be able to meet the required demands when applied in a real application scenario.

4.3 3D Antenna Arrays Performed Tests

After the operation of both antenna elements and RF-DC converter has been validated, it is crucial to evaluate the 3D array operation, more precisely, their coverage capabilities. Due to the existence of at least eight antenna elements in these 3D arrays, measure its global radiation pattern in the anechoic chamber, exciting all antennas in simultaneously becomes a complex task. To perform this measurement, it would be required the use of a power-splitter of 1 input to 8 outputs. These eight output ports, where the signal will be divided, have phase unbalances, not having the same phase-shift. These different phase shift values can not be calibrated and may introduce some errors in the measured results.

Moreover, study the behavior of each antenna individually when all are excited at the same time becomes impractical with a standard VNA, which means that it is not possible to analyze their active reflection coefficients as well as coupling effects that can occur. It was then required to find a measurement system that allows the study of these characteristics, which are crucial to characterize these antenna arrays operation.

4.3.1 Measurement System Description

Multiple-Input Multiple-Output (MIMO) antenna arrays have been explored, mainly due to the advantages that they can bring in 5G panorama since they present the advantage of being able to perform beamforming techniques and provide higher gains.

The multi-sine methodology, firstly presented in [40] to characterize 5G massive MIMO array transmitters, will be used to study and characterize the overall operation of the conceived arrays. The operating principle of this technique focuses on feed all the antenna elements not only by a main tone, equal in all elements, but also for a tickle tone with small power relative to the main one. Each antenna element has its own tickle tone at a distinct frequency. By monitoring the tickle tones frequency, it is possible to characterize each antenna array element individually, which becomes attractive because it would be possible to analyze if occur coupling between elements, which is one of the main challenges raised by the use of these antenna arrays [41], [42].

The primary purpose addressed to the use of this technique is to be able to validate that a full azimuth coverage is ensured. It is expected that through the monitoring of the tickles tones frequency, the azimuth angles where each antenna element most radiate can be identified. The precise identification of each antenna element radiation pattern will help to

understand the azimuth angles, where each one most radiates. This knowledge will allow to understand which elements should be activated in order to achieve a better signal strength, to a specific direction. However, this procedure will only work if the receiver can send feedback of the received signal power to the transmitter, which means that a RSS policy is intended to be followed.

The characterization measurement system from [43], will be used to excite all ports of the 3D antennas at the same time, for different phase shift values and evaluate each port reflection coefficient. This characterization system is composed of transmitters and receivers, where couplers are used to read the incident and reflected waves of each port. Then, a calibration procedure is applied, to have all ports calibrated in terms of magnitude and phase. In this sense, the system perform beamforming and phase sweeps in each port can be made, where the reflection coefficient is obtained in real-time, with all the ports fed at the same time.

This characterization measurement system will be used to evaluate, initially, the 3D antenna array with the structure A. First, the phase shift in each port was swept between -40° and 40°. For each phase shift value, was measured the reflection coefficient in each port. The results are presented in Fig. 4.10. The active reflection coefficients of each antenna remain approximately constant and present magnitudes slightly different from each other. The peak verified in the antenna 7 reflection coefficient (S_{77}) must have occurred due to a small measurement error. These measurements meke it possible to verify the immunity of the antenna elements operation against introduced phase-shifts. This measurement was carried out using the Software Defined Radio (SDR) MIMO system from National Instruments.

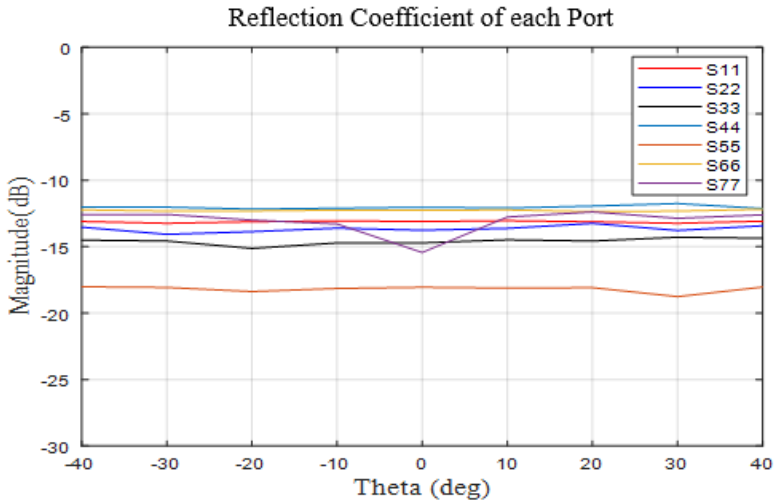

Figure 4.10: Acive reflection coefficients when beamforming is performed.

4.3.2 Received Signal's Power Analysis

In order to evaluate the 3D array coverage capabilities, the operation procedure which follows the described multi-sine methodology was applied in the mentioned measurement system. This system has the advantage of allowing the analysis of the antenna array behavior when all elements are excited simultaneously. Despite the intended array operation, do not consider the simultaneous activation of all the antenna elements, this measure allows us to

identify the exact azimuth angles where each one most radiate. Then, it is possible to conclude when the switch of the active element should be performed, in order to ensure the stronger signal in a receiver, depending on its azimuth direction.

The spacing between the main tone and the tickle tone, as well as the power between them, can be configured. In this measurement, the main tones power was configured as -4 dBm while the tickles tones power was set to -25 dBm. A multi-sine spectrum illustration is shown in Fig. 4.11.

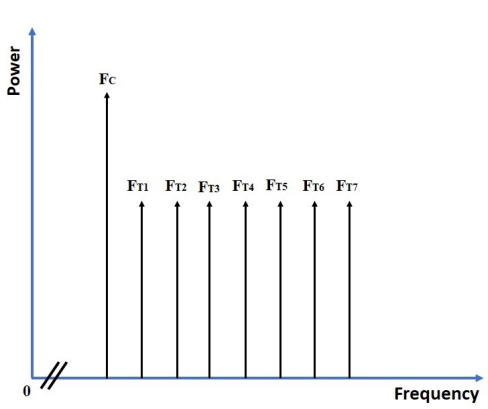

Fc	5,65 GHz
FT1	Fc + 112 KHz
FT2	Fc + 117 KHz
FT3	Fc + 122 KHz
FT4	Fc + 127 KHz
FT5	Fc + 132 KHz
FT6	Fc + 137 KHz
FT7	Fc + 142 KHz

Figure 4.11: Multi-sine spectrum representation (main tone + tickle tone) in each antenna array element.

With this measurement is intended to evaluate if the 3D antenna array can perform a full azimuth coverage. For this reason, the top element (Port 8 in Figure 3.8) will not be considered. This element must cover the plan above the antenna. A single patch, similar to the ones used on the 3D antenna array was used as a receiver. It was placed at a far-field position (0.5 m distance between Rx and Tx), and it was connected to one of the system receivers. The measurement setup is presented in Figure. 4.12.

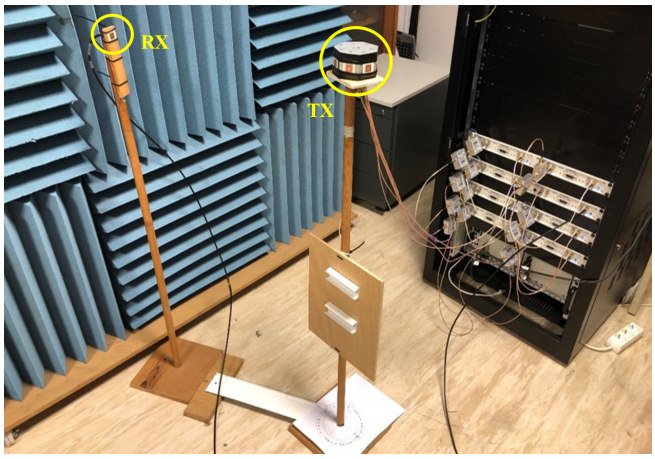

Figure 4.12: Measurement setup.

The far-field and near-field calculations are defined in terms of the *Fraunhofer* distance. In Figure 4.13, a schematic is presented where the regions according to the EM length can be distinguished, based on the *Fraunhofer* distances. D is the largest dimension of the radiating

element, and λ is the wavelength of the radio waves emitted. Concerning the structure A, the far-field zone was considered for distances over 18 cm.

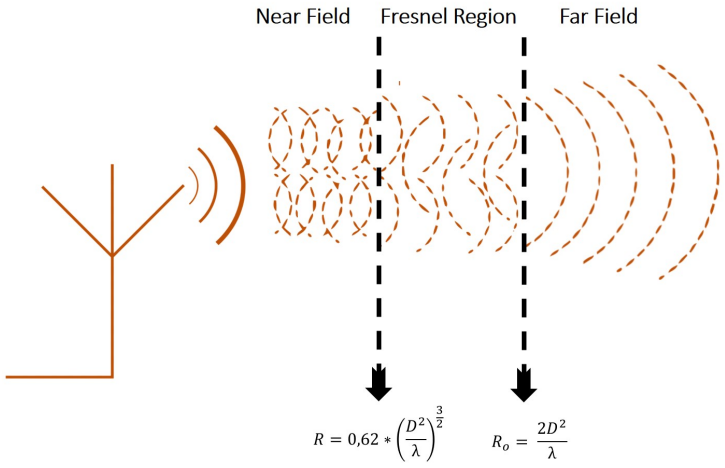

Figure 4.13: EM regions in terms of *Fraunhofer* distances [2]

The signal in the receiver was measured between 0° to 360° with a 10° step. During these measurements, all ports were active and excited by the same phase. The results are depicted in Figure 4.14. The main tone allows us to identify the overall radiation pattern. However, the tickle tones give relevant information about the individual radiation pattern of each single array element, allowing to identify the azimuth angles where they present the highest radiation intensity. Analyzing them, it is possible to conclude that, by switching between the antennas that are activated, the conceived 3D array is capable of maintaining a stable signal over the 360 degrees, and therefore, a full azimuth coverage is ensured.

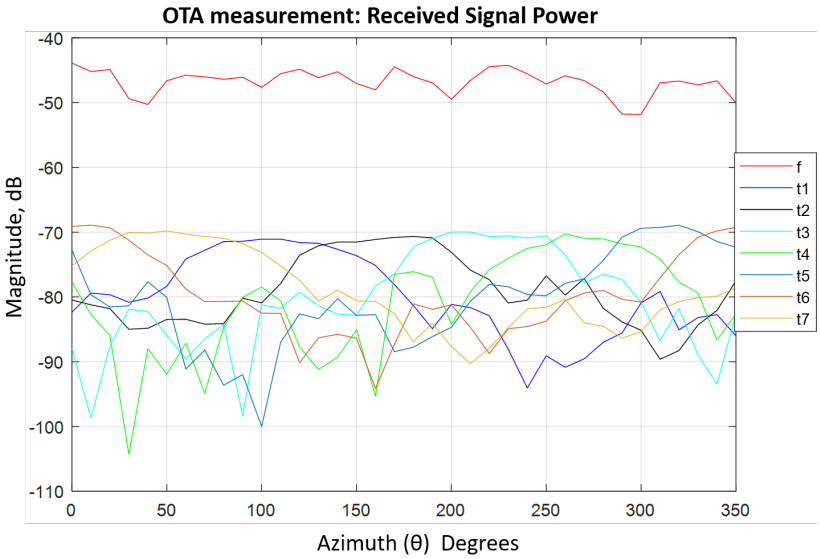

Figure 4.14: Individual contribution of each antenna element to 3D array's global radiation pattern.

If we also analyze the main tone power at the receiver, it is possible to verify oscilla-

tions between approximately -45 and -50 dB. This power should be as constant as possible over the 360 azimuth degrees. These power variations may occur because the measurements were performed in a laboratory, which is subject to multi-path and fading effects. Also, the rotational movement of the receiver (Rx) around the transmitter (Tx) is subject to errors, namely, the distance between RX and TX may be slightly different, which causes different signal attenuations. The receiver's position may also slightly change during the RX rotation, since the bracket used does not guarantee the maximum accuracy when fixing the antenna position.

4.3.3 Phase Sweep Measurement

As mentioned earlier, there are some positions around the 3D array where the signal quality in receiver benefits if it is produced by two antenna elements simultaneously active. An example of those positions is when the receiver is not directly pointed to any array element, like what occurs when it is placed in the angles between two array cells. For this reason, it is crucial to understand which phase shift combinations ensure the strengthened signal at a receiver when it is in those positions. Keeping this in mind, seven measurements were carried out. On each one of them, the receiving antenna was placed at a far-field position directly pointed to the gap that arises between two array cells, as can be seen in 4.15(a). The performed measurement consisted of analyzing the received signal power when one port phase shift was fixed at 0°, and the other one was swept from -90° to 90° with a 10° step.

The results are depicted in Figure 4.15(b) and shown that the received signal power highly depends on the phase relation between the active ports. It also can be concluded that, when the one element has its phase fixed at 0°, the maximum signal strength occurs when the consecutive element has a 30° phase shift. This phase shift value is responsible for causing a maximum of constructive interference in the direction of the receiver placed in the described positions.

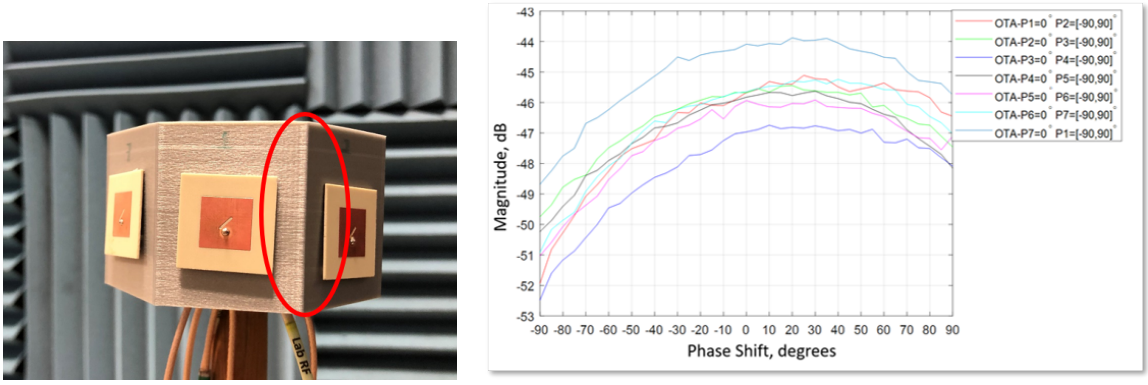

(a) (b)

Figure 4.15: (a) Phase sweep impact on received signal's power and (b) Direction in which the receiver was aligned.

4.3.4 Radiation Patterns Validated in Anechoic Chamber

The multi-sine technique described and applied before has proven to be a reliable solution to study and characterize the individual behavior of antenna arrays elements. The tickle tones analysis distinguished the directions where each antenna element most radiates and hence, validates that by switching between active elements, a full azimuth coverage can be ensured.

The beam-switch approach can, thus, be implemented. However, in order to evaluate the real coverage that the developed 3D antenna arrays can achieve, measurements in the anechoic chamber were performed. The radiation pattern of each antenna element was measured individually and plotted together. The theta angles represent the azimuth plane. The results obtained for structure B are depicted in Figure 4.16.

It is possible to conclude that although the jitter that might occur due to the antenna rotation motion inside the chamber, a small signals gain variations occur between the different the main lobes. This occurrence proves that by switching between the active array elements, a full azimuth coverage is achieved, and the antenna gain is approximately constant.

The same practical procedure was performed on the antenna array with the structure A. However, in these measurements, two radiation patterns were considered and measured: the ones produced for each element individually and those that result from the combination of two active antenna elements.

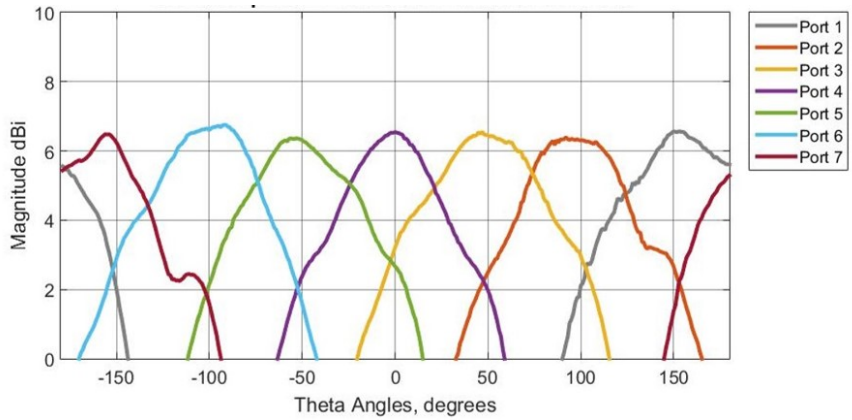

Figure 4.16: Array B radiation pattern measured in anechoic chamber.

The performed measurements consisted of measuring the radiation pattern of each antenna element individually again and, using a power splitter to accomplish a half-power division, measure the radiation pattern produced for two active sequential antennas. The power splitter use allows exciting two antenna elements simultaneously. The overall radiation pattern was then obtained considering these two different sets of measurements. The obtained radiation patterns are plotted together, showing all the coverage capabilities that this array can achieve. The results are presented in Figure 4.17.

Despite some slight differences verified in antenna's gain, the measured results are in line with the simulated ones that were presented in Section 3.2. As expected, when two elements are excited simultaneously, the radiation beams becomes narrower than the ones produced by only one element was excited. This particularity also leads to a higher gain, with an average of approximately 8.1 dBi. When only elements were excited, the antenna gain is approximately constant about the 6.4 dBi.

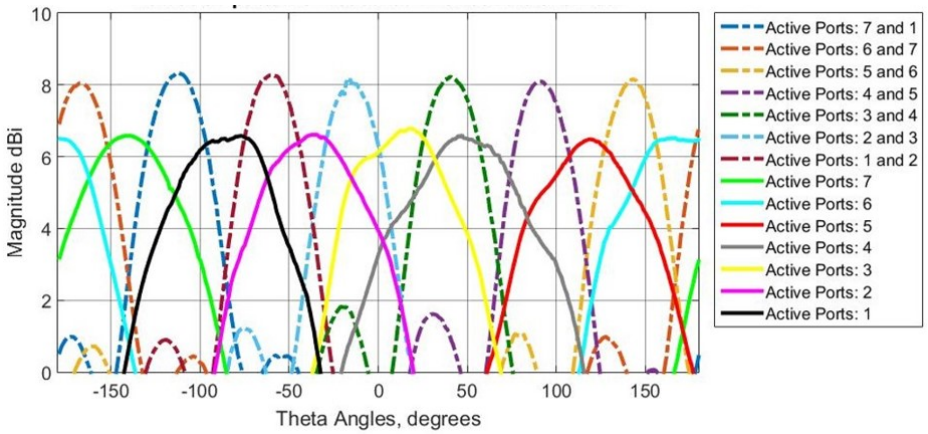

Figure 4.17: Array A: radiation pattern measured in anechoic chamber.

The measurements performed show that by switching between the array antenna elements that are activated, it is possible to keep signal with considerable gain over the 360° azimuth angles, never bellow than 6 dBi. In this way, the developed 3D array is capable of establishing a radio link with considerable gain to a receiver, regardless of its location around itself. However, in order to keep a signal strength stability trough all azimuth directions, the array can be implemented in a system that allows introducing phase shifts, since, as shown in Figure 3.9, the phase shifts make it possible to control the beam produced by two active elements. Following this operation procedure, the 3D array would operate following the same beam-switch approach, but always with two active elements simultaneously, which makes it possible to maintain the signal's stability trough all directions and with the signal's gain that is achieved by two active elements simultaneously (approximately 8.1 dBi). In Figure 4.18 can be seen the 3D array placed in the anechoic chamber holder.

Figure 4.18: Antenna array measurement in anechoic chamber.

4.4 Overall system: 3D antenna array implemented in a WPT system

As mentioned before, one of the main goals of these arrays is to improve the WPT systems performance, more precisely, improve the power transmission efficiency, as well as obtain a more robust coverage. This coverage's robustness results in an increase of directions/positions at which the energy can be focused. A measurement setup was used to simulate a WSN, allowing to study these arrays viability when applied to this kind of system. The measurement setup used was similar to the one described in Section 4.3.2. The only difference is that now the RF-DC converter circuit has been connected to the receiver, and a multimeter was used to measure the output DC power generated by the circuit. The 3D array with the structure C shape operates as a transmitter. In order to test this array's ability to transmit energy to all positions around it, the receiver was rotated around the array, and the signal strength was measured at each one of these positions. This measurement was performed for two different elevation angles, which try to simulate two receiver position scenarios: when it is **higher,** and **lower** than the transmitter array. These scenarios have been already depicted in Figure 3.15. A schematic of the measurement procedure is presented in Figure 4.19. It should be mentioned that all these measurements are performed in a OTA scenario, which implies the existence of several objects that originate several reflections, that may cause a substantial attenuation of the emitted signal's power. However, the primary cause of this attenuation is FSPL, which is given by the Equation 2.2 and represents the power attenuation that a radio signal undergoes while propagating between the transmitter and the receiver antenna, usually through the air.

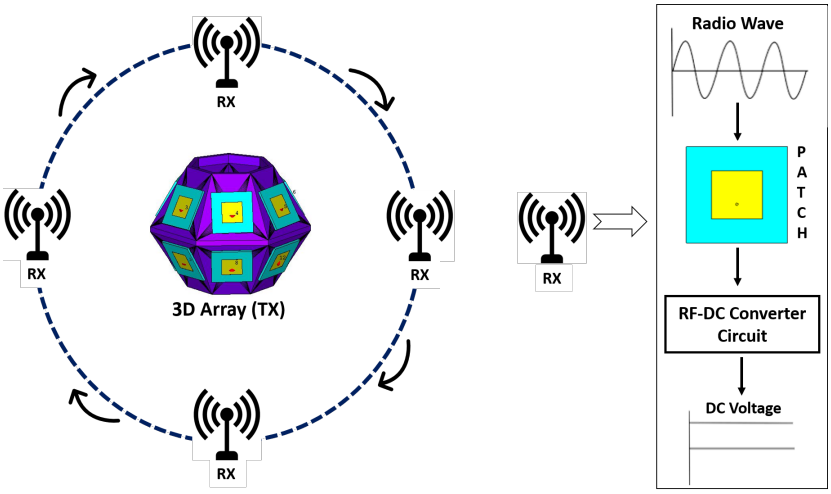

Figure 4.19: Schematic of the measurement system used to test the 3D array C operation.

In order to perform the two sets of measurements mentioned above, the receiver was rotated around the transmitter 3D array at two different elevation angles, namely at the height of 0.7 m and 1.30 m. The transmitter array is placed at 1 m of height. This measurements was performed with the aim of study the coverage capabilities achieved, respectively, by the superior and inferior antenna elements circular bands. Due to space limitations, the receiver antenna only was rotated around the transmitter array, between 0° and 180° azimuth angles with a 5° step. Since that all the antenna elements that constitute the array are equal

and the operation procedure would always be constant, it was considered that the coverage characteristics verified within this range of directions (0° to 180°) would be similar to what would happen in the angles that could not be measured (180° to 360°). The measurement setup is presented in Figure 4.20.

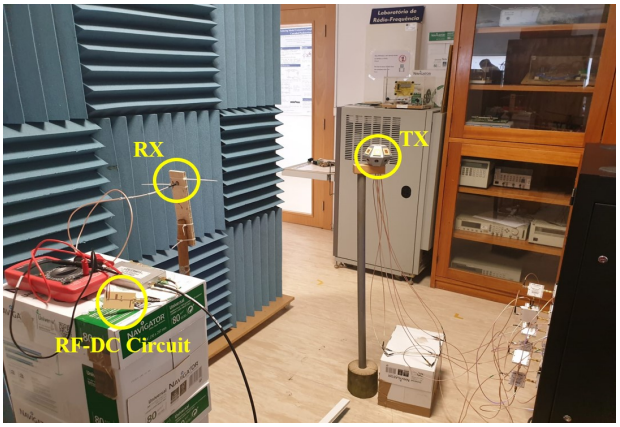

Figure 4.20: Measurement setup used to evaluate the viability of this 3D array in WPT systems.

The measured signal's strength are presented in Figures 4.21(a) and 4.21(b), respectively for the measurements performed with the receiver placed at 0.7 m and 1.3 m. In this measurements the main tones power was configured as -5 dBm, while the tickles tones power was set to -25 dBm.

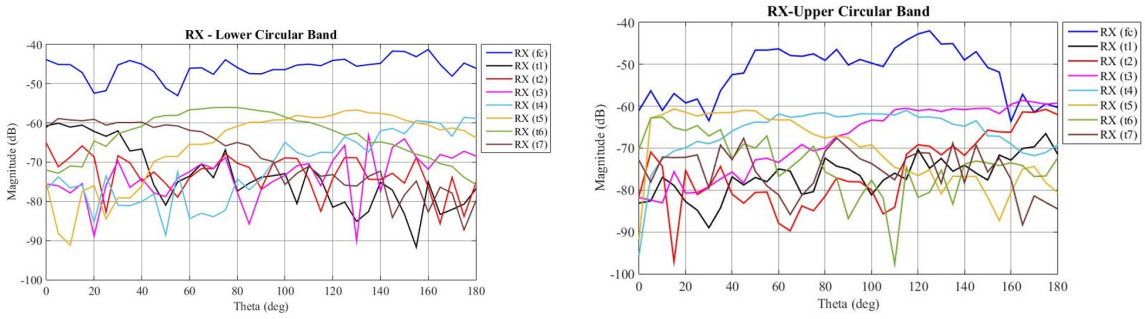

(a) (b)

Figure 4.21: Received signal strength measured with a receiver placed at: (a) 0.7 m and rotated between 0° and 180°. and (b) 1.3 m and rotated between 0° and 180°.

In this case, the multi-sine technique applied to the measurement system, does not provide information to clearly identify the theta angles where each antenna element most radiate. This results may be caused because the chosen measurement setup, does not ensure a complete stabilization of the antenna elements. The antenna motion during the measurements caused some errors in the results. However, some considerations can be made. For the lower circular band of antenna elements, the main tone power at the receiver presents slight changes, with values between -44 dB and -52 dB. However, when we analyze the power of the same tone, but concerning the upper circular band of antenna elements is notorious, the existence of

significant changes along with the measured directions. This occurrence can be justified by multipath and fading effects, that occur in the environment where the measurements were performed. However, a particularity that was already expected has occurred. If we analyze the tickle tone's power in the two performed measurement sets, it can be verified that in both cases is not possible to observe the overlapping of the tickle's tone power of the antennas one and two relative to the others. This occurs because, as mentioned earlier, these measurements were performed between the 0° and 180 ° azimuth angles. These two antennas have it is maximum radiation intensity in the directions that could not be measured, between the 180° and 360° azimuth angles.

Regarding the operation of the RF-DC converter circuit, for the considered emitted power, and remembering that the measurements were performed OTA, the circuit does not generate DC energy. This occurs because the circuit does not have such low sensitivity, what means that the circuit can not start operating for such low-power input signals. Is then required to increase the emitted signal's power, ensuring that the signal that arrives at the converter circuit input has also, more power. Since the SDR MIMO system used only operates with low power signals, an alternative measurement needs to be performed in order to validate the circuit's operation.

So, a VSG was used to generate the RF signal, which was emitted trough one of the 3D antenna array antenna elements. The converter circuit was connected to a patch antenna that works as a receiver. A schematic of the measurement setup used to perform these measurements is presented in Figure 4.22. It should be remembered, that due the considerations made in Section 4.2.2, where it was concluded that the best RF-DC conversion efficiency was obtained when the circuit operates at 5.55 GHz, all the antenna elements used in this section were designed to operate at this frequency.

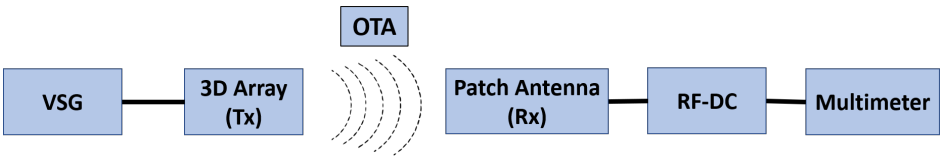

Figure 4.22: Schematic of the measurement setup used to validate the RF-DC operation OTA.

The first performed measurement, consisted of analyze the output DC voltage generated by the RF-DC converter circuit for different distances, between the receiver and the transmitter. So, the emitted power was swept between -10 dBm and 25 dBm with 1 dBm step, when the receiver was placed at 30 cm and 50 cm from the transmitter.

The results are presented in Figure 4.23. The generated DC voltage by the RF-DC converter circuit increases as the emitted signal's power increases. Initially, as the emitted signal's power increases, the DC output voltage generated increases slowly. From approximately 10 dBm, this value increases exponentially. For 15 dBm, it is possible to generate approximately 85 mV and 190 mV for a distance between the receiver and the transmitter of 50 cm and 30 cm, respectively. On the other hand, when the signal power is 20 dBm, the circuit generates, approximately, 150 mV and 360 mV, respectively, for the distances of 50 cm and 30 cm between the two modules.

As expected, the longer is the distance that the signal has to travel, bigger will be the FSPL, and consequently, bigger will be the signal's attenuation. The more significant is the attenuation that the signal undergoes, the lower will be the signal's power that reaches the

receiver and goes to the converter circuit, which results in a produced DC energy decrease. However, the achieved DC energy values are enough to feed passive or low-power sensors that require low current values to operate.

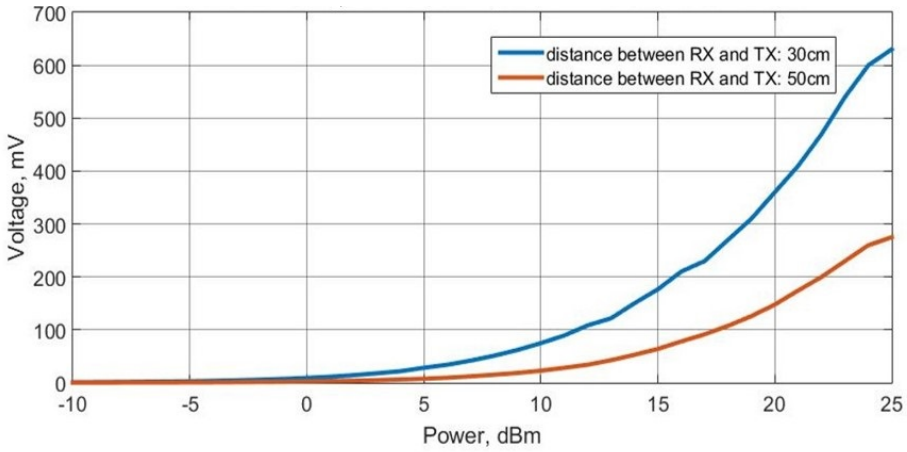

Figure 4.23: OTA measurements: generated DC output voltage vs emitted RF power.

Then, the generated DC energy by the converter circuit was analyzed, but this time, as a function of the distance between the receiver and the transmitter. The distance between these two modules was swept between 30 cm and 100 cm with a 5 cm step for fixed emitted signal's power values (0, 10 and 20 dBm). The obtained results were plotted and presented in Figure 4.24.

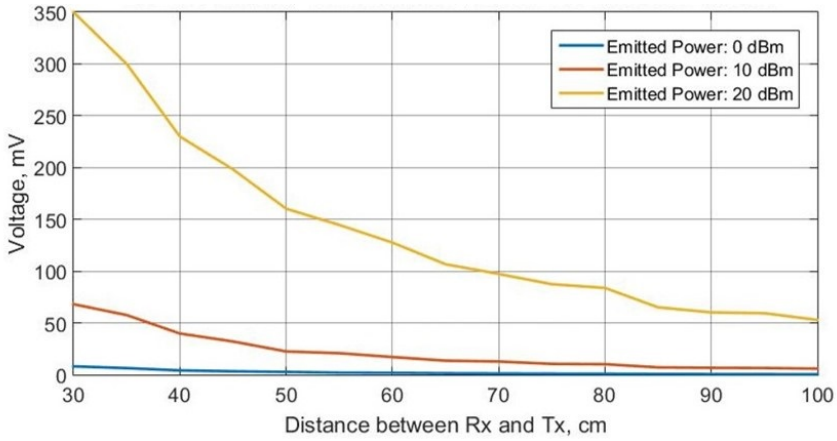

Figure 4.24: OTA measurements: generated DC output voltage vs distance between Rx and Tx.

Several considerations can be made from these results analysis. First, it can be concluded that for the signal strength of 0 dBm, the generated DC energy presents low values, with a maximum of 0.81 mV for the shortest considered distance. For this reason, this power value should be discarded if this system is intended to be implemented in practice. When the emitted power is increased to 10 dBm, the DC energy presents more significant values, obtaining about 25 mV for a distance of 50 cm between the receiver and the transmitter. However, for longer distances, this value drops significantly to a minimum of approximately

8 mV for one meter distance between the two modules. Finally, the most consistent results occur when the RF signal is emitted with a power of 20 dBm. The generated voltage has a maximum of 350 mV for the shortest considered distance and decreases sharply as this distance increases. However, despite this decrease, for one meter of distance between the receiver and the transmitter, the circuit can generate approximately 55 mV.

It can be concluded that, among the tested emitted powers, the RF signal with 20 dBm is the one that guarantees the best overall system operation by ensuring that a significant amount of DC energy can be provided to any sensor that is placed at a considered distance from the transmitter array.

4.5 Conclusion

In this chapter were presented and described all the measurements performed to the developed components individually. Those measurements are carried out, aiming to validate these component's operation behavior.

Initially, using a VNA, the reflection coefficients of the developed antennas were measured. Then, in the anechoic chamber, the antenna's radiation pattern was measured in two orthogonal planes allowing it is AR calculation. Through the AR analysis, it is possible to understand if the antenna is working with circular polarization. These measurements validated the antenna operation to the desired frequency and showed that trough the directions where the radiation intensity is maximum, the antenna is circularly polarized.

In order to validate the RF-DC converter circuit operation, several measurements were taken. Firstly, its S_{11} parameter was measured, aiming to validate the circuit's operation for the desired frequency. Then, the main characteristics of this circuit were evaluated. Using a VSG to simulate the RF wave at the circuit's input, the conversion efficiency was measured as a function of the frequency and power of the input signal. These two measurements were performed separately. In the end, the generated DC output power was measured in the function of the input signal RF power. It was concluded that the ideal circuit frequency is 5.55 GHz, for which with 0 dBm of input signal power, the circuit generates 0.86V, which implies an efficiency of approximately 34 %.

Lastly, the 3D arrays main features were evaluated, most precisely the coverage capabilities and the antenna's gain over the azimuth angles. Measurements in the anechoic chamber were presented, and a multi-sine technique was applied in a proper measurement system already purposed in the literature, which allows to excite all antenna elements simultaneously and analyze in detail the behavior of each one. These measurements allowed us to understand how to ensure the best signal quality, depending on the position of the receiver.

The conclusion of the practical part of this dissertation consisted of simulating a real application scenario where the developed 3D arrays can be implemented. It was evaluated the ability of this array if implemented in a WSN, power-up via WPT several sensors scattered around itself, which can be placed through all azimuth directions and at different elevation angles.

Chapter 5

Conclusions and Future Work

5.1 Conclusion

These alternative arrangements, which can easily be printed in a 3D printer (low-cost), aimed to improve mainly the WPT systems and the WSN's but also the wireless communications systems panorama. It can be considered that the main objective defined for this dissertation was achieved, since, the developed 3D arrays, which followed a beam-switch approach, proved to be capable of a full azimuth plan coverage, being able to transmit a signal with considerable gain to any far-field position around themselves. Thus, the developed 3D arrays are capable of transmitting energy to a sensor, regardless of its location. These 3D shapes also allow the radio link adjustment without mechanical movement, which has advantages over the mechanically steerable antennas since those failures that can occur due to mechanical moving parts are avoided. This beam adjustment is crucial in applications where the receiver does not have a fixed position because it allows the energy focus in the desired directions.

The last developed 3D antenna array aimed not only to ensure a signal's gain stabilization over the azimuth plane but also at different elevation angles. In order to simulate a real application scenario, like a WSN system, it has proceeded to the design and fabrication of a RF-DC converter circuit. In this way, the 3D array could be tested operating as a transmitter, and RF-DC circuit was connected to a patch antenna, which operates a receiver. In this practical scenario, this receiver simulates a passive/low-power sensor of a WSN. It was studied the ability of this array to focus the energy on a specific receiver position in order to power-up him. The ability to establish this radio link between the transmitter and receiver was tested with a fixed transmitter position and with the receiver moving around the transmitter and at different elevation angles. The measured results prove the reliability of this system. However, it is necessary to optimize some system characteristics such as the increase of the output DC power generated by the RF-DC converter.

It should be mentioned that most of the taken measurements were performed in a OTA scenario, which implies the existence of FSPL and of several objects that originate several reflections. If the measurements were performed in a more isolated environment, the results could have been more satisfactory. The measurement system that was used has the advantage of being able to excite all antenna ports simultaneously and carry out measurements in real-time.

This dissertation addressed different RF concepts, most of them related to antennas and

WPT systems, more precisely, the design and characterization of 3D antenna arrays and the design of RF-DC converter circuits, respectively. However, knowledge in other topics like MIMO antenna arrays and characterization systems based on multi-sines techniques was also acquired.

The proposed system met the requirements imposed at the beginning of this work. It can now be explored the benefits this system can bring if implemented in a real WSN.

5.2 Future Work

Different features can be optimized to improve overall system operation. These improvements should focus on the two main components of this system: the 3D arrays and the RF-DC converter circuit.

Regarding the design of the structures that support the antenna arrays, it should be tested the fabrication with different materials, namely different PLA's, in order to verify if their performance improves. Isolation techniques also may be implemented in order to decrease the mutual coupling between antenna elements. The developed antennas operate in a frequency within the ISM band. It would also be interesting to understand which are the best operating frequencies if it is intended to implement this system in a real application.

As for the RF-DC converter circuit, some techniques must be explored in order to improve the receiver-transmitter distance at which this system can operate. Firstly the circuit should be optimized in order to decrease its sensitivity, that is, start producing output DC power for lower power input signals. The use of new components, especially rectifier diodes, should be explored for this purpose. Waveform design should also be explored in order to improve the WPT efficiency. The multi-sines can be tested, aiming to transmit information and energy simultaneously.

At least, a beam-steering algorithm based on RSS techniques should be introduced to this system in order to make its operation autonomous and ensure the tracking of the receivers that can be scattered over a wide area or be in motion.

Bibliography

[1] Mingming Cai. *"Modeling and Mitigating Beam Squint in Millimeter Wave Wireless Communication"*. PhD thesis, 03 2018.

[2] C.A. Balanis. *"Antenna Theory: Analysis and Design"*. Wiley, 2016.

[3] Yi Huang and Kevin Boyle. *"Antennas: from theory to practice"*. Wiley, Hoboken, NJ, 2008.

[4] Silicon Labs. *"The Evolution of Wireless Sensor Networks"*. White Papers, (December 2008):1-5,2013.

[5] M. U. H. A. Rasyid, B. Lee, A. Sudarsono, and I. Mahfud. "Monitoring system of patient position based on wireless body area sensor network". In *2015 IEEE International Conference on Consumer Electronics - Taiwan*, pages 396–397, June 2015.

[6] A. Sudarsono, M. U. H. A. Rasyid, and H. Hermawan. "An implementation of secure wireless sensor network for e-healthcare system". In *2014 International Conference on Computer, Control, Informatics and Its Applications (IC3INA)*, pages 69–74, Oct 2014.

[7] E. Pievanelli, A. Plesca, R. Stefanelli, and D. Trinchero. "Dynamic wireless sensor networks for real time safeguard of workers exposed to physical agents in constructions sites". In *2013 IEEE Topical Conference on Wireless Sensors and Sensor Networks (WiSNet)*, pages 55–57, Jan 2013.

[8] S. Kawasaki. "The green energy harvesting winds by the RF/microwave power transmission". In *2013 IEEE Wireless Power Transfer (WPT)*, pages 111–114, May 2013.

[9] C. L. Palson, A. E. Sunny, and D. D. Krishna. "Circularly polarized square patch antenna with improved axial ratio bandwidth". In *2016 IEEE Annual India Conference (INDICON)*, pages 1–6, Dec 2016.

[10] M. A. Rahman, E. Nishiyama, and I. Toyoda. "A circular polarization antenna with square ring slot loaded on ground plane". In *2017 International Symposium on Antennas and Propagation (ISAP)*, pages 1–2, Oct 2017.

[11] Jieh-Sen Kuo and Gui-Bin Hsieh. "Gain enhancement of a circularly polarized equilateral-triangular microstrip antenna with a slotted ground plane". *IEEE Transactions on Antennas and Propagation*, 51(7):1652–1656, July 2003.

[12] Nasimuddin, Z. N. Chen, and X. Qing. "Asymmetric-Circular Shaped Slotted Microstrip Antennas for Circular Polarization and RFID Applications". *IEEE Transactions on Antennas and Propagation*, 58(12):3821–3828, Dec 2010.

[13] X. Zhang and L. Zhu. "High-Gain Circularly Polarized Microstrip Patch Antenna With Loading of Shorting Pins". *IEEE Transactions on Antennas and Propagation*, 64(6):2172–2178, June 2016.

[14] J. Huang. "A technique for an array to generate circular polarization with linearly polarized elements". *IEEE Transactions on Antennas and Propagation*, 34(9):1113–1124, Sep. 1986.

[15] T. Varum, J. N. Matos, P. Pinho, and R. Abreu. "Microstrip antenna for vehicular communications with improved axial ratio band". In *2011 IEEE EUROCON - International Conference on Computer as a Tool*, pages 1–4, April 2011.

[16] A. Svezhentsev and G. A. E. Vandenbosch. "Analysis of cylindrical microstrip array antennas with patches of a complex shape". In *2013 7th European Conference on Antennas and Propagation (EuCAP)*, pages 2977–2979, April 2013.

[17] D. Sengupta, T. Smith, and R. Larson. "Radiation characteristics of a spherical array of circularly polarized elements". *IEEE Transactions on Antennas and Propagation*, 16(1):2–7, January 1968.

[18] B. Tomasic, J. Turtle, and Shiang Liu. "Spherical Arrays - Design Considerations". In *2005 18th International Conference on Applied Electromagnetics and Communications*, pages 1–8, Oct 2005.

[19] P. Knott. "Design and Experimental Results of a Spherical Antenna Array for a Conformal Array Demonstrator". In *2007 2nd International ITG Conference on Antennas*, pages 120–123, March 2007.

[20] B. Pavan Kumar, C. Kumar, V. Senthil Kumar, and V. V. Srinivasan. "Active Spherical Phased Array Design for Satellite Payload Data Transmission". *IEEE Transactions on Antennas and Propagation*, 63(11):4783–4791, Nov 2015.

[21] M. Geissler, F. Woetzel, M. Bottcher, S. Korthoff, A. Lauer, M. Eube, and R. Gieron. "Innovative phased array antenna for maritime satellite communications". In *2009 3rd European Conference on Antennas and Propagation*, pages 735–739, March 2009.

[22] M. Geissler, M. Bottcher, R. Gieron, M. Eube, and P. Siatchoua. "A Low-Cost Phased Array for Mobile Satellite Communications". In *2007 2nd International ITG Conference on Antennas*, pages 148–152, March 2007.

[23] A. Cidronali, S. Maddio, G. Giorgetti, and G. Manes. "Analysis and Performance of a Smart Antenna for 2.45-GHz Single-Anchor Indoor Positioning". *IEEE Transactions on Microwave Theory and Techniques*, 58(1):21–31, Jan 2010.

[24] L. Bras, N. B. Carvalho, and P. Pinho. "Pentagonal Patch-Excited Sectorized Antenna for Localization Systems". *IEEE Transactions on Antennas and Propagation*, 60(3):1634–1638, March 2012.

[25] Issam Chaour, A Fakhfakh, and Olfa Kanoun. "Enhanced Passive RF-DC Converter Circuit Efficiency for Low RF Energy Harvesting". *Sensors*, 17:546, 03 2017.

[26] J. O. McSpadden, Lu Fan, and Kai Chang. "Design and experiments of a high-conversion-efficiency 5.8-GHz rectenna". *IEEE Transactions on Microwave Theory and Techniques*, 46(12):2053–2060, Dec 1998.

[27] C. Song, Y. Huang, J. Zhou, J. Zhang, S. Yuan, and P. Carter. "A High-Efficiency Broadband Rectenna for Ambient Wireless Energy Harvesting". *IEEE Transactions on Antennas and Propagation*, 63(8):3486–3495, Aug 2015.

[28] H. J. Visser. "Maximizing DC power in WPT using a transient transmit array antenna". In *2016 IEEE Wireless Power Transfer Conference (WPTC)*, pages 1–4, May 2016.

[29] X. Yang, W. Geyi, and H. Sun. "Optimum Design of Wireless Power Transmission System Using Microstrip Patch Antenna Arrays". *IEEE Antennas and Wireless Propagation Letters*, 16:1824–1827, 2017.

[30] A. Massa, G. Oliveri, F. Viani, and P. Rocca. "Array Designs for Long-Distance Wireless Power Transmission: State-of-the-Art and Innovative Solutions". *Proceedings of the IEEE*, 101(6):1464–1481, June 2013.

[31] Y. Li and V. Jandhyala. "Design of Retrodirective Antenna Arrays for Short-Range Wireless Power Transmission". *IEEE Transactions on Antennas and Propagation*, 60(1):206–211, Jan 2012.

[32] A. Costa, R. Gonalves, P. Pinho, and N. B. Carvalho. "Beam steering antenna and network design for WPT applications". In *2016 10th European Conference on Antennas and Propagation (EuCAP)*, pages 1–4, April 2016.

[33] S.M. Sze. *"Semiconductor Devices: Physics and Technology"*. John Wiley & Sons Singapore Pte. Limited, 2012.

[34] S.A. Maas. *"Nonlinear Microwave and RF Circuits"*. Artech House, 2003.

[35] W. Tu, S. Hsu, and K. Chang. "Compact 5.8-GHz Rectenna Using Stepped-Impedance Dipole Antenna". *IEEE Antennas and Wireless Propagation Letters*, 6:282–284, 2007.

[36] C. . K. Chin, Quan Xue, and Chi Hou Chan. "Design of a 5.8-GHz rectenna incorporating a new patch antenna". *IEEE Antennas and Wireless Propagation Letters*, 4:175–178, 2005.

[37] K. Nishida, Y. Taniguchi, K. Kawakami, Y. Homma, H. Mizutani, M. Miyazaki, H. Ikematsu, and N. Shinohara. "5.8 ghz high sensitivity rectenna array". In *2011 IEEE MTT-S International Microwave Workshop Series on Innovative Wireless Power Transmission: Technologies, Systems, and Applications*, pages 19–22, May 2011.

[38] C. R. Valenta and G. D. Durgin. "Harvesting Wireless Power: Survey of Energy-Harvester Conversion Efficiency in Far-Field, Wireless Power Transfer Systems". *IEEE Microwave Magazine*, 15(4):108–120, June 2014.

[39] D.M. Pozar. *"Microwave Engineering, 4th Edition"*. Wiley, 2011.

[40] D. C. Dinis, N. B. Carvalho, A. S. R. Oliveira, and J. Vieira. "Over the air characterization for 5G massive MIMO array transmitters". In *2017 IEEE MTT-S International Microwave Symposium (IMS)*, pages 1441–1444, June 2017.

[41] Z. Li, Z. Du, M. Takahashi, K. Saito, and K. Ito. "Reducing Mutual Coupling of MIMO Antennas With Parasitic Elements for Mobile Terminals". *IEEE Transactions on Antennas and Propagation*, 60(2):473–481, Feb 2012.

[42] J. W. Wallace and M. A. Jensen. "Mutual coupling in MIMO wireless systems: a rigorous network theory analysis". *IEEE Transactions on Wireless Communications*, 3(4):1317–1325, July 2004.

[43] M. Jordão, D. Belo, R. Caldeirinha, A. S. R. Oliveira, and N. B. Carvalho. "Characterization of Electromagnetic Coupling Effects in MIMO Antenna Array Beamforming". In *2019 IEEE MTT-S International Microwave Symposium (IMS)*, pages 1379–1382, June 2019.